An Instantaneous Frequency Based Approach to Estimate Heart Rate and Calculate Heart Rate Variability Metrics

Don Prathap Jayasooriya

Thesis submitted to the faculty of the Virginia Polytechnic Institute and State University
in partial fulfillment of the requirements for the degree of

Master of Science
In
Mechanical Engineering

Alfred Wicks, Chair
Steve Southward
Alexander Leonessa

May 6, 2024
Blacksburg, Virginia

Keywords: Heart rate variability, Instantaneous frequency, Instantaneous heart rate

An Instantaneous Frequency Based Approach to Estimate Heart Rate and Calculate Heart Rate Variability Metrics

Don Prathap Jayasooriya

(ABSTRACT)

An emerging diagnostic tool for detecting heart and physiological conditions is heart rate variability (HRV). Copious research continuously discovers relationships between heart rate variability metrics and physiological functions and cardiac health. The first step in calculating HRV metrics is calculating heart rate. Heart rate is typically calculated using the interval between R peaks in an EKG signal. Consequently, heart rate measurements rely on the presence of distinctive R peaks and the accurate detection of them. The study is motivated by the drawbacks associated with using R peaks to calculate instantaneous heart rate.

In this study we present an alternative method (that does not rely on R peaks) based on the concept of instantaneous frequency to estimate heart rate from electrocardiogram (EKG) signals. The EKG signal is filtered to extract constituent frequency components that correlate with the instantaneous heart rate. The filtered signal is then fed into an algorithm that outputs a signal that shows the variation of the instantaneous heart rate with time. This output signal contains noise due to the behavior of the algorithm at zero crossings of the filtered EKG signal. Two methods for filtering the output signal are also presented in the study.

The proposed method was able to successfully estimate the instantaneous heart rate and allowed the subsequent calculation of frequency domain HRV metrics. This method potentially provides more information for HRV analysis and addresses the drawbacks associated with methods based on R peak detection.

An Instantaneous Frequency Based Approach to Estimate Heart Rate and Calculate Heart Rate Variability Metrics

Don Prathap Jayasooriya

(GENERAL AUDIENCE ABSTRACT)

Heart disease is the leading cause of death in America accounting for about 20% of all deaths. Consequently, both the public and the medical community are engrossed in cardiovascular health, research that enables early detection of heart disease and novel treatments for cardiac conditions. An emerging diagnostic tool for detecting heart and physiological conditions is heart rate variability (HRV). Copious research continuously discovers relationships between heart rate variability metrics and physiological functions and cardiac health. The first step in calculating HRV metrics is calculating heart rate. With the rise in popularity and improvement of wearable technologies, it has become easier than ever to collect data and perform diagnostics, often in real time. As such the need for robust methods and algorithms to perform these calculations are ever more important. The study is motivated by drawbacks associated with the conventional method used to calculate heart rate from electrocardiogram signals. In this study we present a more robust method to calculate heart rate from EKG signals allowing more accurate HRV metrics to be calculated.

In this study we present an alternative method based on the concept of instantaneous frequency to estimate heart rate from electrocardiogram (EKG) signals. We identify the shortcomings of the conventional method of estimating heart rate and discuss the strengths and weaknesses of the alternative method introduced. We then calculate and compare the HRV metrics calculated from the proposed method and the conventional method.

The method presented also has the potential to be used on other signals that measure the heart's activity such as Photoplethysmography signals (PPG) allowing it to be used on wearable devices. We hope that the information provided, and the findings presented in this study will be utilized by the medical community and researchers for future research related to heart rate variability.

Acknowledgments

This thesis would not have been possible without the help and guidance of several individuals. First, I want to thank my advisor, Dr. Alfred Wicks, for his guidance and advice throughout my research. Thank you for always motivating me to think critically and enlightening me during our many research meetings. I would also like to thank my committee members, Dr. Steve Southward and Dr. Alexander Leonessa, for their valuable feedback and guidance.

I am fortunate to have such loving parents and a sister who have supported me throughout my life, especially during graduate school. Thank you for your love, patience, and support. Ammi and Thaththi, you have always encouraged me to reach great heights and achieve my dreams while providing a safety net.

Thank you, Micaela, for being such a wonderful partner and for being my safe place. You bring the best out of me. I am forever grateful for your love, care, patience, and encouragement.

I would also like to thank Chris Russo, Laura Copenhaver, and the crew at the Squires Studio Theater for making work fun and for the lasting friendships. I thoroughly enjoyed my GTA position at the scene shop.

Finally, I want to thank my extended family, friends, and colleagues, whom I could not mention specifically but who made my experience at Virginia Tech truly memorable. Graduate school would have been a much more daunting experience if it had not been for all of you.

Table of Contents

Chapter 1 - Introduction

The human heart is one of the vital organs in the human body. It constantly pumps blood throughout the body delivering oxygen and nutrients to cells. Additionally, the pumped blood removes waste from cells. It is a positive displacement pump and functions in a cyclic manner. For centuries, the medical field has studied this cyclic behavior of the heart. They continually make important discoveries connecting cardiovascular health and wellbeing to observations of the heart's function and its cyclic pattern. An important metric derived from the cyclic nature of the heart's function is the heart rate: a measurement of the number of cardiac cycles the heart undergoes during a set period of time. Usually, heart rate is presented in beats per minute where a beat represents one cardiac cycle which can be felt during arterial palpation as a pulse. An individual's heart rate is controlled by the autonomic nervous system[1] and is sensitive to phenomena such as cardiac sympathetic and parasympathetic nerve activity, the respiratory rhythm, the circadian rhythm, and temperature regulatory functions. [2] Consequently, heart rate is dynamic, and its variability may give insight into the many functions that influence it. This has led researchers to study heart rate variability (HRV) and formulate HRV metrics that can be used as a diagnostic tool in cardiology. Heart rate variability metrics quantify the variations observed in the heart rate during a measurement period of the heart's activity. In [3], the authors present some of the clinical applications where HRV metrics are used as a diagnostic tool. These range from cardiovascular health monitoring [4] to assessing autonomic changes due to psychological and pathological conditions. [5] The first step in calculating HRV metrics is calculating the instantaneous heart rate (IHR) signal from signals that measure the heart's activity. Examples of such signals are electrocardiograms (EKG) and photoplethysmography (PPG) signals. The electrocardiogram signal is preferred by the medical community for its ability to directly detect the electrical activity of the heart. The IHR signal derived from an EKG signal is a time series of heart rates measured at set intervals. It shows how the heart rate changes with time. HRV metrics are calculated from this IHR

signal in the time domain, frequency domain, and through nonlinear methods. As these metrics quantify the variability of the heart rate, the methods used to calculate instantaneous heart rate from EKG signals have a significant effect on them. It is therefore imperative that robust heart rate estimation techniques are used to calculate IHR from EKG signals. This study was motivated by shortcomings present in the conventional methods used in estimating heart rate from EKG signals.

1.1 Motivation

Heart rate variability metrics quantify the variations in the heart rate, and therefore its accuracy is highly dependent on the technique used to measure the heart rate. The most common method used to calculate the heart rate from EKG signals is by measuring the interval between neighboring R peaks, termed the RR interval. These R peaks are the most prominent spikes present in the EKG signals and can be detected using thresholding methods. Enumerable amount of research is available that presents algorithms and signal processing techniques to improving R peak detection. However, anomalies, irregularities and noise in EKG signals make it challenging for peak detection algorithms to correctly identify R peaks. Further, the amplitude and prominence of R peaks greatly depend on the electrocardiogram lead being assessed (more about EKG leads will be discussed later). This subsequently results in missed R peaks and erroneous peak detection. Such errors lead to incorrect heart rate estimation and subsequently inaccurate HRV metrics. Furthermore, the instantaneous heart rate (IHR) signal calculated using RR interval measurements produces samples at irregular time intervals. This is because the heart rate is calculated by measuring the time between neighboring R peaks and a result can only be produced at intervals equivalent to the RR intervals. The RR intervals are not constant and thus RRSIG is sampled at a variable rate. As a result, frequency domain analysis of HRV using techniques such as the Fast Fourier Transform (FFT) cannot be performed directly. This is because the FFT algorithm is only applicable to signals sampled at a uniform sampling rate. Therefore, the IHR signal must be interpolated at a fixed sampling rate before computing the FFT. However, interpolation is not ideal as it deforms the original signal. Other frequency domain analysis

techniques such as the Least Square Spectral analysis [6] that do not rely on a fixed sampling rate are seldom used.

Therefore, it is clear that there are several drawbacks associated with R peak detection to estimate heart rate. The effects of these shortcomings are reflected in the IHR signals and the HRV metrics calculated from them. In this study we aim to introduce a method to calculate instantaneous heart rate using an alternative method that does not rely on R peak detection. The method introduced is based on the concept of instantaneous frequency. In conclusion, the motivation for this study is to provide the medical community with a methodology to assess heart rate and heart rate variability from EKG signals that is independent of RR interval measurements.

1.2 Thesis Outline

This thesis is divided into 4 chapters, each containing subsections. The following is a brief description of the chapters and their content.

Chapter 1 introduces heart rate variability and briefly points out the drawbacks of measuring heart rate from EKG signals using R peaks. These drawbacks provided the motivation to conduct the study presented in this thesis to find a different approach at measuring heart rate from EKG signals.

Chapter 2 provides a review of the literature associated with the cardiac cycle, the electrocardiogram, methods used to calculate heart rate, heart rate variability and instantaneous frequency.

Chapter 3 focuses on the underlying theories associated with the techniques and methods used in this study to process EKG signals, estimate instantaneous heart rate and calculate time domain and frequency domain heart rate variability metrics. This chapter also provides theoretical insight into certain observations made during the process of calculating instantaneous heart rate from an EKG signal.

Chapter 4 is dedicated to the analysis of results obtained from the method introduced in this study to calculate instantaneous heart rate. In this chapter, the developed algorithms will be applied to different EKG

signals and a thorough analysis of the resulting instantaneous heart rate signals and the HRV metrics will be performed. This chapter also discusses how the methods introduced in this study can be extended for future research related to HRV.

Chapter 2 - Literature Review

2.1 The Cardiac Cycle

The human heart is the organ that provides the force to circulate blood throughout the body. [7] It is made up of four internal chambers, namely, the right atrium, left atrium, left ventricle and the right ventricle. The superior vena cava, and the inferior vena cava: both large veins, and the coronary sinus bring oxygen depleted blood from throughout the body to the right atrium. The tricuspid valve, which only allows blood to flow from the right atrium to the right ventricle, connects the two chambers. The right ventricle pushes deoxygenated blood to the lungs through the pulmonary valve and pulmonary artery. [8] The left atrium receives oxygen-rich blood from the lungs through the pulmonary vein and then pushes them to the left

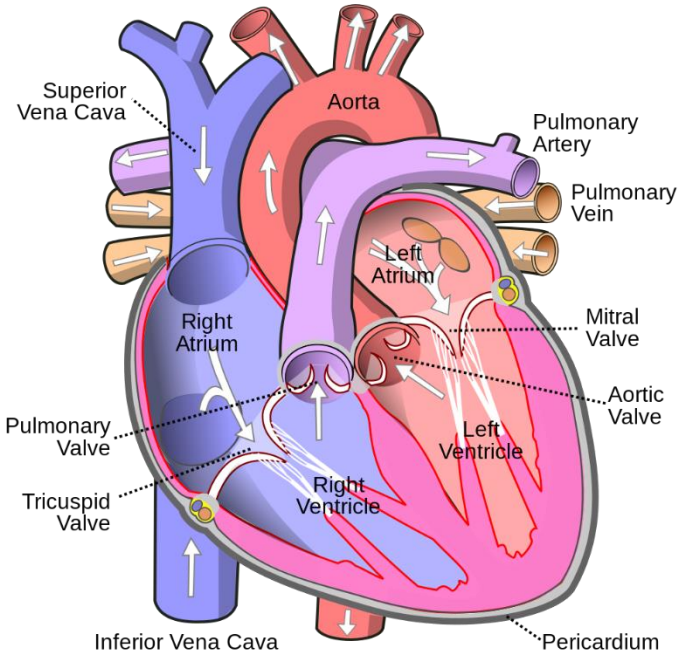

Figure 2.1: The human heart showing its chambers, valves and the major veins and arteries connected to it.

ventricle through the mitral valve. The left ventricle holds the oxygenated blood received from the left atrium and pushes it through the aortic valve and aorta artery to the rest of the body. [9]

The cardiac cycle begins with the contraction of the two atria and ends with ventricular relaxation. The period of time where the heart undergoes contraction to pump blood into circulation is called systole. The period of time when the heart muscles relax and allow blood to fill into its chambers is called diastole. Both atria and ventricles undergo systole and diastole. [10]

At the beginning of the cardiac cycle, both atria and ventricles are relaxed allowing blood to freely flow into the chambers. The pulmonary and aortic valves that only allow blood to flow out of the heart are closed preventing blood from flowing back to the ventricles through the pulmonary and aortic arteries respectively. The tricuspid and mitral valves allow the blood to freely flow from the atria to their respective ventricles.

The sinoatrial (SA) node, which is made up of myocardial conducting cells depolarize, generating an electrical impulse that spreads throughout the atria causing it to contract. Atrial depolarization causes the relatively small P wave in the EKG signal. [11] The impulse then flows to the atrioventricular node and pauses for about 100 milliseconds which allows the atria to contract fully and push all the blood to the ventricles. The impulse then flows through the atrioventricular bundle (bundle of HIS) which branches out and allows the impulse to sweep through the right and left ventricles. [12] The depolarization of the ventricles caused by this creates a large distinctive peak in the EKG signal which is termed the R wave. The impulse is then transmitted to the Purkinje fibers. The impulse transmitting from the atrioventricular node to the Purkinje fibers collectively depolarizes the ventricles causing them to contract and push blood contained within them out of the heart. The tricuspid and mitral valves shut preventing the blood from flowing back to their respective atria. After ventricular systole, both ventricles repolarize in preparation for the next cardiac cycle. This repolarization causes the small T wave in the EKG signal. [13] Figure 2.2 shows the phases of the cardiac cycle that were discussed along with their corresponding EKG signal events.

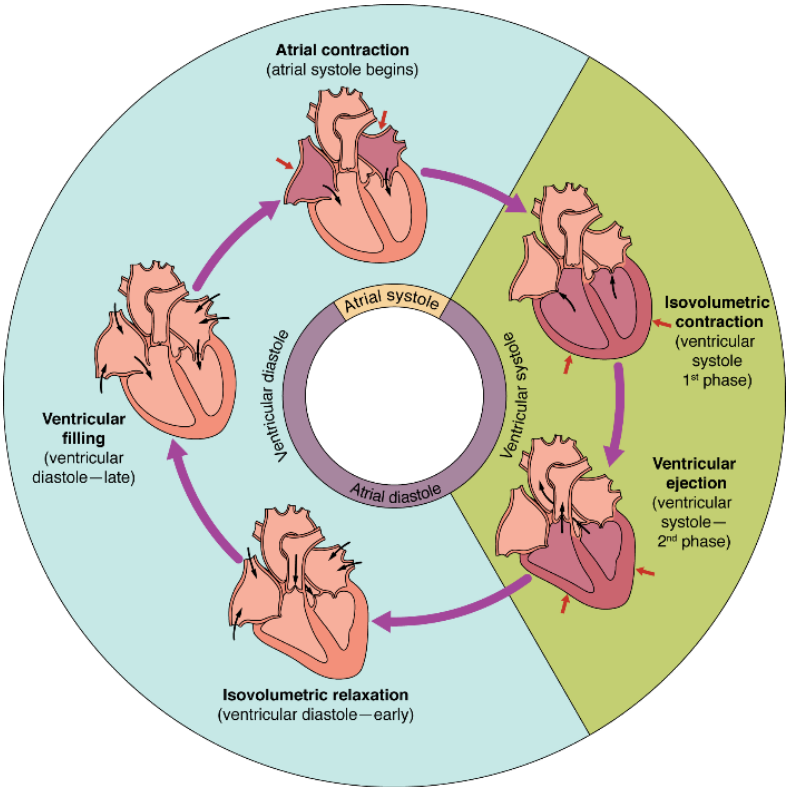

Figure 2.2: The cardiac cycle.

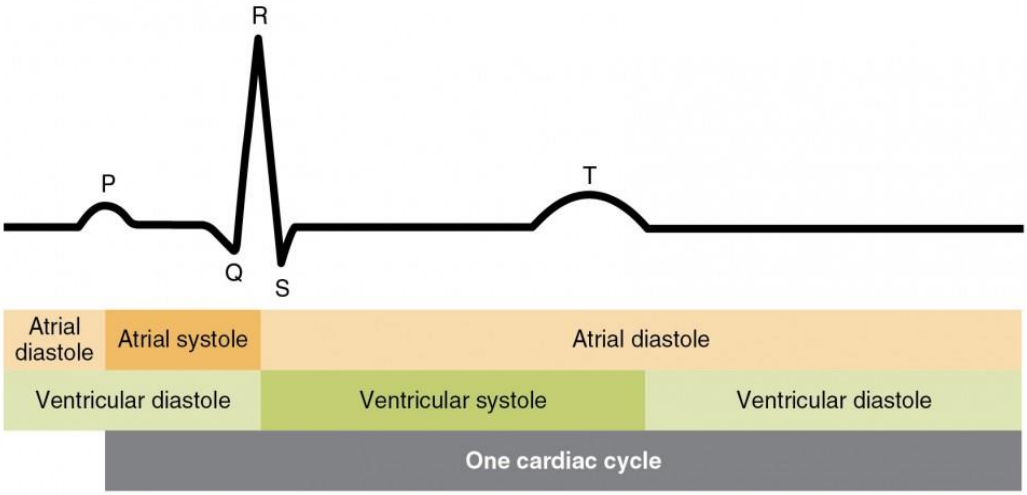

Figure 2.3: Portion of the EKG signal associated with one heart cycle. Notice the EKG events (top) and the cardiac events (bottom) associated with it.

2.2 The Electrocardiogram Signal (EKG)

An electrocardiogram, ECG/EKG for short, is a noninvasive test that detects and records electrical activity in the heart muscles. An EKG lead is a graphical description of the electrical activity of the heart and is constructed by analyzing the electrical potential detected by 2 electrodes. An electrode is a conductive pad that is attached to the skin that allows observation of electrical activity. As the electrical signals generated by the sinoatrial node spread through the heart muscles electrical impulses are created. They are produced by the movement of charged particles: intracellular and extracellular ions (Na^+, K^+, and Ca^{2+}) that pass-through cell membranes which allow for depolarization and repolarization of cardiac muscles. This leads to contractions and relaxation of the cardiac muscles which enables the heart to pump blood throughout the body.

The standard EKG, which is known as a 12-lead EKG (since it utilizes 12 leads), is obtained using 10 electrodes. Six of these electrodes are connected to the chest of an individual while the remaining four are connected to each limb [14]. The electrodes are then connected to an electrocardiogram monitoring device.

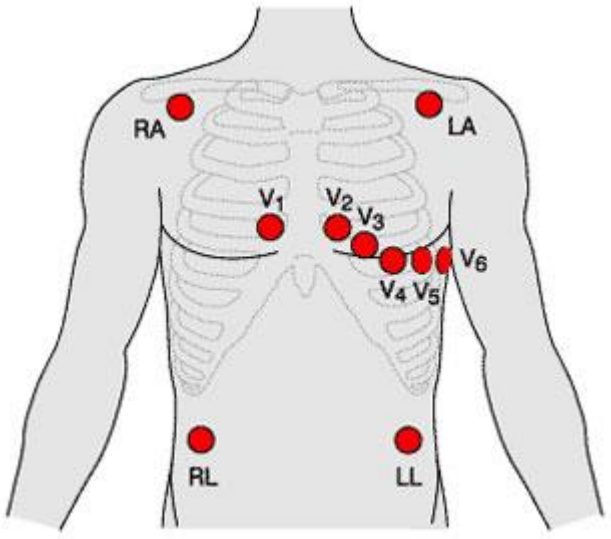

Figure 2.4: Location of the 10 electrodes in a 12 lead EKG. V1 to V6 are chest electrodes while the remaining electrodes are connected to extremities of the body (usually limbs).

These devices can range from standard 12 lead EKG monitors to ambulatory devices such as Holter monitors: used for recordings that exceed 24 hours. [15] The number of electrodes used is also dependent on the type of EKG monitor being used. For instance, single lead EKG monitors that use 2 to 3 electrodes are gaining popularity for personal use. [16]

An EKG lead consists of two electrodes of opposite polarity (bipolar lead) or a reference point and one electrode of positive polarity (unipolar lead) [17]. For example, a 12 lead EKG consists of 3 bipolar limb leads (I, II, III), 3 unipolar limb leads (AVR, AVL, AVF) and 6 unipolar chest leads (V1, V2, V3, V4, V5, V6)[17]. As electrical impulses flow throughout the heart electrical potential differences occurs between electrodes. The EKG leads captures the magnitude and direction of these potential differences. The objective of using 12 leads is to capture the electrical activity of the heart in different directions. Depending on which lead shows irregularities medical personnel can determine which part of the heart they originate from and locate infractions in heart muscles [14]. Figure 2.5 shows a standard 12 lead electrocardiogram recording. The Y-axis represents voltage, while the X-axis represents time. [18]

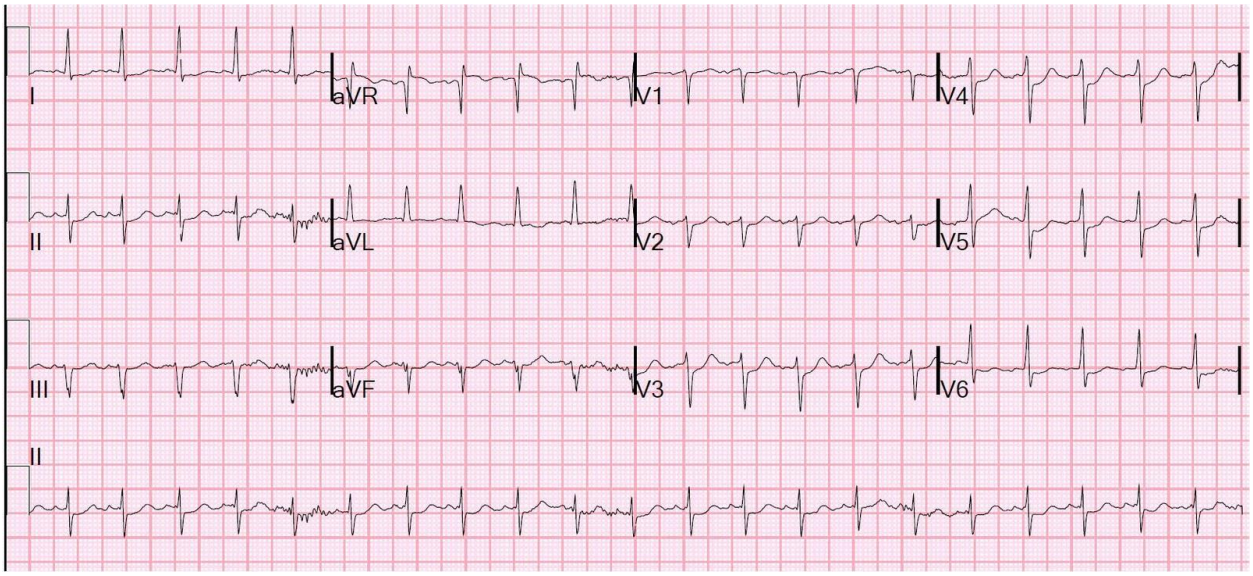

Figure 2.5: Portion of a 12-lead electrocardiogram. Observe the differences in the waveforms obtained from the 12 different leads. Also notice how the R peaks are less prominent in certain leads and inverted in others. Therefore, the algorithm used for R peak detection must account for the lead being used.

The EKG signal consists of deflections from the baseline that indicate an electrical impulse, these are termed as waves.

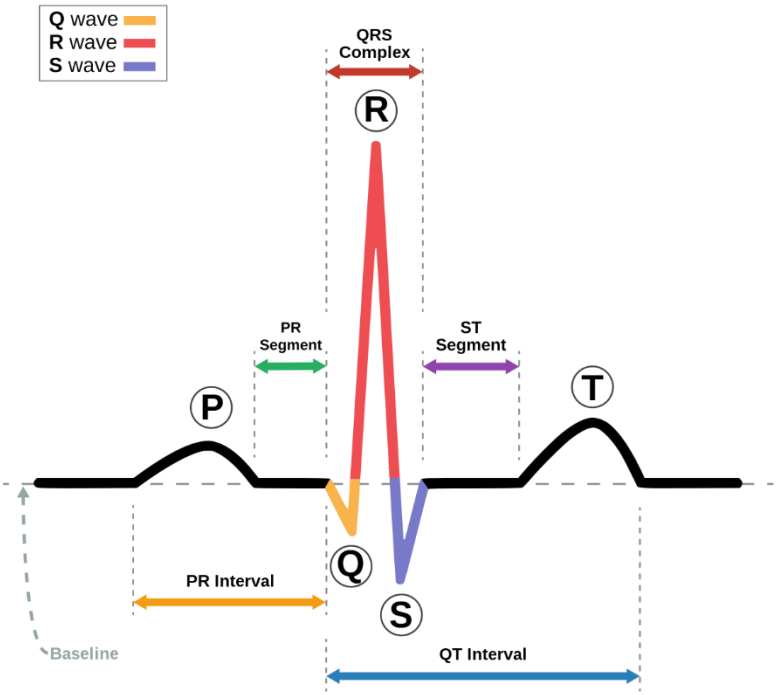

Figure 2.6: Electrocardiogram representation of a heartbeat. The main waves and intervals are marked.

There are 5 main waves in the EKG signal associated with a single heartbeat. They are named the P, Q, R, S and T waves. The Q, R and S waves are usually combined together and assessed as the QRS complex. We discussed the different cardiac events that generate these electrocardiogram events in detail in section 2.1. To summarize, the P wave is generated as a result of atrial depolarization. In a normal sinus rhythm, it is always positive (deflection is upwards) in I and II and always negative in the AVR lead. The shape of the P wave is important for detecting heart anomalies as abnormal P waves may indicate conditions such as atrial enlargement. [19] The QRS plot is the most prominent feature of the EKG wave and represents ventricular depolarization. The R wave within the QRS plot progressively increases in amplitude as it moves across the chest/precordial leads from right to left. As such, V1 has the lowest amplitude and V5 has

the highest. [19] Therefore, it is imperative that leads producing prominent R peaks are used when IHR signals are constructed using RR interval measurements. This is because thresholding algorithms used to detect R peaks require distinctive R peaks in the EKG signal. For EKG signals obtained from single lead EKG machines, it is vital to position the electrodes such that prominent R peaks are present in the EKG signal. Finally, the T wave represents ventricular repolarization and abnormalities of it can give insight to a host of pathological conditions. Another common term associated with EKG signals is the RR interval. It is the time measured between two neighboring R peaks. As the heart functions in a cyclic manner, the RR interval gives the period of this cyclic function. The rate at which the heart beats can therefore be derived from the RR interval. More on this will be discussed in later sections and chapters.

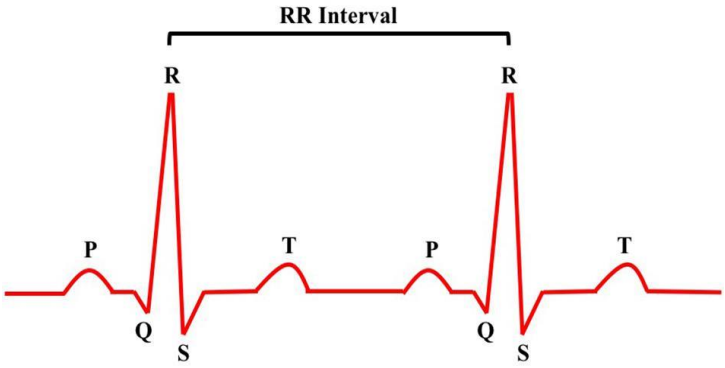

Figure 2.7: The RR interval: time between two neighboring R peaks. This interval is variable and is controlled by the autonomic nervous system.

2.3 Methods used to measure heart rate

Heart rate quantifies the number of cardiac cycles the heart goes through during a set period of time. It is common to present heart rate as beats per minute, that is, the number of cardiac cycles the heart undergoes in one minute. There are several ways to measure heart rate, some more accurate than others. A rudimentary method to estimate heart rate is by taking the radial pulse by placing the fingertips of your index and middle finger over the artery on your wrist and counting the number of pulsations felt in a minute. [20]

2.3.1 Photoplethysmography

With the rising popularity of modern wearables, noninvasive and simple methods for measuring heart rate are becoming attractive. One such technology that is prevalent in wearables is photoplethysmography, or PPG for short. PPG is an optical measurement technique that can be used to detect volumetric changes in blood in the microvascular tissue bed. [21] This technology is utilized in commercially available medical devices and fitness trackers such as pulse oximeters. PPG employs a light source, typically an array of LEDs, and a photodetector, typically a photodiode. The light source emits light that illuminates the tissue, and the reflected or refracted light is captured by the photodetector. During each cardiac cycle, blood is pumped from the heart to the peripheries of the body. The arterial blood volumetric change due to a heartbeat attenuates the light intensity captured by the photodetector. [22] These variations in the light intensity produce an alternating wave pattern that has a frequency equal to the heart rate. The PPG waveform mainly consists of two phases: the upward-trending anacrotic phase and the downward-sloping catacrotic phase. The distinctive peak that separates the two phases is called the systolic peak. The anacrotic phase is correlated with systole, while the catacrotic phase is associated with diastole. [21] The most common method to calculate the heart rate using PPG signals is by utilizing a peak detection algorithm to detect the systolic peaks and then measuring the time between peaks to calculate the period and frequency. Researchers have conducted many studies to assess the suitability and performance of PPG to estimate heart rate. In some studies, the performance of PPG is compared with electrocardiogram signals. This is because the EKG is the gold standard in the medical community for measuring heart rate and observing heart-related conditions. In the study presented in [23], the researchers calculated heart rate by detecting the valleys of the PPG signal and then measuring the interval between valleys. They then compared and quantitatively showed that heart rate variability obtained from PPG and EKG signals closely match. In [24], the authors assess if PPG signals obtained from wearables can accurately estimate heart rate variability. They conclude that wearables using PPG technology perform best under resting to mild exercise conditions and on individuals of certain age groups. This is because signals are affected by motion, respiration, and arterial

stiffness, which changes with age. It should also be noted that PPG measures the blood's volumetric change in the microvascular tissue bed and not the electrical activity of the heart muscle when it goes through the cardiac cycle. It is, however, shown that these phenomena correlate with each other. Since it takes a finite amount of time for blood to rush into the peripheries of the body from the heart, there is a delay associated with the actual heartbeat muscle activity and the inflection points in the PPG signal. This delay is referred to as the pulse transit time (PTT). In [25], Jago and Murray show how the anatomical site where the readings are taken from and body and limb posture affect the PTT.

2.3.2 Electrocardiogram

As mentioned before, electrocardiogram signals are considered the gold standard when it comes to monitoring cardiac activity and health. The nature of the EKG signal, more specifically the presence of distinctive peaks (R waves) makes it possible to measure the heart rate easily. As discussed in previous sections, the peaks are associated with distinctive cyclic events the heart undergoes. Therefore, measuring the time between successive peaks is the easiest way to determine the heart rate. Heart rate can be manually measured using the EKG paper that is printed out by some electrocardiogram machines. The standard EKG paper is output at a rate of 25 mm/second and has a grid comprising of squares. [26] The distance between consecutive vertical edges of the square grid is 1 mm and equals to 0.04 seconds. An estimate for the heart rate can be calculated by counting the number of squares between two successive R peaks and dividing 1500 by the number of squares. For example, if there are 15 squares between two successive R peaks, the heart rate is 1500/15 = 100 beats per minute.

Peak detection algorithms are used to detect peaks in digital EKG signals in order to calculate heart rate. Since this method is heavily reliant on the presence of peaks, it is imperative that raw EKG signals are preprocessed, and robust peak detection algorithms are used. This is because data acquired by the electrodes may contain noise resulting from body movements, weak electrode contact etc. Many studies have been done to come up with EKG preprocessing techniques for effective peak detection. The common procedure

used in many studies is removing noise and accentuating peaks through digital signal processing techniques followed by a peak detection stage that involves the use of thresholds. In [27] the authors present an algorithm to detect QRS complexes from noisy EKG signals. The process comprises several signal preprocessing steps to remove noise and accentuate QRS complexes. Noise is removed using cascaded filters and peaks are accentuated by calculating the derivative of the electrocardiogram and using a moving window integration filter. They then proceed to a peak detection stage which involves determining adaptive thresholds based on signal noise level, previously identified QRS complexes, and RR interval averages. The presented algorithm could detect peaks with an accuracy of 99.325%. In the text [28] the authors discuss common preprocessing and QRS complex detection techniques as well as EKG signal delineation methods used to extract information from the EKG signal. The authors discuss the use of filters ranging from linear time invariant high-pass filters to time-varying polynomial fitting to remove baseline wander from raw EKG signals. Baseline wander is low frequency noise usually induced by body movements and poor electrode contact. [29] When it comes to detecting QRS complexes, the authors discuss about linear and nonlinear methods to enhance the QRS complexes in preparation for peak detection using thresholding methods.

Another common method is the use of wavelet transforms to identify QRS complexes. A wavelet transform involves convolving a signal with a set of wavelets (infinite number in continuous and a finite number in discrete) that are horizontally scaled versions of a particularly shaped wavelet which is termed as the mother wavelet. The process of convolving a signal with a set of wavelets (in the case of discrete wavelet transform) decomposes the original signal into distinctive levels. These levels contain information referred to as coefficients that indicate how much the scaled wavelet correlates with the signal. For instance, if at a certain level, the coefficient value is high at a given location, then the original signal has high similarity to that of the wavelet at that scale. As such, the 1^{st,} and last levels (low frequency and high frequency levels) can be identified as baseline drift and noise respectively and can be removed. Through observation, one can identify the levels that contain valuable information for feature recognition. Consequently, those levels can

be extracted and used to reconstruct a signal that only contains information of interest for further processing. When it comes to EKG signals, wavelets can be used to remove noise and extract the QRS complexes from the original signal. Much research has been done on the type of wavelets that yield the best results for processing EKG signals. It is common to select a wavelet that has a similar shape to that of the feature that is to be extracted from a signal. In the case of EKG signals, this would be the QRS complex. In several studies wavelets in the Daubechies wavelet family were used to extract the QRS complexes as their shape closely match that of the QRS complex. In [30] the authors use Daubechies 6 wavelet to decompose EKG signals into 8 different levels. They then reconstructed signals using selected coefficients which enables them to identify QRS complexes as well as P and T waves. Heart rate can be then calculated using the distance between neighboring R peaks. In the study presented in [31], independent component analysis is performed on noisy EKG signals to eliminate motion induced noise and extract the QRS complexes. The heart rate is then calculated using the RR intervals.

So far, the literature presented in this chapter used the periodicity of signals such as PPG and EKG to measure the heart rate. These methods mainly focused on detecting periodic occurrences such as R waves and measuring the interval between successive events. The study presented in [32] takes a different approach in determining the heart rate. Here, the authors utilize the concept of instantaneous frequency to calculate the heart rate. This is done by first calculating the spectrogram of the EKG signal followed by the use of an algorithm to detect the high-density regions of the spectrogram. A spectrogram visualizes the frequency change of a signal with time. It is a 3-dimensional representation of the signal showing the magnitude of the constituent frequencies of a signal at a given window of time. As a result, a spectrogram is a powerful tool to analyze non-stationary signals. The authors state that since the EKG signal is a periodic signal, the fundamental frequency of the EKG is equivalent to the heart rate. They treat the EKG signal as a frequency modulated signal and use the spectrogram and an algorithm to track this fundamental frequency at each time window. They then use a bandpass filter with a center frequency similar to those of the tracked frequencies to filter the EKG signal and use the Hilbert transform to construct an analytic signal. They then

compute the instantaneous frequency, which in this case is the instantaneous heart rate by taking the derivative of the argument of the analytic signal. They further state that the resultant instantaneous heart rate signal can be sampled at a much lower rate (5 Hz) to minimize required storage capacity. The method requires pre-recorded EKG data as the spectrogram cannot be constructed in real time.

The method presented in this thesis to estimate the heart rate also utilizes the concept of instantaneous frequency. However, rather than using the spectrogram and the Hilbert transform as in [32], an analytical approach is taken to calculate the instantaneous frequency. Although the entire process is performed on prerecorded EKG data in this study, the algorithms presented can be implemented in real-time. This is especially beneficial for real time heart rate monitoring.

2.4 Instantaneous Frequency

In section 2.3 we discussed different methods used in literature and in the medical field to calculate heart rate. In this section we will discuss the concept of instantaneous frequency and associated literature. Through our discussion we will see if concepts of instantaneous frequency can be applied to electrocardiogram signals to measure the instantaneous heart rate. Instantaneous frequency is a concept that can be difficult to grasp as frequency itself is defined as cycles per unit time. A cycle of a process takes a finite length of time and thus it can be paradoxical to define such a thing as instantaneous frequency. However, frequency can be assumed to be a local or instantaneous feature of a signal if the signal in question is periodic, continuous, and harmonic. [33] Instantaneous frequency can be thought of as a time varying parameter of a signal which defines the spectral peak (constituent frequency with the highest magnitude) of the signal at that given time. This only holds true for a signal that has a single constituent frequency (monocomponent) or has a very narrow frequency range. [34] The concept of instantaneous frequency is meaningless for a multicomponent (made up of a broad spectrum of frequencies) signals. This is because at any given instant, the signal is composed of multiple frequency components.

In [35] Van Der Pol defines instantaneous frequency (IF) as the rate of change of phase, arriving at the equation,

$$\text{IF} = \frac{1}{2\pi}\frac{d\phi(t)}{dt} \tag{2.1}$$

J. Ville in his paper [36] published in 1948, expanded on the concept of analytical signals to define instantaneous frequency. An analytic signal of a real signal is constructed by summing up the real signal and its Hilbert transform in the time domain. This converts the real signal into a complex signal z(t), and J. Ville showed that rate of change of the argument of this complex signal gives the instantaneous frequency at a given time.

$$\text{IF} = \frac{1}{2\pi}\left(\frac{d}{dt}\, arg(z(t))\right) \tag{2.2}$$

In [37], the authors compare 3 different instantaneous frequency algorithms to estimate the instantaneous frequency from synthetic frequency modulated signals. They compare an algorithm based on the analytic signal with two other algorithms based on wavelet transform and generalized pencil of function (GPOF) method. They conclude that the GPOF method is the least sensitive to noise and that the wavelet transform method is the simplest to implement.

In some studies, analytical methods have been introduced to estimate the instantaneous frequency of a harmonic monocomponent signal. Adelson in [38] introduces a method in which the instantaneous frequency of a harmonic monocomponent signal is calculated using 3 data points. He proposes that such a signal can be modelled as,

$$y(t) = \text{A}\sin(\omega t + \phi) \tag{2.3}$$

With the 3 unknowns being, amplitude (A), frequency (ω) and initial phase (ϕ). It is therefore possible to find these unknowns if 3 data points are known by substituting and solving 3 linear equations. The frequency found using this method would be the instantaneous frequency associated with the 3 data points. Adelson further went on to present an averaging method to estimate the instantaneous frequency from a

noisy harmonic signal when more than 3 data points are available. His method utilizes a weighting function to estimate the average IF of a data window. For noisier signals, the data window must be increased. Adelson's method is only applicable to signals that are harmonic and have no bias. A bias adds another unknown term and thus 4 points are necessary to find them. This is usually not a problem in post processing as the bias can be removed by subtracting the mean value of the signal. However, for real time applications this is not possible. In [39], Vizireanu builds on Aldersons method by modifying the sinusoidal equation by adding a bias term. He then proposes a method where 4 data points are used to calculate the unknowns.

In the study presented in [40], Romulus et. al. assesses 3 popular methods of estimating IF on a frequency modulated signal covered with Gaussian noise. Analytical methods such as the one introduced by Adelson are extremely sensitive to noise as the method relies on the assumption that the data points belong to a perfect sinusoidal function. Romulus et. al. compares time-frequency IF estimation methods such as Short-Term Fast Fourier Transform (STFT), Winger-Ville transform and time domain IF estimation methods such as phase differentiation at estimating IF from noisy signals. They conclude that for low signal to noise (SNR) ratios (high noise level), IF estimates from time-frequency methods are superior.

Although instantaneous frequency is associated with monocomponent signals, studies such as [41], [42] have been done to estimate IF frequency of multicomponent signals with varying success. In these studies, the most prominent frequency component in the signal (peak with the highest magnitude in the spectrum) is found to be the instantaneous frequency. In [42], the authors conclude that calculating the IF from multicomponent signals is only possible when the frequency components are well separated in the time domain. In [41], the researchers present a method where the signal is represented in the time frequency domain (spectrogram) and for each time section, utilizes an algorithm to detect the most prominent frequency component and the trajectory of that frequency component. The algorithm then removes that frequency component from the spectrogram and repeats the process to identify the next most prominent frequency component. Therefore, this process is able to identify the instantaneous frequency components at a particular time section of the multicomponent signal.

Although an electrocardiogram signal is multicomponent and nonstationary (signal characteristics change with time), we can preprocess the EKG signal to convert it into a form that is close to a monocomponent and harmonic signal. As mentioned in [34], instantaneous frequency can be estimated fairly easily for a signal having a very narrow spectrum. In later chapters, we will assess the spectrum of the EKG signal and see how filtering methods can be used to convert it to a form from which the instantaneous heart rate can be calculated.

2.5 Heart Rate Variability

Heart rate is dynamic: fluctuations in the heart rate are caused by changes in the balance between the sympathetic and parasympathetic nervous systems. [43] Heart rate variability quantifies the variations in the period between successive heartbeats of a sequence of heat beats. Therefore, heart rate variability (HRV) is an indicator of the autonomic nervous system's activity and is an increasingly popular metric for assessing different health conditions. The technique is also favorable due to its non-invasive nature. HRV can be evaluated in several methods: time domain, frequency domain, and through nonlinear measurements. [44] Further, HRV can be measured at different intervals and yield varied results that are not necessarily interchangeable. The most popular intervals are 24-hour, short-term (~5 minutes), and ultra-short-term (less than 5 minutes). The reason for varied HRV results at different intervals is the effects of low-frequency fluctuations induced by processes such as the circadian rhythm in longer measured intervals. HRV is more commonly evaluated using electrocardiogram data. However, in recent years with the rising popularity of wearables, studies have been conducted on assessing the accuracy of HRV measurements derived from data retrieved from other techniques, such as Photoplethysmography. [24]

2.4.1 Time domain measurements

Time domain measurements are based on the calculated period between adjacent peaks (R waves). [45] This interval is termed as the RR interval. However, R waves can also occur due to arrhythmic events and can distort heart rate measurements. The normal-normal (NN) intervals are calculated after filtering

electrocardiogram data to remove these abnormal peaks that do not originate from the right atrium's sinoatrial node. [44] Many statistical parameters are calculated based on the NN interval. The most common time domain HRV parameter is the standard deviation of NN intervals (SDNN) calculated for the entire duration of the EKG. The SDNN is more accurate when calculated for extended periods, such as 24 hours. Careful processing of ECG data is vital as SDNN is sensitive to deviations caused by abnormalities such as ectopic beats and missed beats. [45] It has been shown that higher SDNN values indicate lower risk of mortality. In one study performed on patients who've had heart attacks, survival rate in the 31 month follow up period was 5.3 times higher for individuals having SDNN values over 100 ms than those who had a SDNN lower than 50 ms. [46]

Standard deviation of averaged NN intervals (SDANN) is another time domain HRV metric. Here the 24-hour recording is divided into 5-minute segments before calculating the average NN interval of each segment. The standard deviation of the averaged NN interval values is then computed. Average of the standard deviations of NN intervals (SDNNI or ASDNN) is the average of the standard deviations of the NN intervals calculated during 5-minute segments. SDNNI has been shown to correlate with autonomic activity and its effect on HRV. Another popular metric to quantify HRV is the (Root Mean Square of Successive Differences) RMSSD value. As the name suggests, this is calculated by taking the root mean square value of the time differences in successive NN intervals. The time difference is represented in milliseconds. RMSSD reflects the effects of the vagal verves on the heart rate variability. [47] Researchers have also found correlation between RMSSD and power contained within the high frequency band of the spectrum of IHR signals. NN50 quantifies the total number of times the difference between successive NN intervals is greater than 50 ms. A closely related parameter – pNN50, calculates the percentage of NN50 compared to all measured NN intervals.

Most of these time domain HRV metrics rely on the measurement of NN/RR intervals and thus correct detection of R peaks is vital. Therefore, their accuracy is heavily reliant on the quality of the EKG signal (less artifacts, less noise) and the robustness of the peak detection algorithm used to detect the R peaks.

However, from these HRV metrics SDNN and ASDNN can be estimated without relying on RR intervals. This is because these metrics essentially calculate the standard deviation of the IHR signal. The conventional way to compute the IHR signal is by using RR intervals (RRSIG). However, if we compute an IHR signal using a different method, the standard deviation of that signal should closely match that of the RRSIG. Furthermore, we will see in the next section how SDNN is closely related to some frequency domain HRV metrics as well.

2.4.2 Frequency domain measurements

Heart rate variability can also be evaluated by assessing the RR interval data in the frequency domain. The RR interval data can be calculated in a couple of different ways. It can be presented as a time series of RR interval times or as a series of instantaneous heart rates. In this study we will only consider RR data presented as a time series of instantaneous heart rates. Instantaneous heart rate can be calculated by simply taking the reciprocal of the RR interval and multiplying it by 60 to present it in beats per minute. We will call this signal the RRSIG. The RRSIG is a signal sampled at a variable sampling rate. This is because each instantaneous heart rate (IHR) is calculated using the RR interval between neighboring R peaks and the time index of the IHR is equal to the summation of previous time stamps and the current RR interval. Algorithms such as the Fast Fourier Transform (FFT) are commonly used to convert time domain signals such as RRSIG to the frequency domain.[43] However, it is essential to resample the RRSIG at a constant sampling rate before the Fast Fourier Transform algorithm is applied to compute the Power Spectral Density. This is because the FFT algorithm can only be implemented on signals sampled at a fixed sampling rate. Some studies such as [6] use the least square spectral analysis to perform frequency domain analysis of RR data. The advantage of the least square spectral analysis is that this method allows spectral analysis of signals sampled at variable sampling rates. Another popular method used in frequency domain analysis of HRV is the autoregressive model. The autoregressive model is a technique used to describe time varying processes and assumes that future values of a time series linearly depend on previous values.[48] It's a parameter-based model where certain techniques are used to determine the best parameter values to produce

the optimum model. This method is sometimes preferred over the FFT due to its ability to obtain higher frequency resolution for shorter data sets. It also allows the evaluation of the power of specific frequency components. The resolution of the FFT on the other hand depends on the size of the data set. Furthermore, the power of a certain frequency component cannot be estimated if it is not a multiple of f_s/N, where f_s is the sampling frequency and N is the length of the dataset. Due to the discrete nature of the frequencies, power from neighboring frequencies leak into the frequency bins defined by the FFT algorithm. This is termed as leakage. However, the FFT has a low computational cost compared to the autoregressive model. Further, it can be somewhat difficult to estimate the optimum autoregressive model. [49] In this study we will focus our attention on the FFT algorithm to estimate the power spectral density (PSD) of the IHR signals (RRSIG and the instantaneous frequency-based heart rate signal introduced later in the study). A more in-depth discussion of the Fourier transform can be found in chapter 3. In frequency domain analysis, HRV is parameterized by calculating the power contained within certain frequency bands in the IHR signal. Researchers have identified 4 frequency bands that constituent frequencies in the IHR signal fall into. These are the ultra-low frequency (≤0.003 Hz), very-low-frequency (0.003 – 0.04 Hz), low frequency (0.04 – 0.15 Hz), and high frequency (0.15 – 0.4 Hz). [44] Studies have found correlations between these frequency bands and certain bodily functions. The ultra-low frequency (ULF) band is mainly influenced by the circadian rhythm. Some researchers think functions such as temperature regulation and metabolism may also have an influence on the ULF band. It has been shown that the very low frequency (VLF) band indicates sympatho-vagal balance and is a strong indicator of mortality. Low VLF powers are associated with arrhythmic death, PTSD and low levels of testosterone.[44] The low-frequency (LF) band, sometimes termed as the baroreceptor range reflects baroreceptor activity.[44] Baroreceptors relay blood pressure information to the autonomic nerve system which then regulates blood pressure to maintain it at a normal range.[50] It has also been shown that the power of the LF range is affected by vagal activity at low respiration rates: usually having a period greater than 7s. [48] The high frequency (HF) band indicates vagal activity [51] and is significantly affected by the respiratory rate. The power within the HF band reflects the

heart rate variations induced by the respiratory cycle. Because of this, this range is sometimes called the respiratory band.[44] Since the power contained within the frequency bands vary among individuals and even different data sets obtained from the same individual, it is common to divide the power of frequency bands by the total power to normalize it. [48] Similar to time domain measurements, care must be taken when comparing parameters derived from different data vector lengths. Depending on the measurement length, the frequency distribution of the signal changes. As the measurement length is increased the power contained in the ultra-low frequency and very low frequency bands also increase. This is because effects of ultra-low frequency components manifest in longer measurements such as 24-hour recordings. In short-time recordings (5 minutes) effects of ULF and LF are negligible or are present in the form of linear trends, that can be removed during pre-processing. [48]

Some studies have further shown a correlation between some time domain measurements and spectral data. For instance, SDNN, which is the standard deviation of all NN intervals measured during the measurement period, is highly correlated with the total power of the frequency distribution. This is due to the total power of the spectrum being equivalent to the variance, which is the square of the standard deviation calculated in SDNN. [45]

Chapter 3 – Methods

3.1 Overview

This chapter discusses the theoretical background of the techniques and methods used to calculate the heart rate and heart rate variability metrics in the frequency domain. Section 3.2 of this chapter will present an introduction to the data set being used in this study. In section 3.3, a brief introduction to the IHR signal constructed using RR intervals is presented. Section 3.4 will discuss the initial EKG signal processing stage which involves the use of digital filters to extract frequency components near the mean heart rate. Section 3.5 will present the instantaneous heart rate algorithm. This section will discuss the instantaneous frequency algorithm. A supporting algorithm used to clean the instantaneous frequency signal is presented in Section 3.6. In section 3.7, the instantaneous heart rate algorithm will be applied to the filtered EKG signal to calculate the instantaneous heart rate (IHR). The final section of the chapter is dedicated to a discussion on frequency domain HRV metrics and how they are calculated using the IHR signals.

3.2 Electrocardiogram (EKG) signal characteristics.

The electrocardiogram data used in this study is from the data set published under Kansas State University IRB protocol #9386, available at [52]. The EKG signals have been acquired using a GE Datex CardioCap 5 patient monitor. The EKG signals in this dataset have already been filtered using a bandpass filter with a passband between 0.5 Hz to 40 Hz. All EKG signals have been sampled at 1 kHz. The dataset contains EKG signals collected from 40 individuals at rest in the supine position. The database also provides information about the participants such as gender, age, height, weight and known heart conditions.

3.3 Calculating Instantaneous Heart Rate using RR intervals.

In this section we will briefly discuss how the heart rate can be calculated using RR intervals. It is important to understand how this is done as this is the most common technique used in literature to calculate heart rate and subsequently the IHR signal. As previously discussed in Chapter 2, the EKG signal records the electric activity of the heart. R peaks are the most noticeable peaks in the EKG signal. Since an R peak occurs during each cardiac cycle, the time between two neighboring R peaks gives the cycle time. By taking the reciprocal of this cycle time we can estimate the heart rate at that given moment. It is therefore essential to correctly detect R peaks. Numerous studies have introduced robust methods to identify R peaks and record their temporal location. However, in this study, we rely on a simple thresholding method to detect R peaks. We only need to detect R peaks to generate the instantaneous heart rate signal using RR intervals. This signal, which is termed RRSIG will be compared with the IHR signal generated using instantaneous

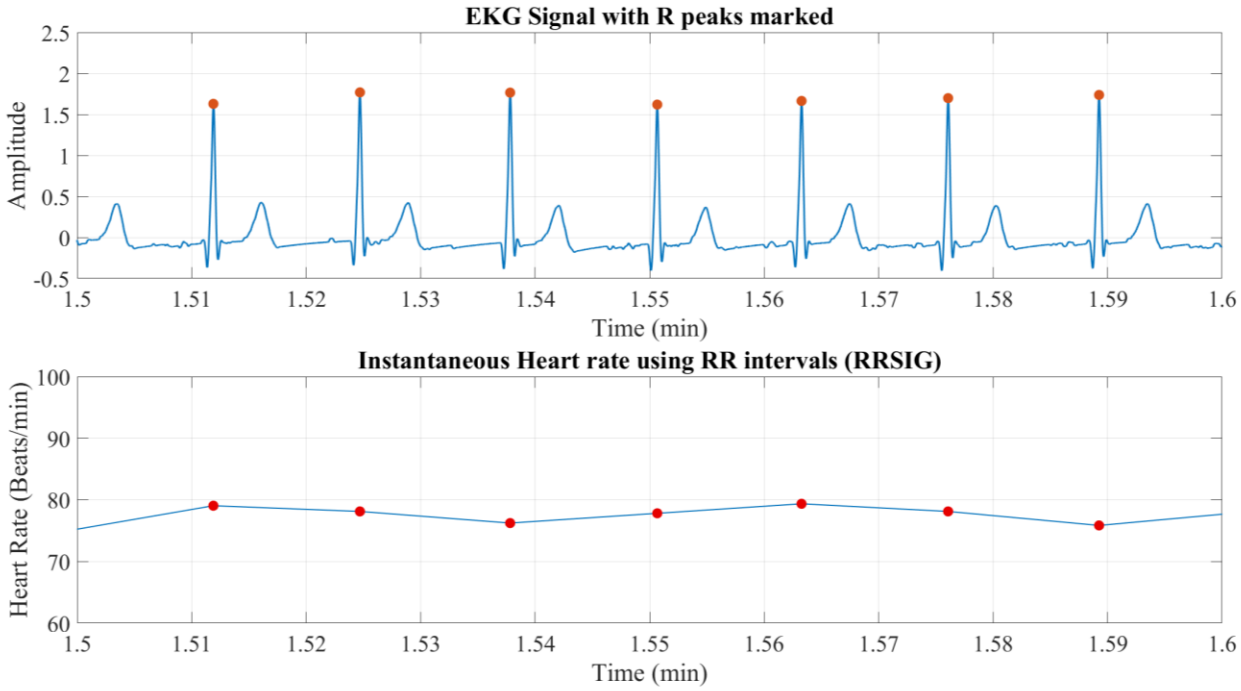

Figure 3.1: EKG signal at the top and the heart rate calculated using RR intervals at the bottom. The heart rate signal is termed RRSIG in this study. The red markers in RRSIG corresponds to the heart rate calculated using the backward difference of time stamps of neighboring R peaks. As such the IHR at a particular time stamp could be thought of as the average heart rate between the current time stamp and the previous time stamp.

frequency method. Using the findpeaks function in MATLAB, the temporal locations of the R peaks were found. RR intervals were then calculated by taking the backward difference between the time stamps of neighboring R peaks. The heart rate was then determined by taking the reciprocal of the intervals and multiplying it by 60. The resulting data vector was termed as RRSIG and a portion of it is shown in Figure 3.1. Note that a data point in the RRSIG is produced at irregular intervals when R peaks occur in the EKG signal. Therefore, RRSIG can be considered as a signal that is sampled at a varying sampling rate. This property of the RRSIG is unfavorable for frequency domain HRV analysis as we will discuss later.

3.4 Preprocessing the EKG signal.

The main objective of the preprocessing stage is to prepare the EKG signal before being fed into the instantaneous heart rate algorithm which will be introduced later in this chapter. As mentioned in section 3.2, the electrocardiogram signals used in this study have already been filtered using a bandpass filter. This was done to remove as much noise as possible from the EKG signal and to remove any low frequency baseline drifts. Preprocessing steps mentioned hereupon in this section are additional processes done on these filtered signals. Our goal is to estimate the instantaneous heart rate and observe the heart rate variability from an EKG signal. Previous chapters discussed what is meant by the heart rate: the rate at which the heart undergoes cardiac cycles. The EKG signal is a non-stationary, multi-component signal. This means that the EKG signal contains multiple constituent frequencies, and the frequency content changes with time. [53] We can visualize this with the use of a spectrogram of the EKG signal. A spectrogram is a powerful digital signal processing tool that allows the analysis of a signal in the time-frequency domain. It shows how a signal's frequency content changes with time. This is especially useful for analyzing nonstationary, multicomponent signals as their constituent frequency components change with time. To understand the spectrogram, one must first understand the Discrete Fourier Transform (DFT).

3.4.1 Discrete Fourier Transform, Power Spectral Density, and the Spectrogram.

In this study we will extensively use the Fast Fourier Transform (FFT) to convert signals from the time domain to the frequency domain. The FFT is an algorithm that calculates the Discrete Fourier Transform (DFT) more efficiently. Before we discuss the DFT, let's understand what is meant by the Fourier transform and the Discrete – Time Fourier Transform (DTFT). Any periodic signal of period T can be represented as a summation of an infinite series of weighted sinusoidal waveforms whose frequencies range from a fundamental frequency (derived from the period T) and its harmonics.[54] This representation is called the Fourier series and can be expressed as follows,

$$\mathrm{x(t)} = \sum_{\mathrm{n}=-\infty}^{\infty} \mathrm{C_n e^{jn\omega_0 t}} \tag{3.1}$$

Where C_n is the weight/coefficient of a particular sinusoid, ω_0 is the fundamental frequency and j is the imaginary quantity. For n < 0, the series contain negative frequencies and for n>0 the frequencies are positive. When the negative and positive waveforms of a given harmonic are added together it results in a real signal having an amplitude twice as much as the two harmonic waveforms. Therefore, when the magnitude of a certain frequency component is calculated, the value must be doubled. We cannot discretize an aperiodic signal into sinusoids of a fundamental frequency and its harmonics as we did previously. However, using complex exponentials we can expand the aperiodic signal. This process is called the Fourier transform and is computed as follows,

$$\mathrm{X(\omega)} = \int_{-\infty}^{\infty} x(t) e^{-j\omega t} dt \tag{3.2}$$

As you can see $\mathrm{X(\omega)}$ is continuous unlike the discrete sinusoidal components that constructed the periodic signal discussed before. The original signal x(t) can then be computed by the inverse Fourier transform which takes the form,

$$\mathrm{x(t)} = \int_{-\infty}^{\infty} X(\omega) e^{j\omega t} dt \tag{3.3}$$

So far, we have considered continuous signals. In digital signal processing we deal with discrete signals and thus we must expand the concepts we discussed into the digital domain. The Fourier transform equivalent in digital signal processing is the discrete-time Fourier transform (DTFT). The DTFT converts a periodic time domain sequence $x[n]$, (where n corresponds to positive integers) into the frequency domain continuous function, $X(\omega)$ (where ω is frequency in rad/s). [55] The time sequence $x[n]$ represents a continuous function that has been sampled at a constant sampling rate. The relationship can be expressed as follows,

$$X(\omega) = \sum_{n=-\infty}^{\infty} x[n]e^{-jn\omega} \tag{3.4}$$

Therefore, the DTFT converts a sequence of data from the time domain to a complex and continuous function in the frequency domain. The DTFT cannot be calculated using a digital computer for two reasons. Firstly, $X(\omega)$ is a continuous function and digital systems cannot produce such functions. Secondly, the time sequence ranges from -∞ to +∞ but digital systems can only work with finite data lengths. However, it is possible to approximate $X(\omega)$ as a set of finite discrete frequencies given the spacing between the frequency samples is sufficient. $X(\omega)$ is a periodic function with a period of 2π. Therefore, for a time sequence of N length, $X(\omega)$ can be discretized into N number of frequency samples/bins that are integer multiples of $\frac{2\pi}{N}$. We can represent the k^{th} frequency component of this approximation as,

$$X[k] = \sum_{n=0}^{N-1} x[n]e^{-\frac{j2\pi kn}{N}} \tag{3.5}$$

This is termed as the Discrete Fourier Transform (DFT). One can question why $X(\omega)$ is discretized into N number of frequency samples. Wouldn't choosing a higher number of discretized frequency bins provide higher resolution? This is not the case as the information contained within the signal is dependent on its length. Increasing the number of frequency bins is equivalent to zero padding the signal in the time domain: adding zeros to the end of the signal. [56] Thus, no additional information is present in the signal. Increasing the number of bins essentially interpolates the data in the frequency domain and does not provide any

additional information. However, zero padding can be useful when trying to reduce spectral leakage. [57] Spectral leakage happens when the energy contained within one frequency component "leaks" to a neighboring frequency component. Since we defined frequency bins as integer multiples of $\frac{2\pi}{N}$, certain constituent frequencies might not exactly match a bin. In such a situation, we can zero pad the signal so that frequency components will match integer multiples of $\frac{2\pi}{N}$. Furthermore, when visualizing signals in the time-frequency domain, large number of frequency bins will give a smoother appearance to the distribution (due to interpolation).

The time sequence $x[n]$ can be recalculated through the inverse DFT from X[k] as follows,

$$x[n] = \frac{1}{N}\sum_{k=0}^{N-1} X[k] e^{\frac{j2\pi kn}{N}} \tag{3.6}$$

X[k] is a complex number and provides information of the magnitude and the phase of a constituent frequency component of the time series data. To find the amplitude of a constituent frequency component X[k], one can simply take the absolute value of the complex quantity X[k], double it (to account for the contribution by both negative and positive frequencies) and divide by N. Division by N is necessary to get the average value from the summation expressed in equation 3.5. For a periodic continuous signal, the power contained within it is infinite as it is infinitely long. However, if we consider a segment of the signal, the energy/power contained within it is finite. We can isolate a segment of the signal by applying a window to the signal (we will discuss windowing functions later in this section). Most often, we use a rectangular window. We know that the average power of a sinusoid is equal to its squared amplitude divided by 2. Therefore, for a discrete signal the one-sided (combined effect of both negative and positive frequencies represented together) power contained within the frequency component X[k] is expressed as,

$$P[k] = 2\left(\frac{|X[k]|}{N}\right)^2 \tag{3.7}$$

If we plot the power calculated in the above method against frequency components, it is called the power spectrum. The expressions we derived for amplitude and power only hold true if certain conditions are met.[58] First the signal being assessed should be stationary which means that signal characteristics do not change with time. We also assume that a rectangular windowing function is applied to it before the DFT is computed. Finally, we assume that the signal is comprised of discrete frequency components represented by X[k]. The final assumption is most often not the case for real world signals that are created by a broadband of frequencies and have continuous spectra. For such signals it is more appropriate to present power as a density. This is because closely placed frequency components around a discrete frequency component will all contribute power to this discrete spectral component giving an erroneous spectrum. This kind of spectral "leakage" also occurs when a signal is segmented using a window. To compensate for this, we calculate the power spectral density (PSD). To compute the PSD, we must first calculate the equivalent noise bandwidth (ENBW) for the window being used. The ENBW accounts for the alterations made by the window on the spectrum and calculates a new bandwidth that we can use to normalize the spectral power to calculate the spectral density.[59] The ENBW is calculated as follows[60],

$$\text{ENBW} = f_s \frac{\sum_{n=1}^{N-1} w_n^2}{(\sum_{n=1}^{N-1} w_n)^2} \tag{3.8}$$

Where w_n is the nth data point of the window and f_s is the sampling rate. Now we can calculate the one-sided power spectral density (PSD) as follows,

$$\mathbf{PSD}[\boldsymbol{k}] = \frac{\boldsymbol{P}[\boldsymbol{k}]}{\boldsymbol{ENBW}} \tag{3.9}$$

When a rectangular window is used, we can substitute from equation 3.7 to 3.9,

$$\text{PSD}[k] = \frac{2|X[k]|^2}{N^2 ENBW} \tag{3.10}$$

Further, for a rectangular window with unity gain, the ENBW can be computed as follows:

$$\text{ENBW} = f_s \frac{N}{N^2} \tag{3.11}$$

$$\text{ENBW} = \frac{f_s}{N} \tag{3.12}$$

Therefore, the power spectral density can be expressed as,

$$\text{PSD}[k] = \frac{2|X[k]|^2}{N f_s} \tag{3.13}$$

When talking about ENBW it is important to have some understanding of what a windowing function is. A windowing function essentially acts as a window, segmenting a signal temporally for analysis. Signals can be infinitely long or too long for storage and/or fast processing. In such situations, a window is used to isolate a portion of the signal. A window does this by driving all data beyond the boundaries of the window to zero and extracting the information in the signal within the window. There are many types of windows, each with their advantages and disadvantages. The simplest window is the rectangular window that drives all data points beyond the window to zero and setting a unity gain to all data points within the window. Sometimes segmenting a signal with a rectangular window can create sharp transitions at the edges of the segmented signal. This creates broadband transient events that lead to spectral leakage. [61] To prevent this some windows are designed to create a smooth transition from zero at the window boundaries to the actual amplitudes of the signal at the center of the window. An example for such a window is the Hann (Hanning) window shown in Figure 3.2. Observe how in the time domain the Hann window provides a smooth transition at the boundaries of the signal segment, eliminating any sharp transitions. However, when looking at the frequency domain representation of the window, we can see that its spectrum is not just a single impulse at the center frequency. Rather it contains side lobes of delta frequencies. A window is applied to a signal by multiplying the signal in the time domain with the windowing function. This is equivalent to the periodic convolution of the spectra of the signal and the window in the frequency domain. Therefore, the side lobes present in the spectrum of the window lead to power from neighboring frequency components in the signal to leak into the frequency component being assessed in the signal. This is why applying any kind of windowing function leads to spectral leakage.

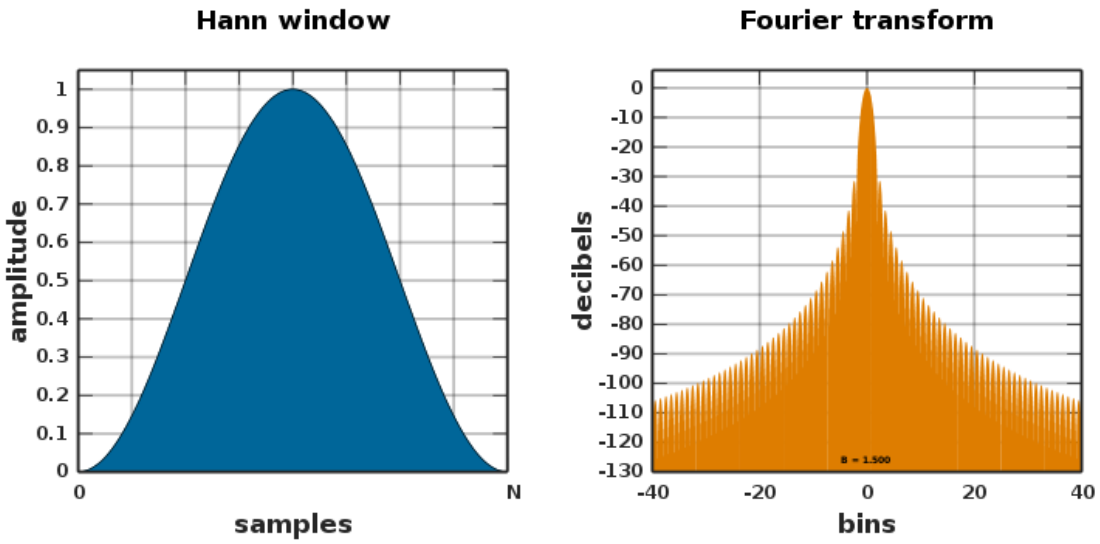

Figure 3.2: Hann window represented in the time domain (left) and the frequency domain (right).

Now let's focus our attention on the spectrogram. Consider a discrete signal made up of N points. A windowing function of length M is slid across this signal while maintaining an interval of R data points between neighboring segments. Therefore, there is an overlap (L) of M-R data points between each segment (see Figure 3.3). When a signal is multiplied with a windowing function, all values of the signal outside the windowing function's interval are driven to zero. This allows the original signal to be segmented and analyzed. After the signal is segmented, the DFT is calculated for each segment of the signal. The resulting complex values of each segment give information of the magnitudes and phases of the constituent frequencies of that particular segment of the signal. Now, if we compute the power spectrum of each signal segment and line them up sequentially, we create a spectrogram. The spectrogram is 3 dimensional, as it provides information related to time, frequency and spectral magnitude. When represented in 2 dimensions,

the magnitude is represented using a colormap. The spectrogram therefore gives us information on how the spectrum of a signal changes with time.

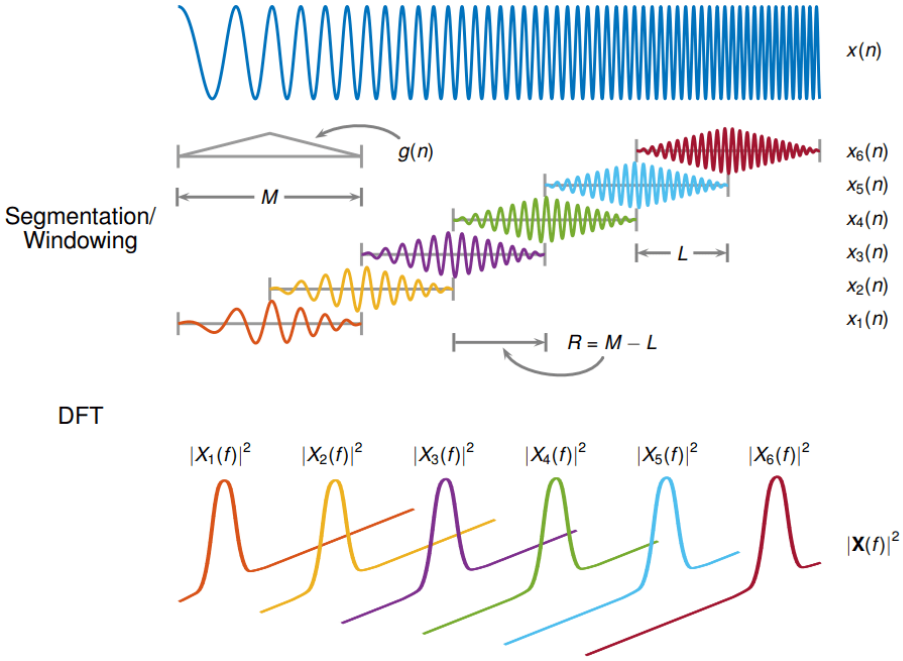

Figure 3.3: Procedure of calculating the spectrogram. The signal is divided into segments of M length and the DFT is calculated for each segment. The magnitudes of the constituent frequencies are calculated by taking the squared value of the magnitude of the complex numbers resulting from the DFT.

Source: Adapted from [62]

3.4.2 Spectrogram of the EKG signal.

To observe an EKG signal in the time-frequency domain, we used one of the EKG signals from the database that does not have any anomalies. The mean heart rate of the EKG signal considered is 78.89 bpm or 1.315 Hz. A portion of the EKG signal can be seen in Figure 3.4 and the associated spectrogram of the EKG signal is shown in Figure 3.5. To compute the spectrogram shown in Figure 3.3, we used a Hamming window of 2^{13} samples in length with an 87.5% overlap. The reason for choosing such a high overlap was to essentially "stretch" the time axis and improve time domain resolution.[63] The spectrogram was also evaluated with a DFT length of 2^{17}. This means that each segment is evaluated using 2^{17} points in the frequency domain.

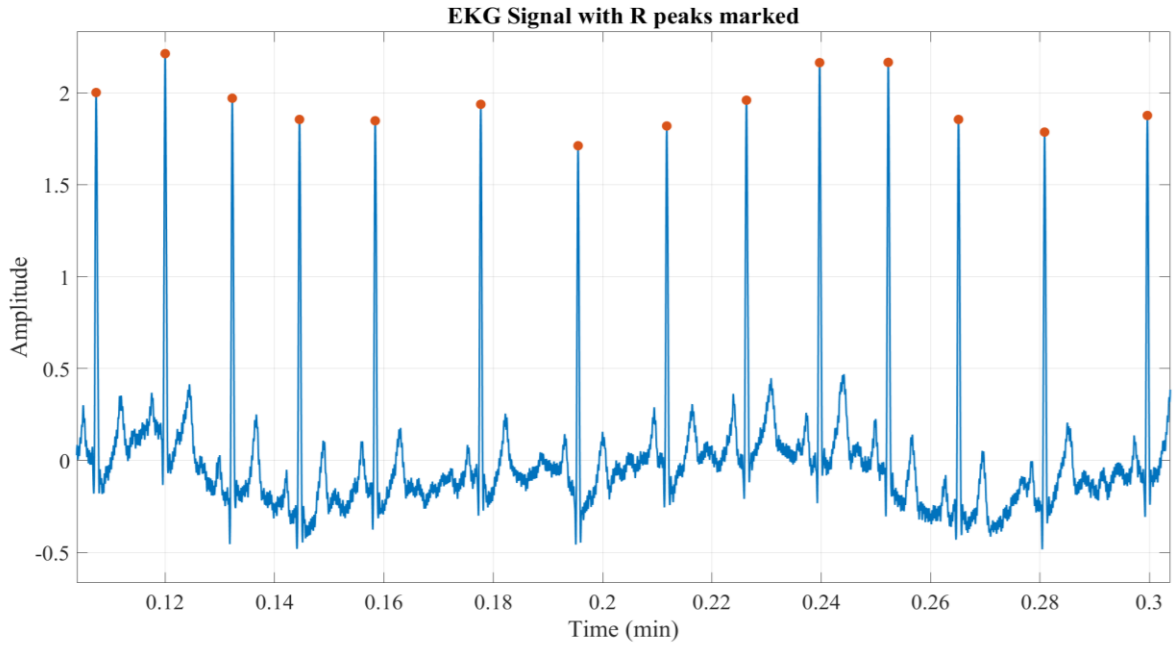

Figure 3.4: A portion of the EKG signal before being processed.

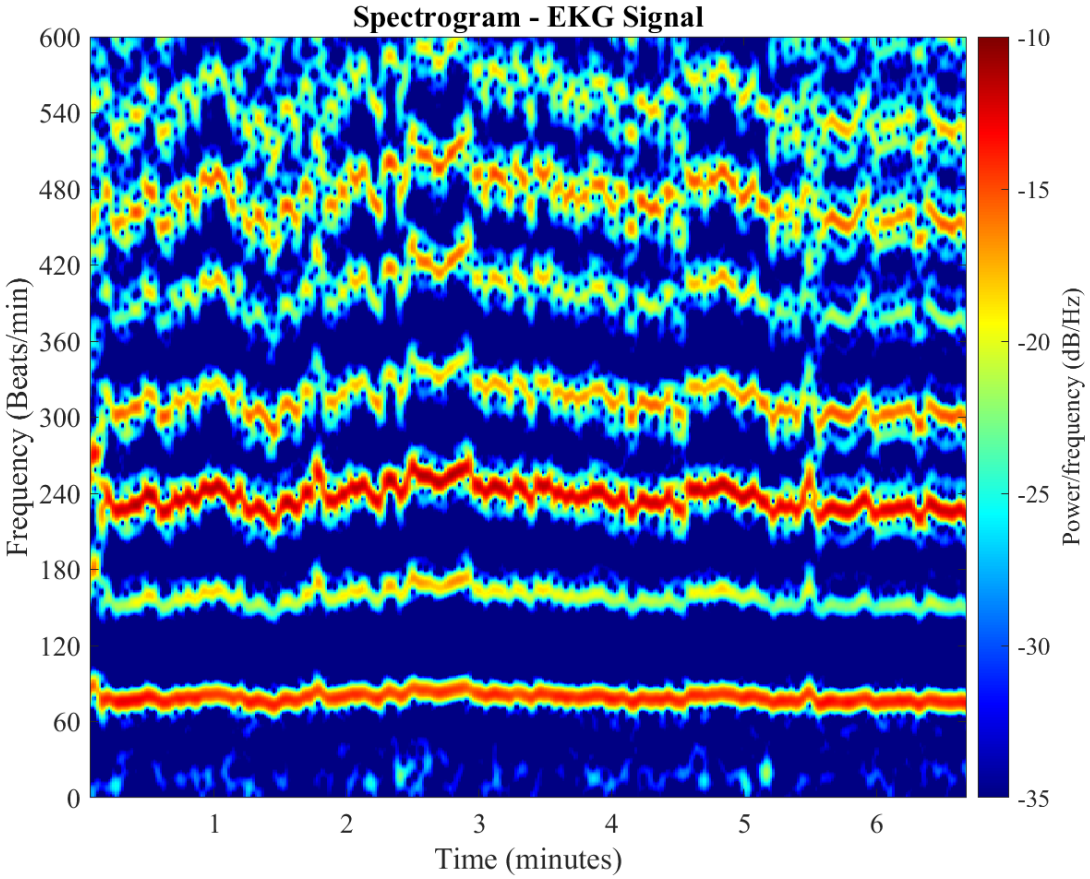

Figure 3.5: Spectrogram of EKG signal within 0 Hz to 10 Hz frequency range (0 to 600 beats/min). The colormap on the right indicates the power contained within the frequencies. Higher powers are represented by warmer shades. Power is represented as a density.

The power contained within a frequency component is represented as an intensity in the spectrogram according to the colormap on the right-hand side of figure 3.5. Higher powers are represented by warmer shades and lower powers by cooler shades. As you can see, the EKG signal is made up of multiple constituent frequencies. Although the spectrogram can be used to visualize temporal frequency changes in the signal, it does not provide good resolution in both time and frequency axes. There is always a trade-off between the achievable resolution in the time domain versus the frequency domain in a spectrogram. On the contrary, the method introduced in this study to estimate the IHR is able to provide a time domain resolution equivalent to the sampling period of the EKG signal. Focusing our attention back on the spectrogram, we see that most of the constituent frequencies of the EKG signal are in the 0 to 20 Hz (0 to 1200 beats/min) range. The bands in the spectrogram are not perfectly horizontal, as the constituent frequencies of the EKG signal change with time. For this EKG signal, we can observe that the bands of the spectrogram occur at approximate multiples of the lowest frequency band, which is at around 79 beats/min. This frequency band corresponds to the instantaneous heart rate.

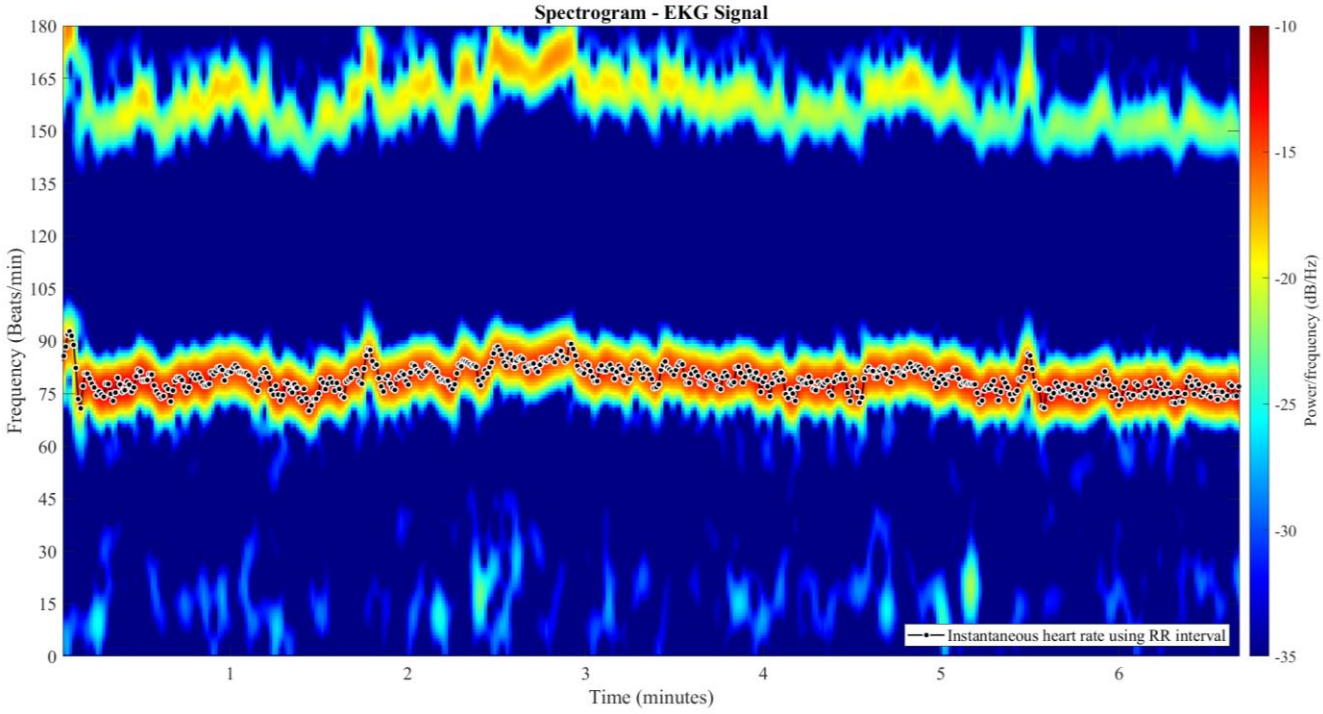

Figure 3.6: Instantaneous heart rate calculated using RR intervals (RRSIG) is plotted on top of the spectrogram. Observe how RRSIG land on the IHR band.

This can be shown by plotting RRSIG on top of the spectrogram as seen in figure 3.6. Here, the instantaneous heart rate was calculated for each heartbeat of the EKG signal using the RR interval between neighboring R peaks (RRSIG) and plotted on top of the spectrogram as black dots. We can see that they land on the lowest frequency band. Let's call this frequency band the instantaneous heart rate band (IHR band). Therefore, we only need the IHR band to assess the variability of the heart rate. We can filter the EKG signal using a bandpass filter to extract the IHR band. Since the EKG signal is non-stationary, the instantaneous heart rate may change with time. To track this instantaneous heart rate, we must first design a bandpass filter that is able to filter out all other frequencies except for frequencies near the instantaneous heart rate. Since the heart rate is variable, the center frequency of the bandpass filter must be equivalent/close to the instantaneous heart rate of the signal. Therefore, it is essential that the filter coefficients are updated based on the variable heart rate. Such a filter is called an adaptive filter. Designing an adaptive filter is out of the scope of this study. For the purpose of filtering the EKG signal in this study, we have used a bandpass filter with a center frequency equivalent to the mean heart rate of the EKG signal being assessed. Since the EKG signal is post-processed, we can estimate the mean heart rate by taking the average of RRSIG. A digital infinite impulse response, 4^{th} order Butterworth bandpass filter with a center frequency equivalent to the mean heart rate was designed.

3.4.3 Bandpass filter Design

A bandpass filter, as the name suggests, passes through frequencies within a specified range (termed as the passband) and attenuates all other frequency components of the signal. A bandpass filter can be described by the center frequency (f_0), bandwidth ($f_2 - f_1$), gain in the passband, and filter order. The transfer function of a digital filter can be derived from the transfer function of an analog filter with the use of the Bilinear transform. This transforms a system from continuous time to discrete time. The Bilinear transform is given by the equation,

$$s = \frac{T}{2}\frac{z-1}{z+1} \tag{3.14}$$

Where T is the sampling period.

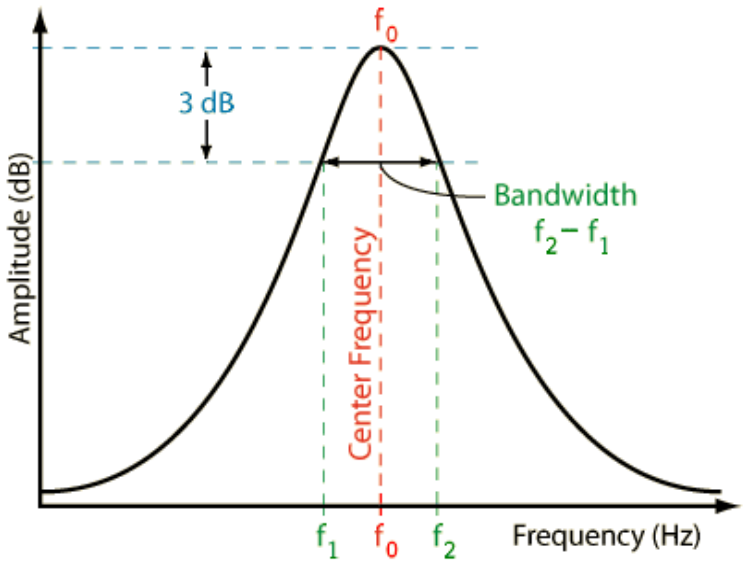

Figure 3.7: Frequency response of a bandpass filter.

This converts the system from the s-plane to the z-plane. We do not need to dive deep into the theory of converting a system from continuous to discrete time for the purpose of designing the bandpass filter. However, for lower-order filters, it is usually easier to first derive the transfer function in continuous time (s-plane) based on filter characteristics and then transform the system to discrete time.

Since we calculated the mean heart rate using the RR intervals, the center frequency of the bandpass filter will be as follows. [64]

$$f_0 = f_{mean\_HR} \tag{3.15}$$

Where, f_0 is the center frequency of the bandpass filter and f_{mean_HR} is the mean heart rate in Hz. The bandwidth of the filter is predefined according to the expected heart rate variability. In this study, we are focusing on resting heart rate. For a person at rest, typically the heart rate varies around the mean heart rate by about 10 beats per minute. [65] Therefore, the bandpass filter was designed to have a pass band with a lower cutoff frequency (f_1), 15 beats/min lower than the mean heart rate.

$$f_1 = f_{mean\_HR} - \frac{15}{60} \tag{3.16}$$

The center frequency of a bandpass filter is defined as the logarithmic mean of the lower and upper cutoff frequencies. Therefore, the center frequency has the following relationship with the cut-off frequencies.

$$f_{mean\_HR} = \sqrt{f_1 f_2} \tag{3.17}$$

Where f_2 is the upper cut-off frequency. Then the upper cut-off frequency can be found as follows,

$$f_2 = \frac{f^2_{mean_{HR}}}{f_1} \tag{3.18}$$

All frequencies are in Hz.

A 4th order digital Butterworth bandpass filter was designed in MATLAB. As mentioned before, further work can be done to create an adaptive bandpass filter to better filter the incoming EKG signal. Such a filter will be able to adapt based on the mean heart rate of the EKG signal. The frequency response of the bandpass filter is as follows,

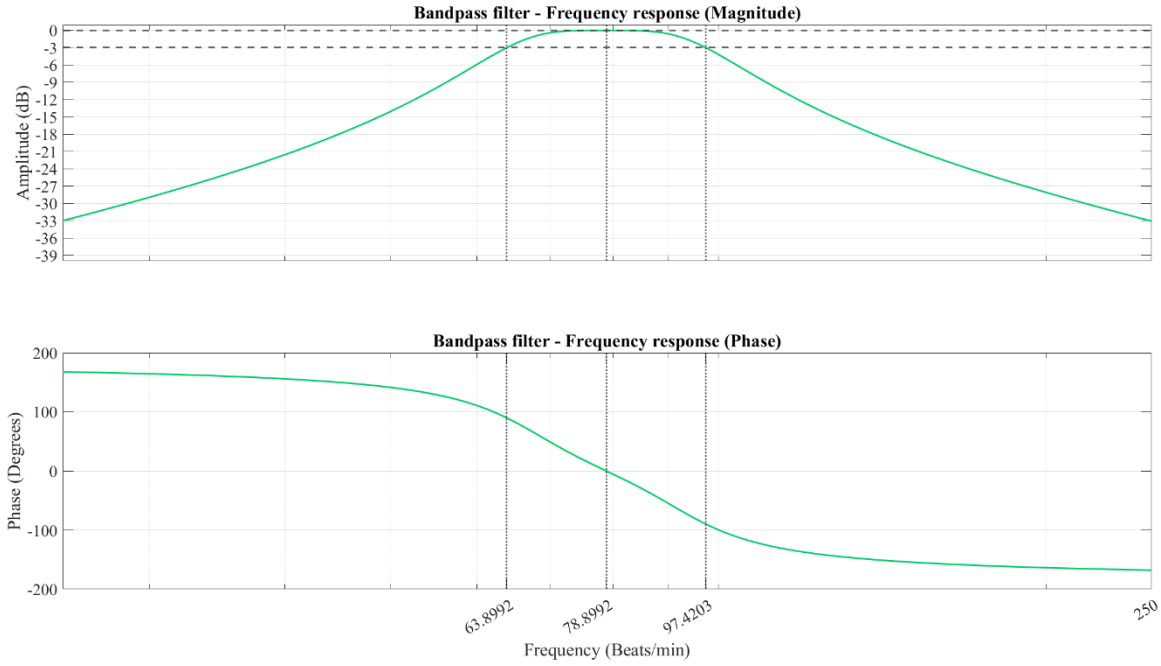

Figure 3.8: Frequency response of Bandpass filter designed for the EKG signal being assessed. For ease of interpretation, the frequencies are presented in beats/min. The center frequency (1.315 Hz) is 78.8992 beats/min. The lower and upper cut-off frequencies are also marked as the dotted lines. Note that for a different EKG signal, the center frequency and the cutoff frequencies will be change according to the mean heart rate.

Let's now observe the spectrogram of the filtered signal. The bandpass filter was able to remove most of the high-frequency components from the EKG signal. However, the filtered signal still contains faint harmonics of the IHR band. One can suggest increasing the filter order of the bandpass filter to achieve a higher roll off rate to attenuate high frequency components. However, doing so makes the bandpass filter unstable due to numerical errors. Therefore, a 4^{th} order lowpass filter was cascaded with the bandpass filter to further attenuate the high frequency components.

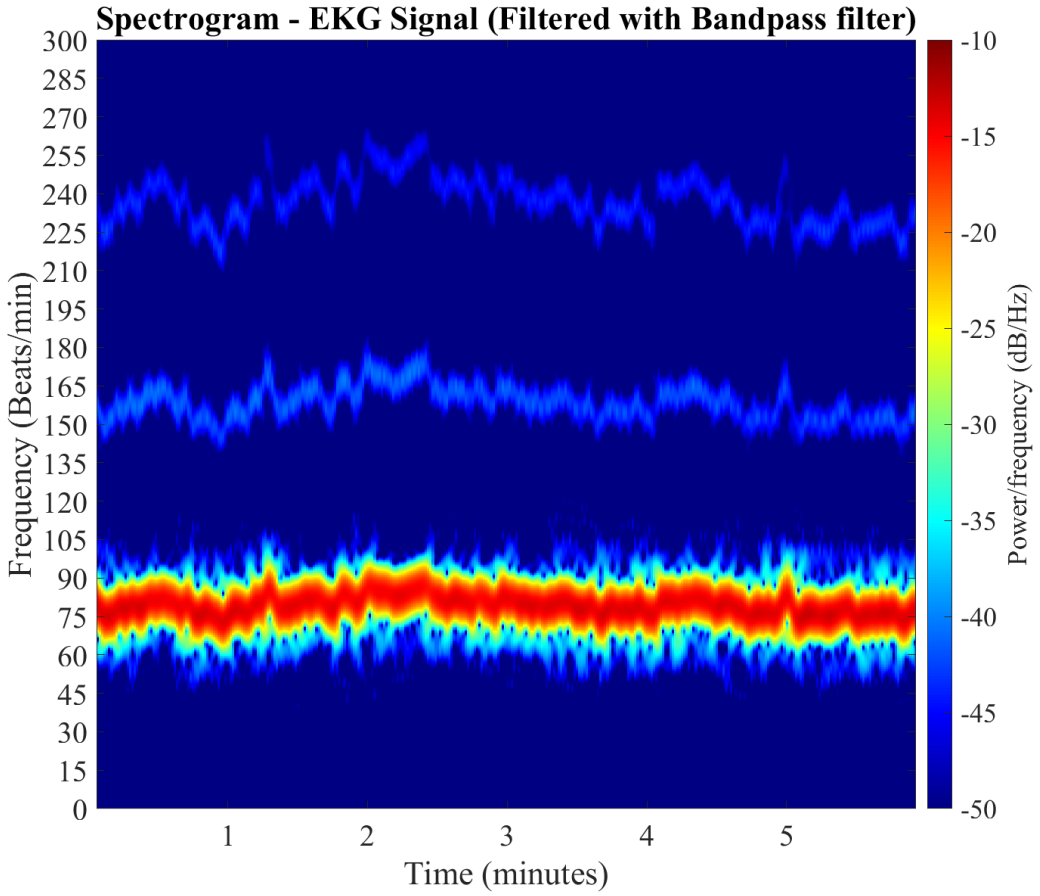

Figure 3.9: Spectrogram of EKG after filtering with Bandpass filter. Note how most of the high frequency spectral components were removed by the bandpass filter. However, observe the faint frequency band present at harmonics of the IHR.

3.4.4 Low-pass filter Design

A low-pass Butterworth filter was designed using MATLAB to remove high frequency components which remain in the EKG signal after the initial filtering performed using the bandpass filter. A Butterworth filter was chosen as it maintains a flat passband (no ripples in the passband) [66] , and the roll-off rate provided by it is sufficient for this application. A 4th order digital filter with a cut-off frequency equivalent to 1.6x the mean heart rate was found to be the most effective. Choosing this cut-off frequency ensured that the high frequency components within the IHR band are not attenuated by the low pass filter. If we assume that the highest frequency within the IHR is equivalent to the upper cut off frequency of the bandpass filter (f_2), and substituting the expression derived in equation (3.16) to f_1 and (3.18) to f_2 we arrive at,

$$\frac{f_{mean_{HR}}^2}{f_{mean\_HR} - \frac{15}{60}} = 1.6 * f_{mean\_HR} \tag{3.19}$$

Solving this expression, we get the value for $f_{mean\_HR} = 0.53\ Hz$ or 32 beats/min. This means that the mean heart rate must be 32 beats/min (0.53 Hz) or lower for the low pass filter to have an effect on the

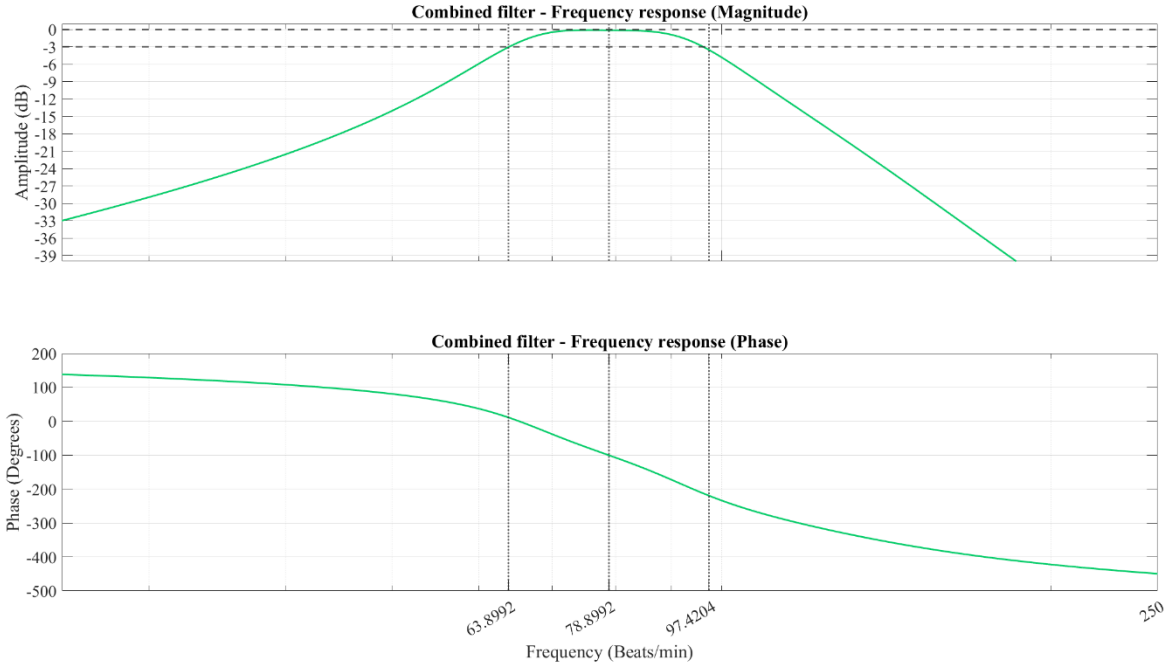

Figure 3.10: Frequency response of the cascaded filtering stage. Magnitude response (top) and the phase response (bottom). This shows the combined effect of the bandpass filter and the lowpass filter. Note how the -3dB points are still at the original cut-off frequencies of the bandpass filter.

frequency components within the IHR band. Typically, the human heart beats at a rate between 60-100 beats/min with the lowest rates at around 40 beats/min. [67] Therefore, it is safe to assume that the likelihood of the mean heart rate reaching below 40 beats/min is very low. Thus, the low pass cut-off frequency will have minimal effect on the IHR band. The frequency response of the combined filtering stage is shown in figure 3.10. This represents the combined effect of both the bandpass filter and the lowpass filter. Note how a higher roll-off rate is achieved at the high stop band compared to the low stop band. The effective roll-off rate at the high stop band is -120 dB/dec while the low stop band has a roll-off rate of -40 dB/dec. The choice of the cut-off frequency of the lowpass filter also ensured that the original cut-off frequencies of the bandpass filter are preserved.

A segment of the EKG signal after filtering with the bandpass filter and the low-pass filter is shown in Figure 3.11. The filtered signal contains some amplitude modulation apparent by the variation in the amplitude seen in Figure 3.11. Although this is not favorable for instantaneous frequency estimation, it is difficult to eliminate amplitude modulation. Furthermore, due to the cut-off frequency's proximity to the IHR band, the phase of the frequencies especially closer to the cut-off frequency are significantly affected.

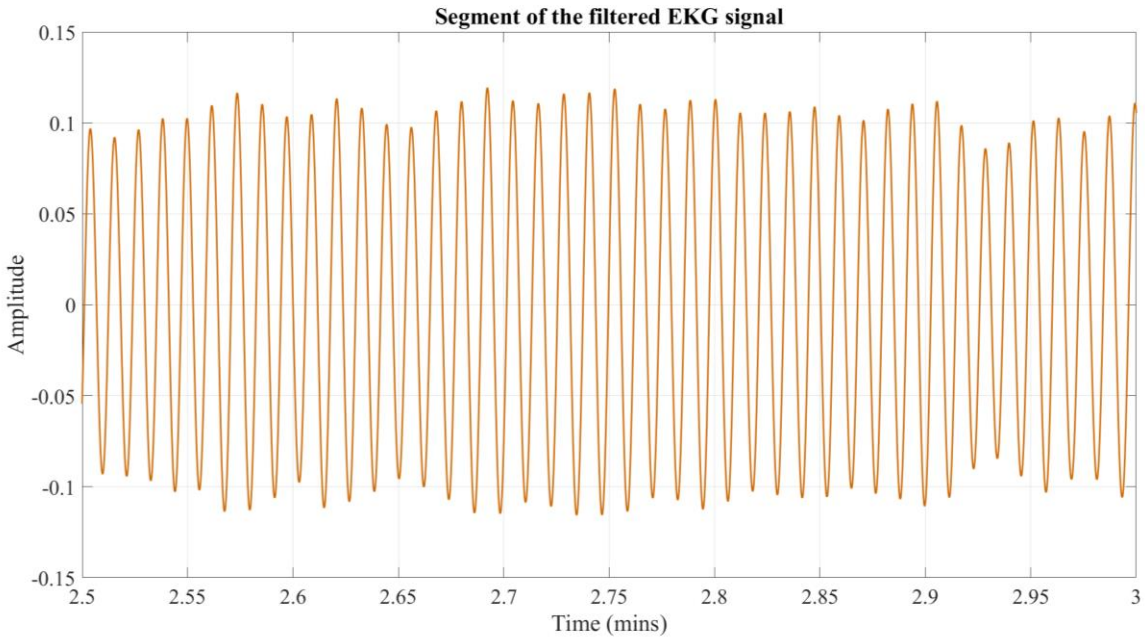

Figure 3.11: Segment of the filtered EKG signal. Observe the variation in the amplitude of the signal. We term this as amplitude modulation.

The only way this can be avoided is by choosing a higher cut-off frequency for the low-pass filter. However, this reduces the effectiveness of the low pass filter in attenuating the undesirable high frequency content.

The spectrogram of the filtered signal is shown in Figure 3.12. The high-frequency components of the EKG signal have been significantly attenuated by the filtering stages. The frequency components with the highest power are within the IHR frequency band. The frequency bins around the heart rate with relatively lower power (weaker intensity in the spectrogram) give rise to the amplitude modulation in the EKG signal that we observed in Figure 3.11. This can be shown through a brief discussion on amplitude modulation.

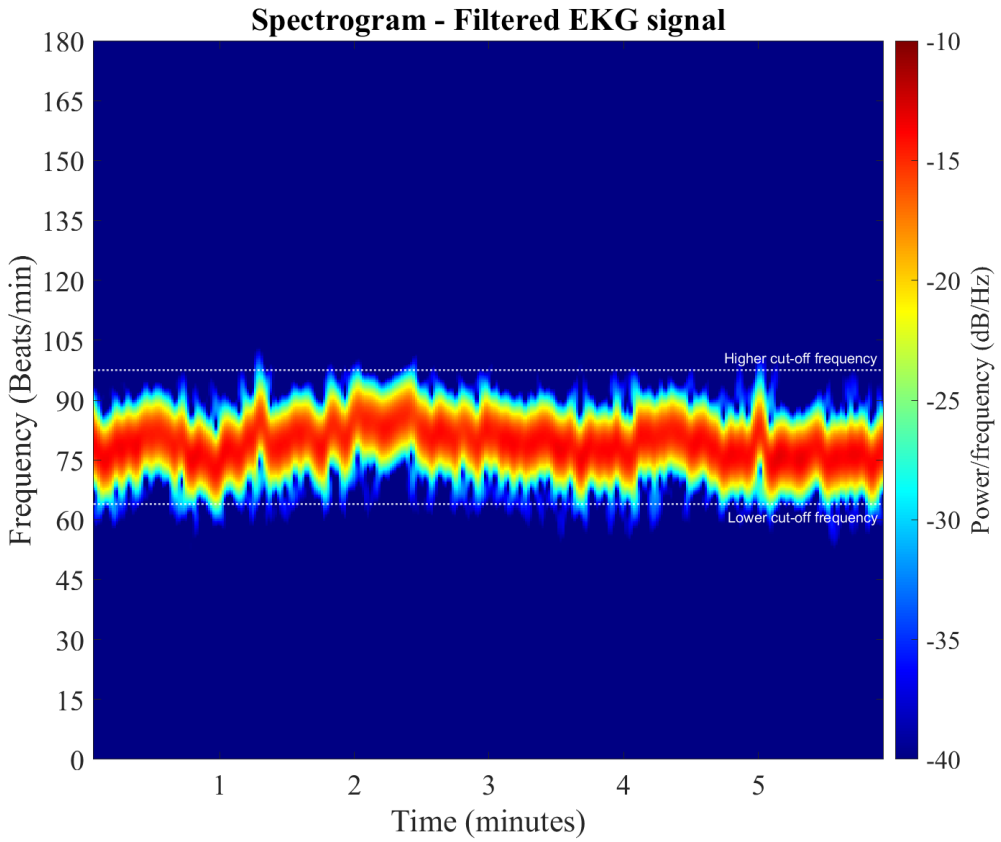

Figure 3.12: Spectrogram of the filtered EKG signal. The cut-off frequencies of the filtering stage are represented by the white dotted lines.

3.4.5 Amplitude modulation

The process of changing the amplitude of a carrier signal based on the instantaneous value of a message/modulating signal is termed amplitude modulation. [54] As the nomenclature suggests, the information that is to be transmitted is contained in the message signal, and the carrier signal acts as the

vessel to transmit the information. If the message signal is considered to be a sinusoidal signal, amplitude modulation (AM) can be expressed as follows,

$$signal_{AM} = [1 + msin(\omega_m t + \phi)]Asin(\omega_c t + \psi) \tag{3.20}$$

Where,

ω_m = Message signal frequency (angular velocity).

ω_c = Carrier signal frequency (angular velocity).

ϕ = Message signal initial phase.

ψ = Carrier signal initial phase.

A = Carrier signal amplitude.

m = Modulation index.

This expression can be expanded and then expressed using trigonometric identity,

$$signal_{AM} = Asin(\omega_c t + \psi) + \frac{Am}{2}\cos[(\omega_c - \omega_m)t + \psi - \phi] - \frac{Am}{2}\cos[(\omega_c + \omega_m)t + \psi + \phi] \tag{3.21}$$

The initial phases are constants; therefore, their trigonometric functions are also constant. Using angle sum trigonometric identities, we can rewrite the above expression as follows,

$$signal_{AM} = A_1 \sin(\omega_c t) + A_2 \cos(\omega_c t) + B_1 \cos(\omega_c - \omega_m)t - B_2 \sin(\omega_c - \omega_m)t + C_1 \cos(\omega_c + \omega_m)t - C_2 \sin(\omega_c + \omega_m)t \tag{3.22}$$

Where A_1, A_2, B_1, B_2, C_1, C_2 are constants. As you can see, amplitude modulation adds two frequency components to the original carrier signal. These frequencies are $\omega_c - \omega_m$ and $\omega_c + \omega_m$, and are termed as the lower and upper side bands respectively. When the modulating signal is not a simple sine wave as considered above, the modulated signal will contain all the constituent frequencies of the message signal

shifted by the carrier frequency and within the side bands. This is what we see in the filtered EKG signal as well. From the spectrogram in Figure 3.12, we see how frequency components (cooler shades) exist around the instantaneous heart rate (warmer shades). These side bands give rise to the amplitude modulation we see in the filtered EKG signal in Figure 3.11. Due to the close proximity of the side bands to the instantaneous heart rate, we cannot filter them out. However, the instantaneous heart rate algorithm is robust enough to account for some amplitude modulation, as we will see in the next section.

3.5 Instantaneous Heart Rate Algorithm

3.5.1 Calculating Instantaneous frequency using 3 data points.

The instantaneous heart rate algorithm is developed based on the assumption that the filtered electrocardiogram signal is monocomponent and is sinusoidal. A signal is considered monocomponent if a signal's energy is concentrated in one single frequency. [68] The filtered EKG signal is not monocomponent, as demonstrated in previous sections. However, it can be assumed as such because it only contains frequencies within a narrow band about the instantaneous heart rate. On that account, the signal is not distorted by high-frequency noise. If the signal contains no baseline drift and vertical shift, under above mentioned assumptions, the signal can be expressed in the following form,

$$y(t) = \text{Asin}(\omega t + \phi) \tag{3.23}$$

Where,

t = Time stamp

y = Magnitude of the signal at t = t,

A = Amplitude of the signal

ω = Angular velocity (rad/s)

ϕ = Initial phase

Now consider this signal is sampled at a constant sampling rate, which is much higher than two times Nyquist frequency of the signal. The Nyquist frequency is defined as the highest frequency of a signal that can be reliably measured by a data acquisition system (DAQ). The Nyquist frequency is half the sampling rate of the DAQ. Let the sampling period be Δt. From equation (3.23), we can determine the amplitude, phase and frequency of the signal if we have 3 data points.

Consider 3 consecutive data points, (t_1, y_1), (t_2, y_2) and (t_3, y_3). These data points can be expressed as follows,

$$y_1 = \text{Asin}(\omega t_1 + \phi) \tag{3.24}$$

$$y_2 = \text{Asin}(\omega t_2 + \phi) \tag{3.25}$$

$$y_3 = \text{Asin}(\omega t_3 + \phi) \tag{3.26}$$

Since,

$$t_2 = t_1 + \Delta t \tag{3.27}$$

$$t_3 = t_1 + 2\Delta t \tag{3.28}$$

Equations (3.25) and (3.26) can be rewritten as,

$$y_2 = \text{Asin}(\omega t_1 + \omega\Delta t + \phi) \tag{3.29}$$

$$y_3 = \text{Asin}(\omega t_1 + 2\omega\Delta t + \phi) \tag{3.30}$$

Substituting $\omega t_1 + \phi = \alpha$,

$$y_1 = \text{Asin}(\alpha) \tag{3.31}$$

$$y_2 = \text{Asin}(\alpha + \omega\Delta t) \tag{3.32}$$

$$y_3 = \text{Asin}(\alpha + 2\omega\Delta t) \tag{3.33}$$

From the compound angle formula, we can rewrite the (3.32) and (3.33) equations,

$$y_2 = \text{Asin}\alpha\cos(\omega\Delta t) + \text{Acos}\alpha\sin(\omega\Delta t) \tag{3.34}$$

$$y_3 = \text{Asin}\alpha\cos(2\omega\Delta t) + \text{Acos}\alpha\sin(2\omega\Delta t) \tag{3.35}$$

Substituting $y_1 = \text{Asin}(\alpha)$,

$$y_2 = y_1 \cos(\omega\Delta t) + A\cos\alpha \sin(\omega\Delta t) \tag{3.36}$$

$$y_3 = y_1 \cos(2\omega\Delta t) + A\cos\alpha \sin(2\omega\Delta t) \tag{3.37}$$

From double angle formulas, we can rewrite (3.37) as,

$$y_3 = y_1(2\cos^2(\omega\Delta t) - 1) + 2A\cos\alpha \sin(\omega\Delta t)\cos(\omega\Delta t) \tag{3.38}$$

Multiply (3.36) by $2\cos(\omega\Delta t)$,

$$2y_2 \cos(\omega\Delta t) = 2y_1 \cos^2(\omega\Delta t) + 2A\cos\alpha \sin(\omega\Delta t)\cos(\omega\Delta t) \tag{3.39}$$

(3.38) – (3.39) and rearranging yields,

$$\omega = \frac{1}{\Delta t}\cos^{-1}\left(\frac{(y_1 + y_3)}{2y_2}\right) \tag{3.40}$$

Let $P = \left(\frac{(y_1+y_3)}{2y_2}\right)$,

The inverse cosine can be calculated using the complex inverse trigonometric function [69],

$$\cos^{-1}(\mathrm{P}) = -i\log(\mathrm{P} + i\sqrt{1 - \mathrm{P}^2}\,) \tag{3.41}$$

Since the instant frequencies are all real values, $-1 \leq P \leq 1$ and $0 \leq \cos^{-1} P \leq \pi$

From equation (3.40), one can calculate the frequency corresponding to a signal segment that is 3 data points in length. This frequency is as close as we can get to the instantaneous frequency. If the signal is frequency modulated with a low-frequency message signal, equation (3.40) can be used to extract the message signal. Essentially, this can be used to demodulate a frequency modulated signal. In the next section we will do a brief discussion on frequency modulation as it will help us understand the output we obtain from the expression 3.40.

3.5.2 Frequency modulation

A frequency modulated signal is a signal where its instantaneous frequency is varied in proportion to the message signal. [54] A frequency modulated signal contains a carrier signal, which is a constant frequency signal modified based on the amplitude of a message signal. The message signal contains the information that must be transmitted. A frequency modulated signal can be mathematically expressed in the form shown in equation (3.42).

$$signal_{FM}(t) = \quad Acos(\omega_c t + m\int_0^t x_{msg}(t)dt + \phi) \tag{3.42}$$

Here the carrier frequency is ω_c, the message signal is denoted as x_{msg} and m is the modulation index. The modulation index determines the frequency sensitivity of the modulated signal to the amplitude of the message signal. In other words, "m" determines how much the frequency changes in the frequency modulated signal based on the amplitude of the message signal. Therefore, the instantaneous frequency of $signal_{FM}$change according to the instantaneous amplitude of x_{msg}. We can construct an IF signal by calculating the IF of the $signal_{FM}$ at each time instance. The IF signal will therefore have the same shape as x_{msg} because its instantaneous amplitude governs the IF of $signal_{FM}$.

3.5.3 Instantaneous frequency algorithm.

In the above section we went through the derivation of the equation for calculating the instantaneous frequency. However, obtaining the instantaneous frequency from equation (3.40) is not trivial. Consider a scenario where $y_2 = 0$. Such an instance can occur when the center data point lands on a zero crossing. A zero crossing happens when the signal crosses the horizontal axis (y = 0). Further, at such a point, theoretically, $y_1+y_3 = 0$ due to the constant sampling period. Therefore, at such data points, the instantaneous frequency equation is undefined as it involves division by 0. To avoid such scenarios, the algorithm will ignore data points when the product of y_1 and y_3 yields a negative result. This is because the sign of y_1 and y_3 will be different only when y_2 lands on or is extremely close to the x-axis. The algorithm will hold on to

the calculated "P" value of the previous y_2 data point and not calculate P at zero crossings. Further, due to rounding errors, the value of P may exceed the limits [-1,1]. In such instances, the value of P is rounded to +/- 1 depending on the sign of P. The developed MATLAB algorithm considers 3 consecutive data points (data window) to calculate the instantaneous frequency. Once IF is calculated, the data window is advanced by one data point. This allows the overlapping of data points, improving resolution. The process of the algorithm is shown in the flow chart in Figure 3.13 "Sig" is the input signal to the algorithm.

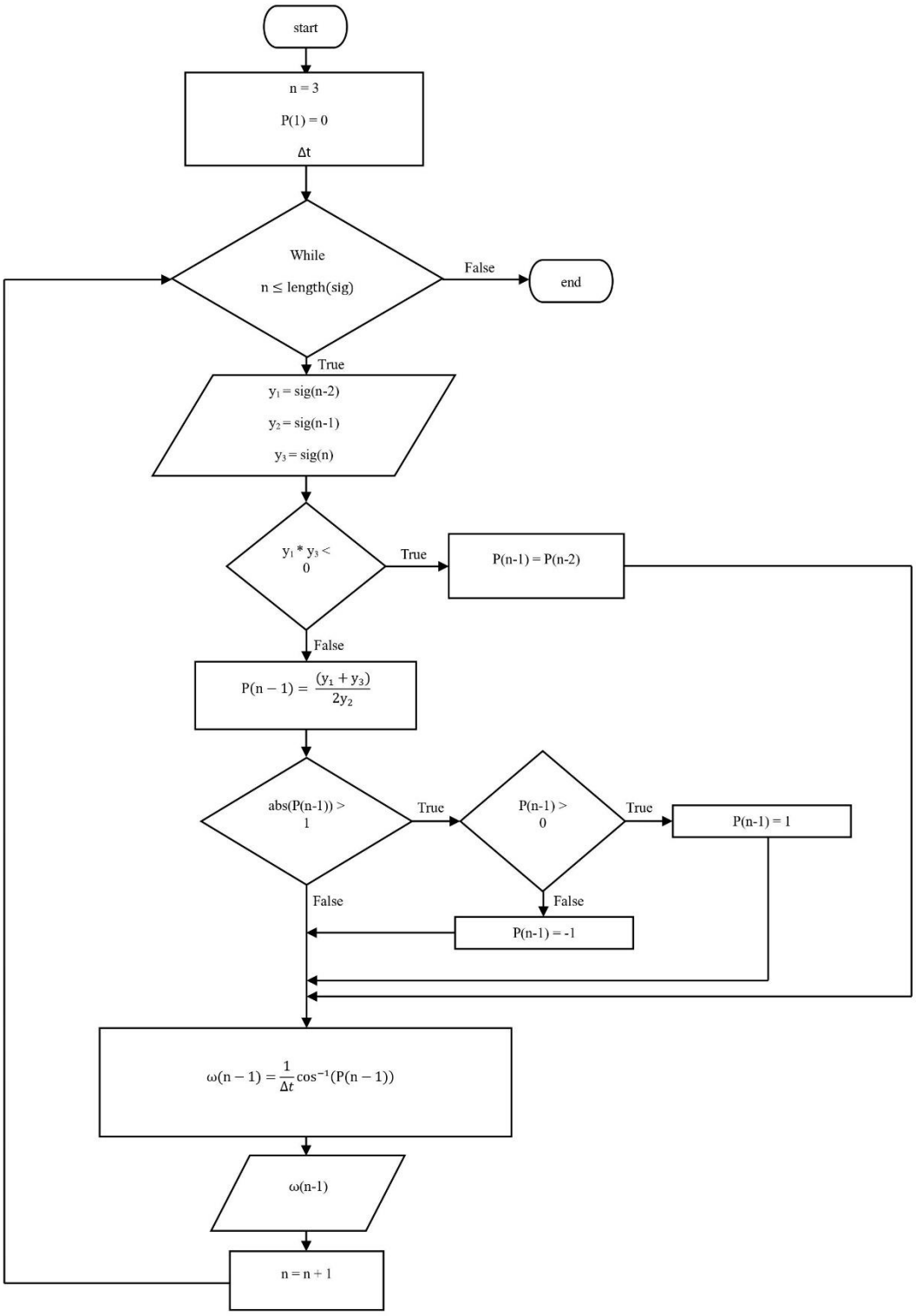

Figure 3.13: Flow chart that represents the logic followed by the instantaneous frequency algorithm.

To test the algorithm, let's consider a mono-component cosine wave with a frequency of 10 Hz and an amplitude of 1. Let the sampling rate be 1 kHz and the length of the signal be 2 complete cycles (0.2 seconds). In theory when we feed this signal to the instantaneous frequency algorithm, we should expect a horizontal line at y = 10 Hz as the frequency of the signal is 10 Hz. The algorithm was implemented as a function on MATLAB and the output of the function is shown in figure 3.14.

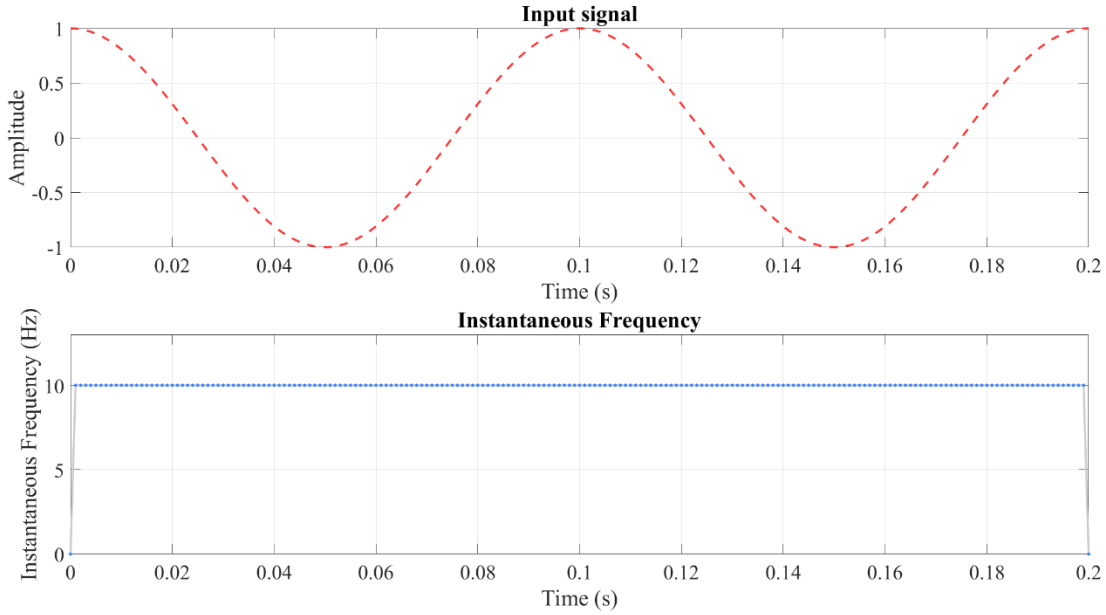

Figure 3.14: Input sinusoidal signal of 10 Hz (above) and the Instantaneous frequency signal calculated from it (below).

As you can see, the algorithm is able to track the constant frequency of the 10 Hz signal. Note that since the algorithm holds the previous value of P and ignores the data points at zero crossings, we do not observe any spikes or discontinuities in the output signal. Now that we assessed the algorithm's performance on a single-frequency sine wave, let's consider a signal that more closely resembles the filtered EKG signal.

The filtered EKG signal can be considered as a frequency modulated signal. This is because the instantaneous heart rate of the signal varies within an upper and lower boundary around the mean heart rate with time. Therefore, equation (3.40) can be used to track the instantaneous frequency of the filtered EKG signal. The resultant signal from equation (3.40) will reveal the heart rate variability. The filtered EKG signal is also amplitude modulated as seen in Figures 3.11 and 3.12.

To demonstrate the MATLAB algorithm on a frequency and amplitude-modulated signal, consider the following example input signal. We will feed this signal into the IF algorithm we developed.

f_msg = 1 Hz (frequency modulating/message signal frequency)

f_carrier = 10 Hz (carrier signal frequency)

A_carrier = 1.0 (carrier signal amplitude)

f_dev = 3 Hz (frequency deviation of the frequency modulated signal)

f_amp = 0.5 Hz (frequency of amplitude modulating signal)

m = 0.1 Amplitude modulation index

f_s = 1000 Hz (sampling frequency)

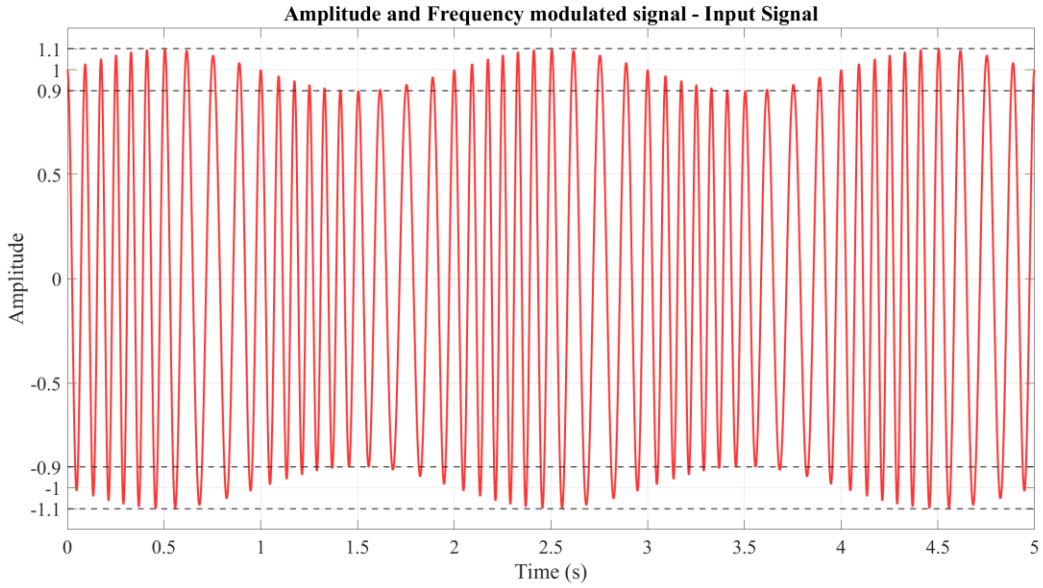

Figure 3.15: Frequency and amplitude modulated input signal. See how the amplitude modulation index of 0.1 produces amplitude deviations of +/- 0.1 around the amplitude of the original carrier signal which is 1. We will feed this signal into the IF algorithm.

The output of the IF algorithm for the input signal shown in Figure 3.15 is presented in Figure 3.16.

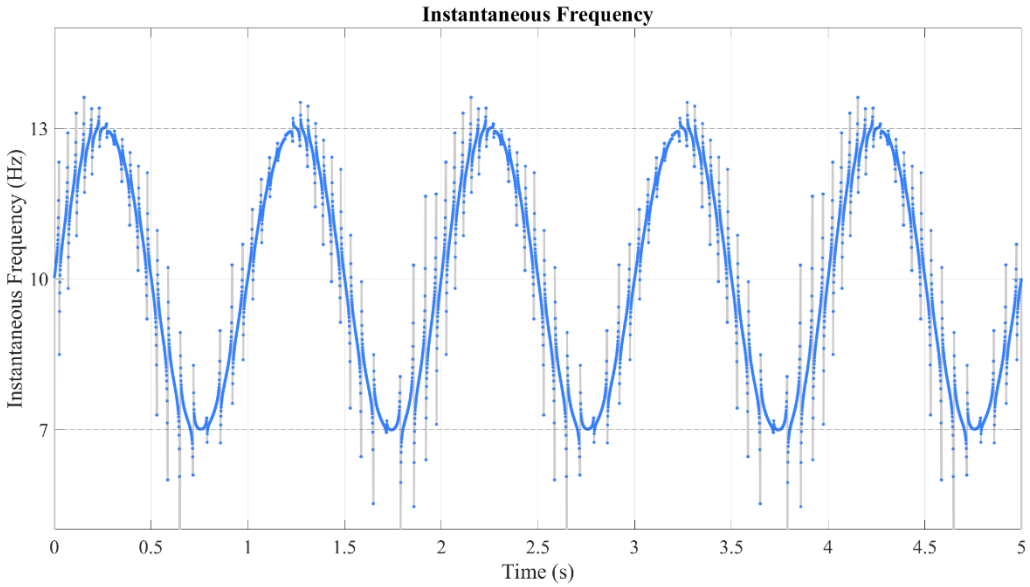

Figure 3.16: Output of instantaneous frequency algorithm. Observe how the instantaneous frequency oscillates between 7 and 13 Hz. This is equivalent to +/- 3 Hz of frequency deviations from the original carrier frequency of 10 Hz. Also notice how the frequency of the Instantaneous frequency signal is 1 Hz. This is equivalent to the message signal frequency.

The output signal is sinusoidal and has a frequency of 1 Hz. This is equivalent to the modulating signal/message signal frequency. Also note that the amplitude of the signal fluctuates between 7 Hz and 13 Hz with a mean frequency of 10 Hz. This reflects the carrier frequency of 10 Hz and the frequency deviation of 3 Hz in the frequency modulated signal. The algorithm has therefore tracked the instantaneous frequency of the frequency and amplitude modulated signal.

Close observation of the instantaneous frequency signal shows that spikes occur at zero crossings of the input signal. Observe the green dotted vertical line that passes through a zero-crossing point of the input signal in Figure 3.17. These spikes result from asymptotes present in the region where the center data point lands on the x-axis ($y_2 = 0$). When a rational function's denominator approaches zero, a vertical asymptote occurs at the point where the denominator reaches zero. Although the algorithm ignores y_2 points that exactly land on the x-axis, the output curve's shape is still affected by the asymptotes. This generates the undesirable spikes present in the instantaneous frequency signal.

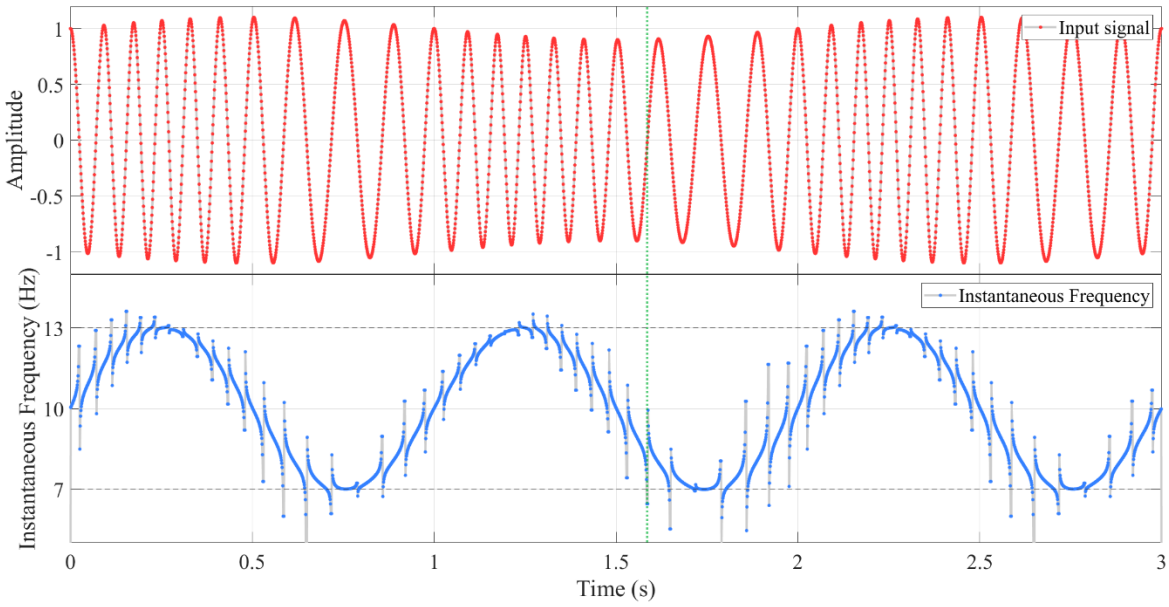

Figure 3.17: Spikes in the instantaneous frequency signal occurring at zero crossings of the input signal.

Let's now observe characteristics of these spikes. As mentioned before, these are the result of vertical asymptotes occurring near zero-crossings of the input signal. Therefore, the spikes occur at a frequency equivalent to the zero-crossing rate of the input signal. Since the input signal is frequency modulated, the zero-crossing rate is variable and is about double the instantaneous frequency of the input signal. One way to potentially remove the spikes from the instantaneous signal (IF signal) is to send it through a low pass filter having a cut-off frequency lower than the average zero crossing rate of the input signal. However, this cut-off frequency should be high enough to still pass the message signal through. Usually, the carrier frequency of a frequency-modulated signal is much higher than the message signal frequency. Therefore, a carefully chosen low-pass filter will be able to remove most of the unwanted spikes from the IF signal.

For a filtered EKG signal such as the one depicted in Figure 3.11, the carrier signal frequency is analogues to the mean heart rate. This is because we assume that the heart rate varies about the mean heart rate. In that case the low pass filter cut-off frequency must be set below double the lower bound of the IHR band of the signal. Careful consideration must be given when choosing this cut-off frequency so that important information is not lost.

In the next section of this study, we introduce another method that could be used to eliminate spikes from the IF signal. Unlike the message signal we used in the above example, we do not possess a priori knowledge of the message signal of an EKG signal. Therefore, we do not want to lose important information contained within the IF signal calculated from the EKG signal during filtering. The motivation for the spike elimination method introduced below stems from this need to retain as much information as possible within the IF signal. After presenting the method, we will assess its performance against using a low pass filter to mitigate the effects of unwanted spikes.

3.6 Removing spikes from the IF signal.

In the previous section, the input signal was represented in the analytical form as shown in equation (3.23). The first derivative of equation (3.23) is as follows,

$$\dot{y}(t) = A\omega\cos(\omega t + \phi) \tag{3.43}$$

For a miniscule portion of a frequency and amplitude modulated signal, Aω can be assumed to be constant. Therefore, equation (3.42) reduces to the form,

$$\dot{y}(t) = B\cos(\omega t + \phi) \tag{3.44}$$

Where "B" is a constant. $\dot{y}(t)$ at a given data point can be approximated using central difference involving neighboring data points. For instance, consider data point (t_n, y_n), the value of the derivative at that data point can be approximated as,

$$\dot{y}_n = \frac{y_{n+1} - y_{n-1}}{t_{n+1} - t_{n-1}} \tag{3.45}$$

Since the sampling rate of the signal is constant, $t_{n+1} - t_{n-1}$ is constant and is equal to 2x the sampling period. For the purposes of this research, we are not concerned with the actual value of the derivative but only the shape of the derivative signal. Therefore, we can ignore division by the time period and approximate the shape of the derivative signal with the following equation,

$$\dot{y}_n = y_{n+1} - y_{n-1} \tag{3.46}$$

For higher sampling rates the sampling period can get very small and division by such a value will produce large values. With the expression in (3.46) we can mitigate the value of the derivative growing exceptionally large. Whenever a derivative of a signal is calculated in this study, expression (3.46) is used.

We can now substitute from (3.46) to (3.44) which yields,

$$\dot{y}_n = B\cos(\omega t_n + \phi) \tag{3.47}$$

The derivative of the signal approximated using central difference method is shown in Figure 3.17. Observe the green vertical line that crosses through a peak in the input signal and a zero crossing of the derivative signal. The difference in phase angle can be understood by looking at equations (3.23) and (3.47). The derivative of the input signal is a cosine function which is orthogonal to the original sine function which represents the signal. We can check the orthogonality of the two signals by calculating the inner product of the two signals.

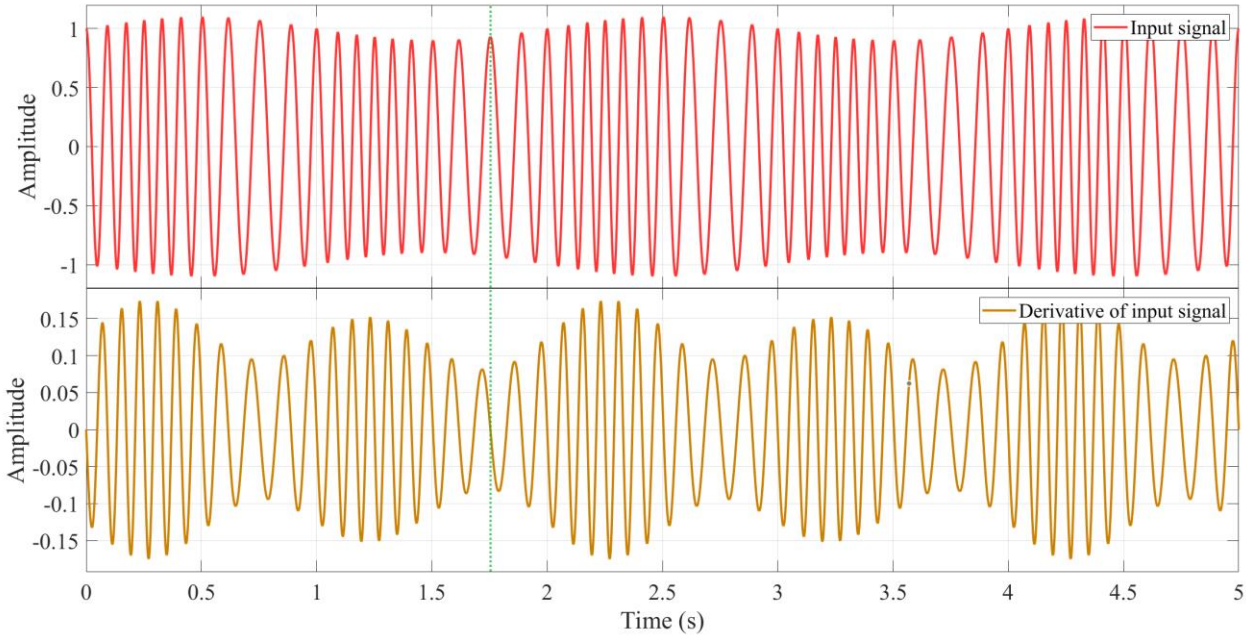

Figure 3.18: Input signal and its derivative calculated using central difference method.

The inner product of two signals is define as, [70]

$$cos\theta = \frac{X^T Y}{\|X\|\|Y\|} \tag{3.48}$$

Where, X and Y are the two signals in the form of column vectors and θ is the angle between the two signals. If the inner product is zero, $\theta = \pi/2$, which means the two signals are orthogonal. The inner product of the two signals was calculated in MATLAB. The value was found to be 2.2513e-8, which is extremely small and therefore, $\theta = \pi/2$.

Considering 3 adjacent data points in the derivative signal and following a similar process presented in the previous section to solve 3 equations we obtain an analytical solution for the angular frequency:

$$\omega = \frac{1}{\Delta t}\cos^{-1}\left(\frac{(\dot{y}_{n+1} + \dot{y}_{n-1})}{2\dot{y}_n}\right) \tag{3.49}$$

From the expression (3.49) we can conclude that the first derivative of the original signal can also be used to calculate the instantaneous frequency. Now, we have two signals that can be used to calculate instantaneous frequency. The advantage of this is the input signal is orthogonal to its derivative signal. Therefore, the derivative signal has zero crossings when the original signal is at a peak or trough and vice versa. Hence, spikes in the IF signals calculated from the original and derivative signals will never occur at the same temporal location. This could be useful when trying to remove spikes from the IF signal.

As seen in Figure 3.19, IF signals calculated using the original and its derivative have the same basic appearance and are similar in shape to the message signal. However, close inspection shows that the location of the spikes/asymptotes are different in the two signals (see Figure 3.20). Observe the orange vertical dotted line that goes through a spike in the IF signal calculated using the derivative (IFDS), and the green line that goes through a spike in the IF signal calculated using the original input signal (IFIS). This validates the previous statement of the spikes never occurring at the same temporal location on both signals. Therefore, we can replace a spike in one signal with the corresponding portion of the other signal that has no spike. To do this we need to come up with an algorithm to identify where the spikes occur and replace

them with the signal portion from the other IF signal. Next, we will discuss a methodology to detect spikes in the IF signal.

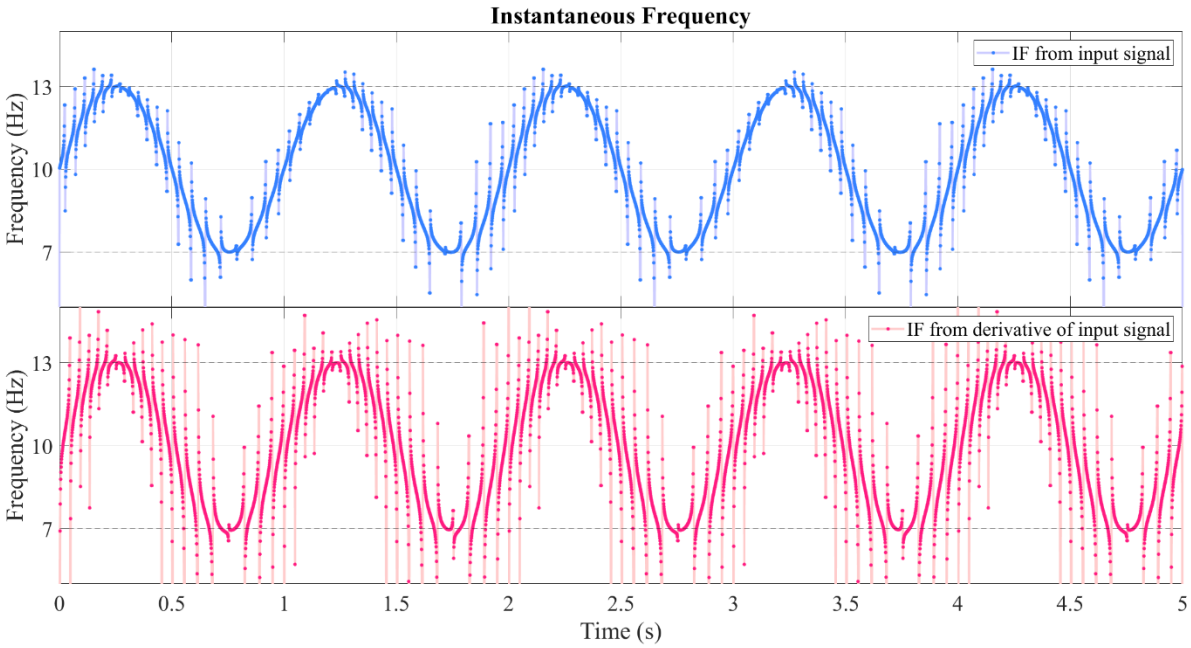

Figure 3.19: Comparison between IF signals obtained from the original signal and its derivative.

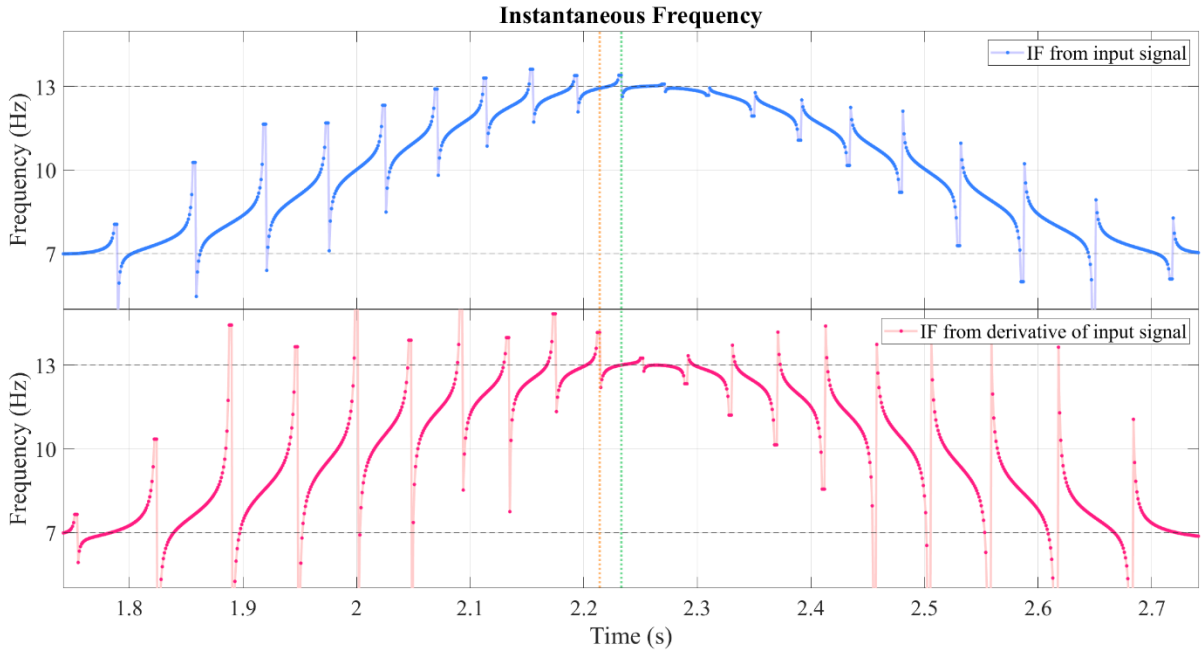

Figure 3.20: Comparison of the location of spikes in the two signals. Observe how the dotted lines passing through spikes in one IF signal passes through regions with no spikes in the other IF signal.

The derivative of a signal is sensitive to the slope of the signal at a given location. Thus, the derivative of the IF signal is sensitive to the asymptotes/spikes present in the signal. Therefore, we can expect higher values in the derivative of the IF signal at points where asymptotes are present. The derivative of the IF signal can also be approximated using the central difference method. Figure 3.21 shows the derivative of the IF signal, calculated using the central difference method in the region of a spike. Observe how the value of the derivative remains small for points away from the spike and increases as the influence of the asymptote gets stronger. However, since the IF algorithm holds the previous value of P for data points closest to zero crossings, we see flat regions in the IF signal at zero crossings. This is reflected in the derivative signal having a value of zero for points near zero crossings. The derivative value then becomes negative as the slope of the spike goes negative and then returns to a small value for data points further away from the spike. Although the derivative was able to capture the spike, it is not of much use as it is. Let's consider the squared value of the derivative of the IF signal instead.

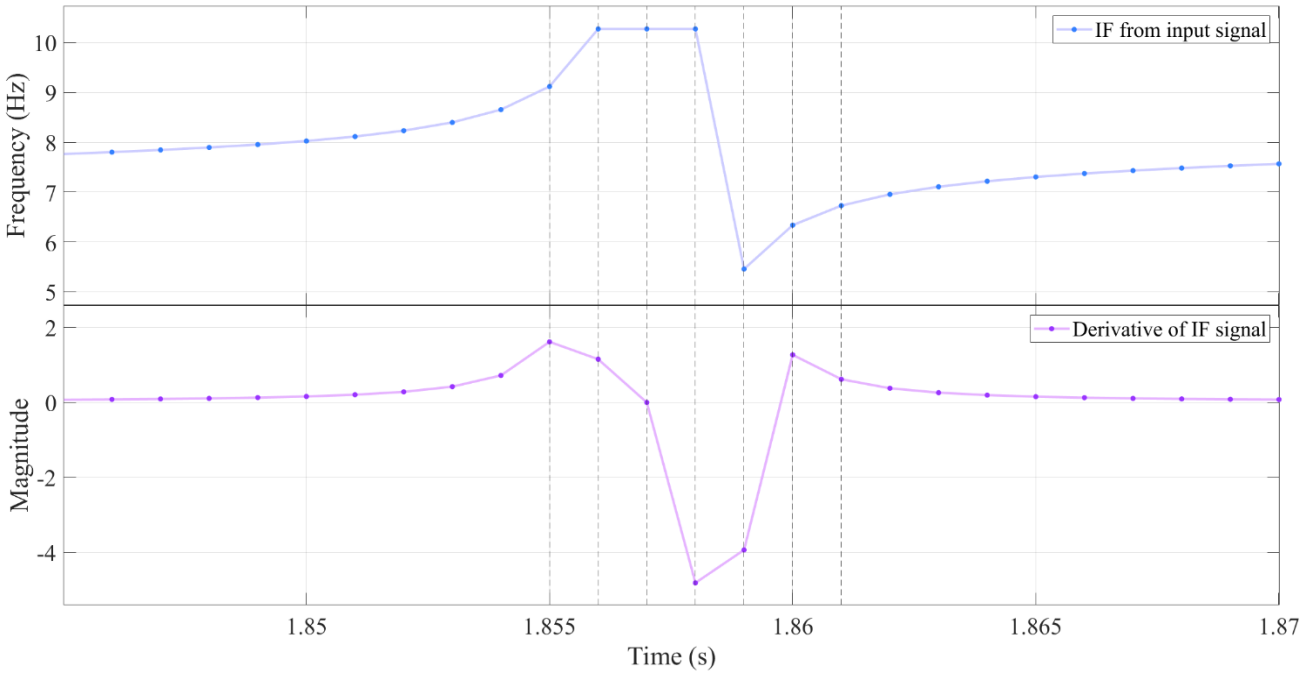

Figure 3.11: A spike in the IF signal (top) and the corresponding region in the derivative of the IF signal (bottom).

The squared derivative of the IF signal is shown in Figure 3.22. Squaring the derivative signal accentuates the rate of change of the IF signal and thus makes the locations of the spikes more prominent. Further, taking the squared value also flips the sign of the negative portion of the derivative signal. We could potentially use the squared derivative signal with a thresholding/comparison algorithm to detect the location of spikes in the IF signal. However, the sudden drop to zero of the value of the squared derivative near zero crossings prevents it being used with any such algorithm.

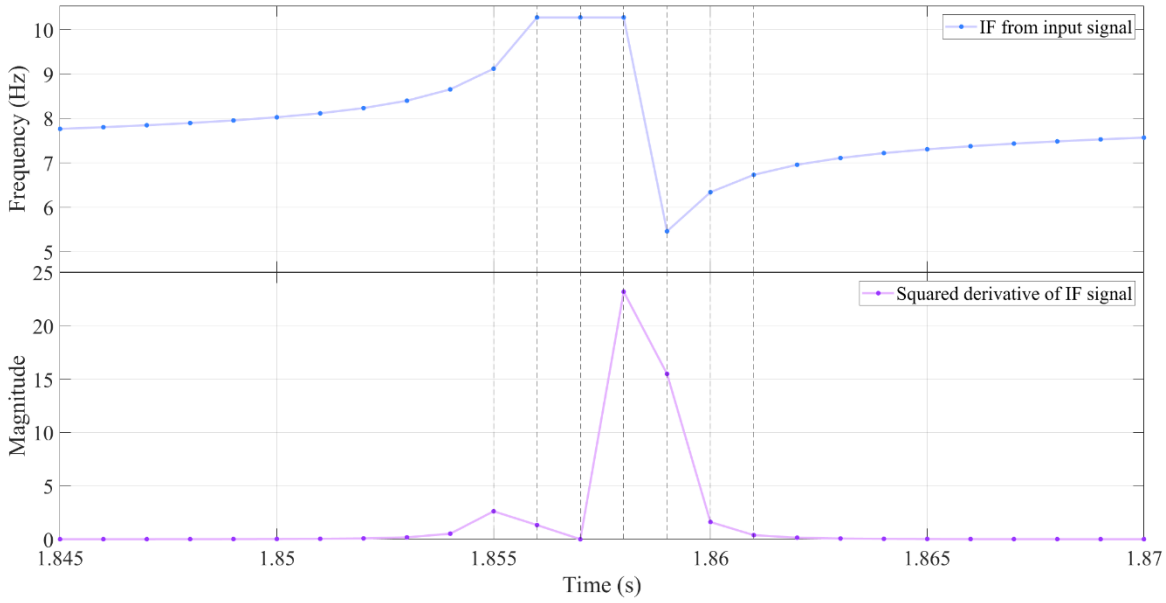

Figure 3.22: Close-up of the IF signal near a spike (top) and the squared derivative (bottom).

To eliminate this undesired feature of the derivative signal, we could utilize a moving window integrator. A moving window integrator as the name suggests, integrates a signal portion within a specified window. For a discrete signal, the moving window integrator (MWI) can be expressed as follows,

$$\mathrm{MWI(n)} = \sum_{i=n-\frac{N-1}{2}}^{n+\frac{N-1}{2}} y(i) \tag{3.50}$$

Where N is the size of the window. N is an odd number to ensure that the window is centered around the data point y(n) being assessed. The size of the window is chosen empirically. More will be discussed about

the size of the window later in this chapter. Principle inspiration for using a moving window integrator came from the study mentioned in [71], where the integrator was used to extract information from QRS complexes.

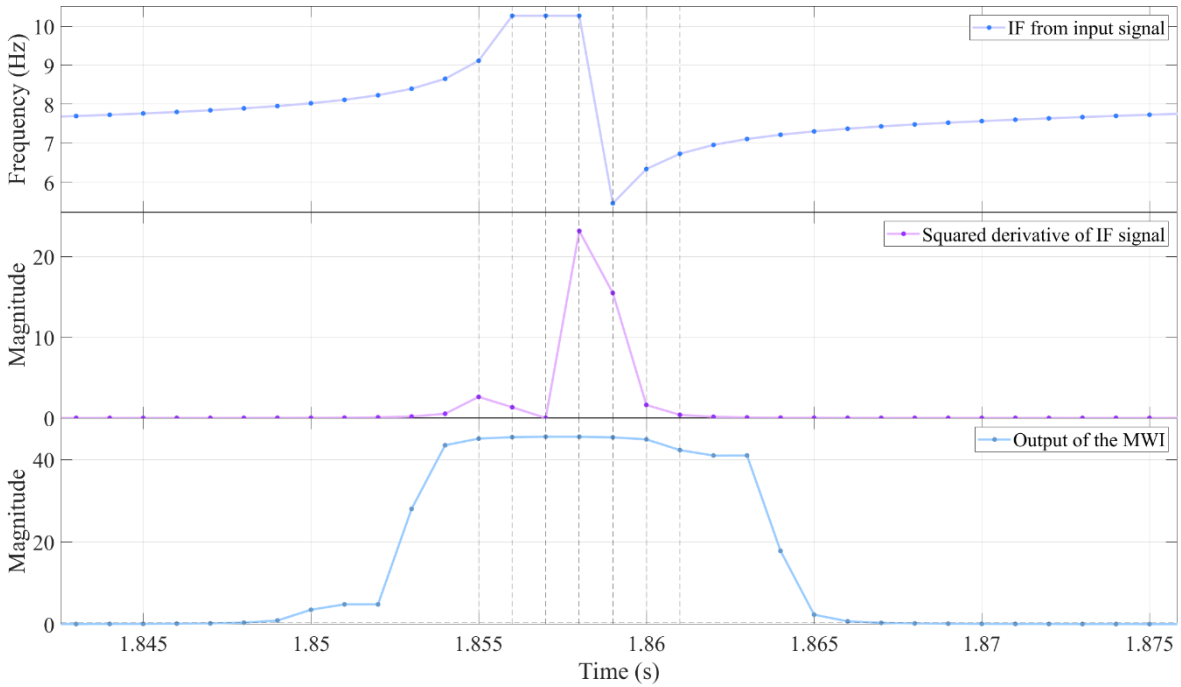

Figure 3.23: IF signal in the region of a spike (top), the squared derivative of the IF signal (middle) and the output of the moving window integrator with a window size of 11 data points (bottom).

Figure 3.23 shows the output of the moving window integrator utilizing a window size of 11 data points for the squared derivative of the IF signal. Observe how the output of the integrator has a single column that envelopes the two peaks in the squared derivative signal. As mentioned before the size of the window is chosen empirically. It should be chosen in a way that the closely placed peaks in the squared derivative signal corresponding to the same asymptote are captured within the window while peaks corresponding to neighboring asymptotes are not included. For the IF signal considered in this chapter, a window of 11 data points was sufficient to create an envelope around the peaks corresponding to the same asymptote. Since the MWI output encapsulates the region affected by asymptotes/spikes, we can finally come up with a methodology to remove spikes from the IF signal.

Since we have 2, IF signals that were calculated using the original signal and its derivative, we can process both IF signals in the above-mentioned procedure to obtain two outputs from the moving window integrator. We will name them MWIIFIS (output for IFIS) and MWIIFDS (output for IFDS). These two outputs can be used in a comparison algorithm (discussed later in this chapter) to remove spikes from the IF signals and produce a significantly cleaner signal.

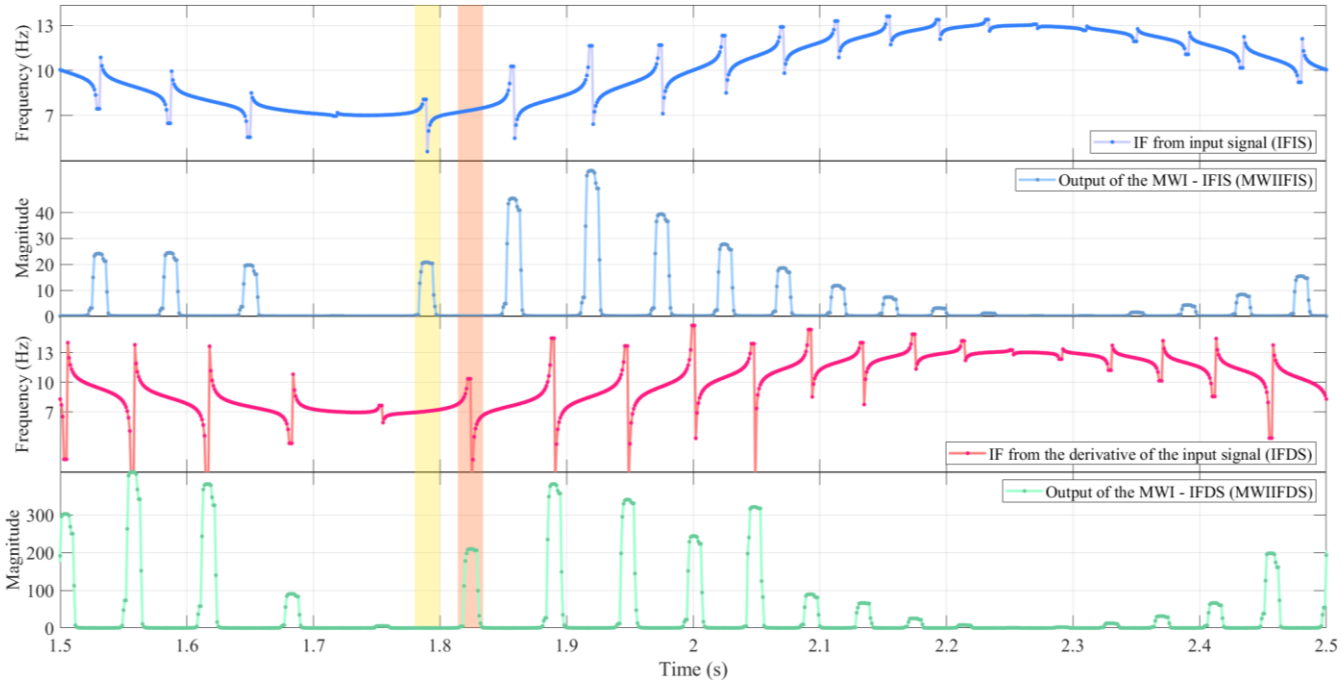

Figure 3.24: Comparison of the outputs of the moving window integrator. The second and forth plots from the top show the outputs of the MWI for the two IF signals. Observe how the columns in the MWI outputs never occur at the same time, rather they alternate between the two signals.

Figure 3.24 shows the final outputs from the moving window integrator for the IF signals calculated from the original input signal and its derivative. The yellow and orange bands in the plot mark the temporal regions of two spikes in the IFDS and IFIS respectively. Note how a column exists in the MWIIFIS and none in the MWIIFDS when a spike occurs in IFIS and vice versa. We now have two outputs that show where the spikes are in each IF signal. These two outputs can be used to detect spikes in the IF signal and remove them using a comparison algorithm.

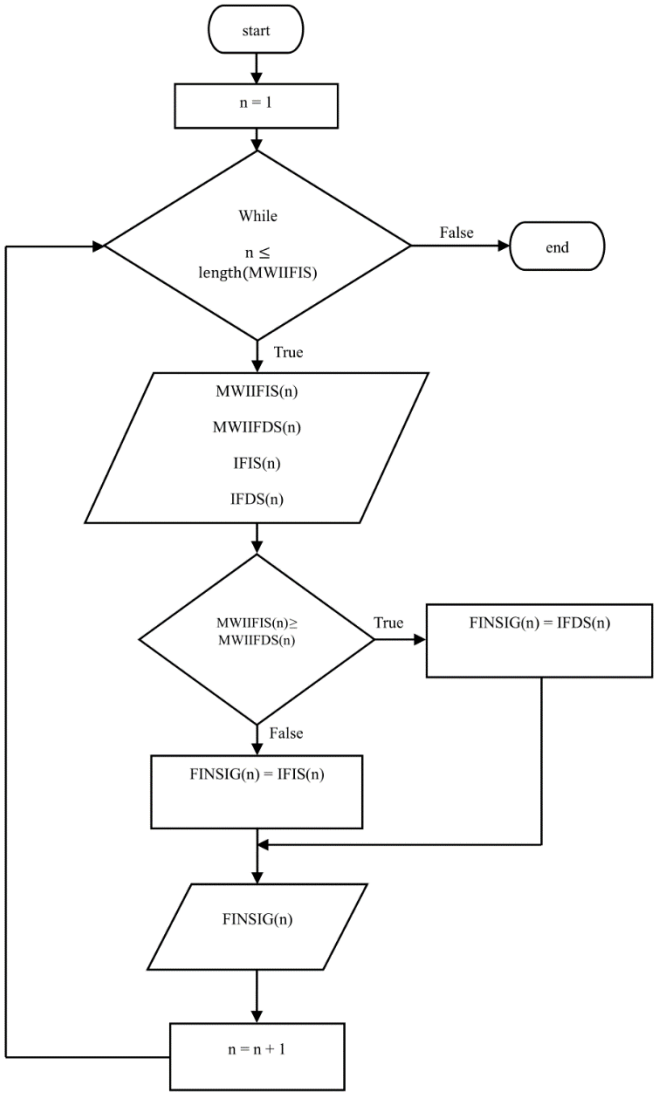

Figure 3.25: Flow chart of the comparison algorithm.

The comparison algorithm receives 4 inputs – IFIS, IFDS, MWIIFIS and the MWIIFDS. All 4 signals are synchronized (no time shifts). The comparison algorithm compares the value of the two outputs from the moving window integrator (MWIIFIS and MWIIFDS) at each data point. It then outputs the value of either the IFIS or IFDS depending on which MWI output is smaller. For example, for a particular data point, if the value of MWIIFIS is smaller than that of MWIIFDS, the comparison algorithm outputs the corresponding value of IFIS. This is because the moving window integrator output value of one signal is always higher compared to its counterpart in the region of a spike. This process produces a signal that only

contains the portions of the IF signals that do not contain spikes. Figure 3.26 shows the logic of the comparison algorithm. FINSIG is the output of the comparison algorithm.

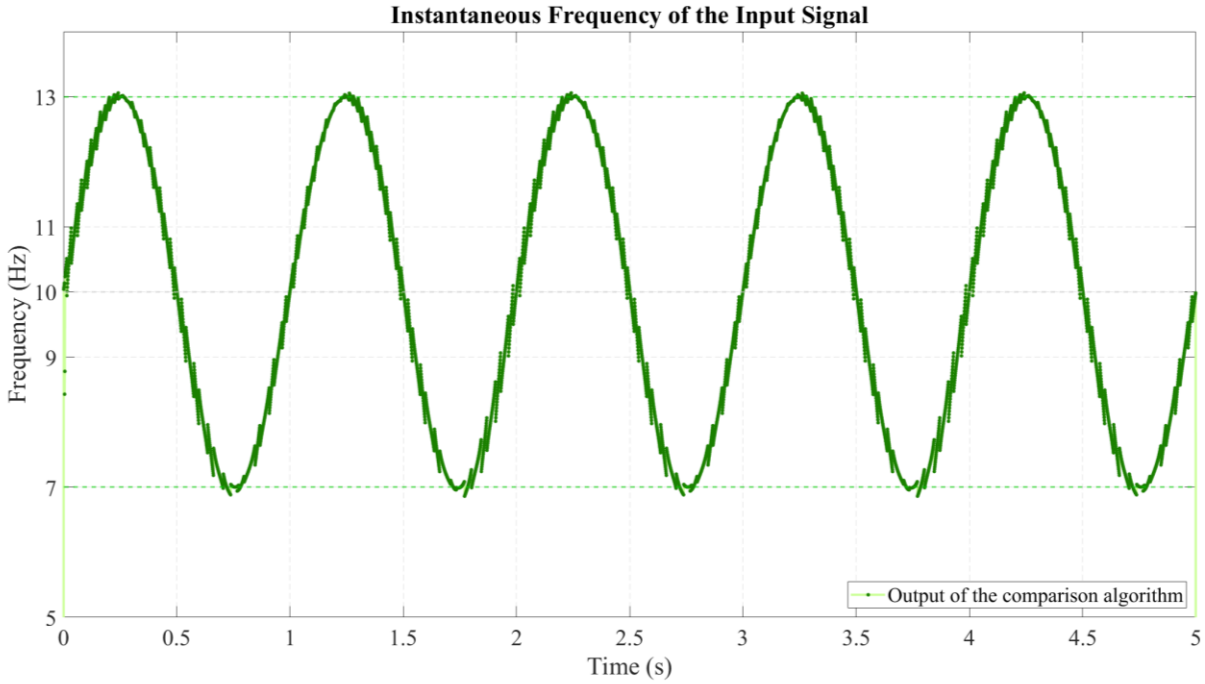

Figure 3.26: Output of the comparison algorithm.

Figure 3.26 shows the output of the comparison algorithm (FINSIG). The spikes present in the IF signals that were produced from the instantaneous frequency algorithm have been significantly attenuated in FINSIG. The amplitude of the signal fluctuates between 7 Hz and 13 Hz (frequency deviation was set to 3 Hz) with a mean value of 10 Hz which is the frequency of the carrier signal. FINSIG also has a frequency of 1 Hz which is equivalent to the message signal frequency. We can verify this by calculating the Spectrum of the FINSIG. In Figure 3.27, the Fourier transform of FINSIG and IFIS were calculated after removing the bias from the signals (centered around the x-axis). As you can see, a distinctive peak is present at 1 Hz, in both signals. This peak corresponds to the frequency of the message signal. In the IFIS signal, the next highest peak has a magnitude of -28.5 dB while in the FINSIG it has a magnitude of -40 dB. Theoretically, since the message signal is a monocomponent signal, the only frequency component that should be present in the IF signal is that of the message signal frequency (1 Hz). However, we see that FINSIG has a much lower noise level compared to IFIS. This means that the spike removing algorithm has successfully

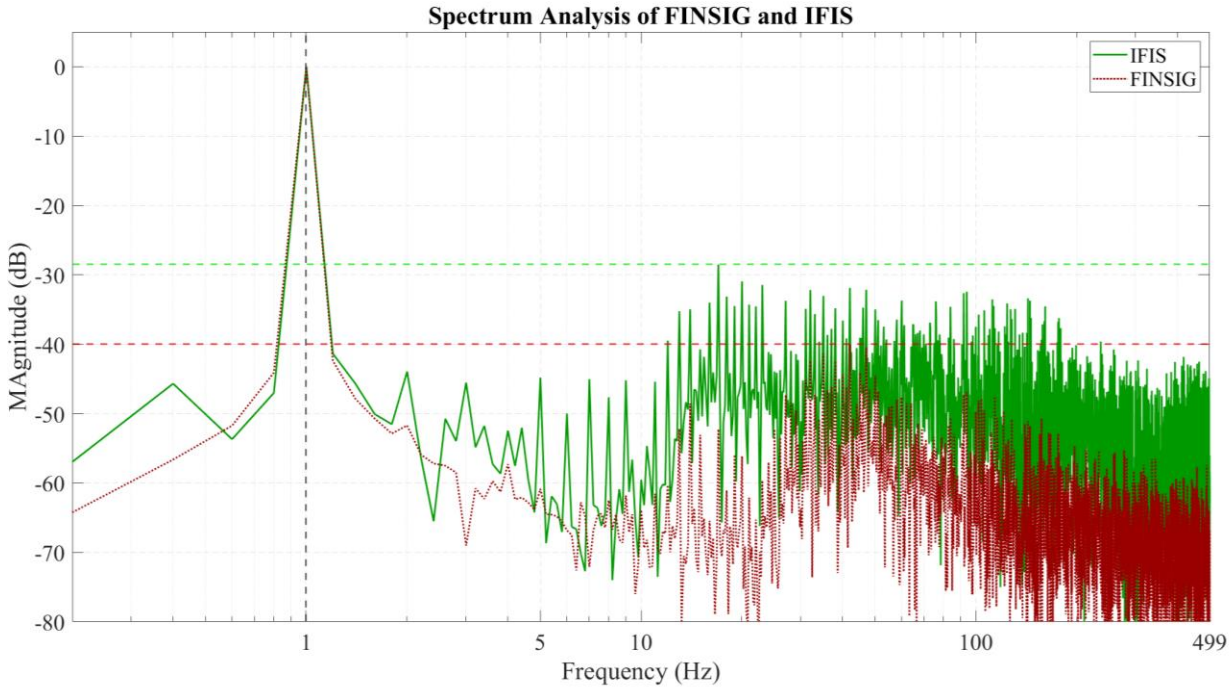

Figure 3.27: Spectrum analysis of the output of the comparison algorithm (FINSIG) and IFIS. The frequency axis is in logarithmic scale.

attenuated "noise" induced by the spikes. To visualize the noise present in FINSIG, we can create an ideal IF signal/message signal and subtract it from FINSIG. The result is shown in Figure 3.28. The noise level can be assessed using signal to noise ratio. Signal to noise ratio (SNR) compares the level of the signal that carries the information to that of the unwanted noise. A higher SNR value means that the signal is clearer and is less distorted by noise. SNR is calculated using the below mentioned equation.

$$\mathrm{SNR} = 10\log\left(\frac{\mathrm{P_{signal}}}{\mathrm{P_{noise}}}\right) \tag{3.51}$$

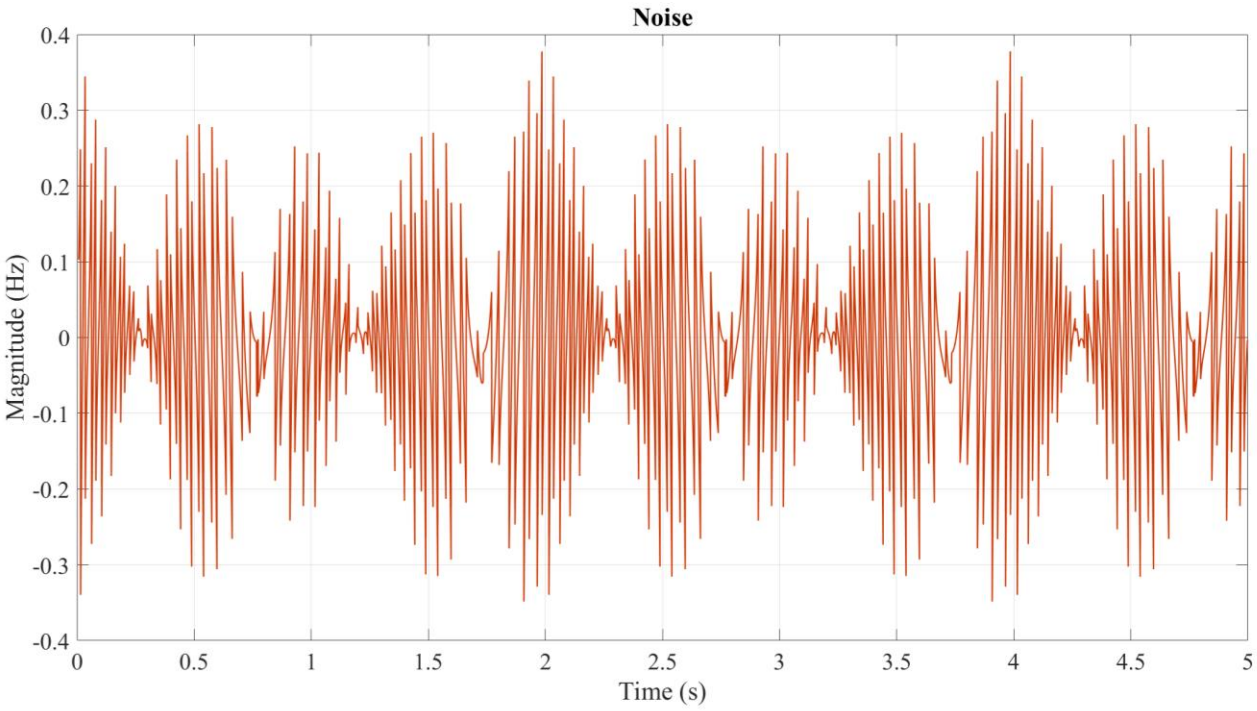

Figure 3.28: Noise in the final signal.

Here, P_{signal} is the power of the signal that does not contain noise and P_{noise} is the power of the noise included in the signal. SNR is expressed in decibels. The SNR value of FINSIG is 40.07 dB. This means that the desired signal is over 100 times greater in amplitude than the noise. We calculated the SNR value for the IFIS as well and it was found to be 26.19 dB. This means that the desired signal amplitude is only 20.4 times greater than the amplitude of the noise. This further proves that the spike removing algorithm has successfully attenuated the noise induced by the spikes.

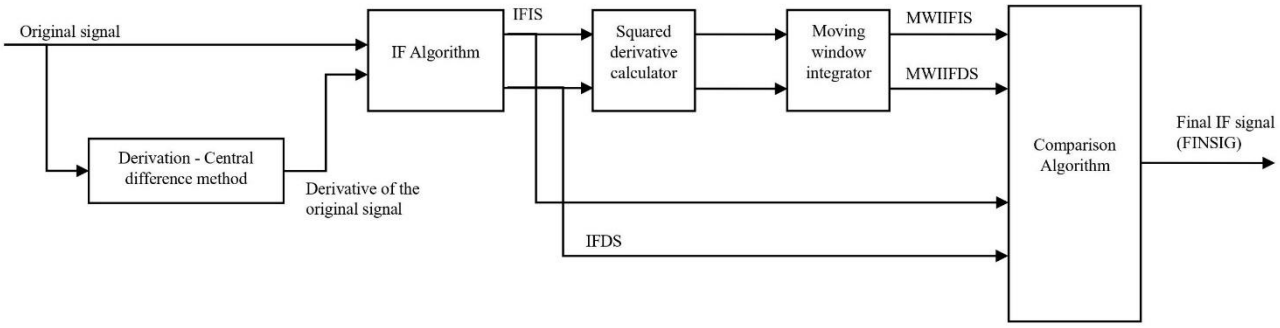

Figure 3.29: Overall process of calculating the instantaneous frequency and cleaning it up using the spike removing algorithm presented in this study.

The overall process of calculating the final, cleaned up IF signal (FINSIG) from the original frequency and amplitude modulated signal is shown in figure 3.28. The process to obtain the denoised IF signal from the input frequency and amplitude modulated signal involves 5 distinctive steps. For the theoretical FM-AM signal that was used to demonstrate the process, we were able to obtain an IF signal with an acceptable SNR. However, an EKG signal could contain a message signal that is not a simple sinusoid. Further, the performance of the spike removing algorithm on filtered EKG signals is yet to be assessed. In the next section of this chapter, we will apply the techniques introduced thus far on the filtered EKG signal presented in section 3.4.

3.7 Calculating the Instantaneous Heart Rate from the EKG signal.

In section 3.4, we discussed the process of preparing the EKG signal for calculating the Instantaneous heart rate. Refer to Figure 3.11 to see a segment of the EKG signal after the preprocessing stage. As mentioned in section 3.4, we have a signal that has frequency components within the IHR band.

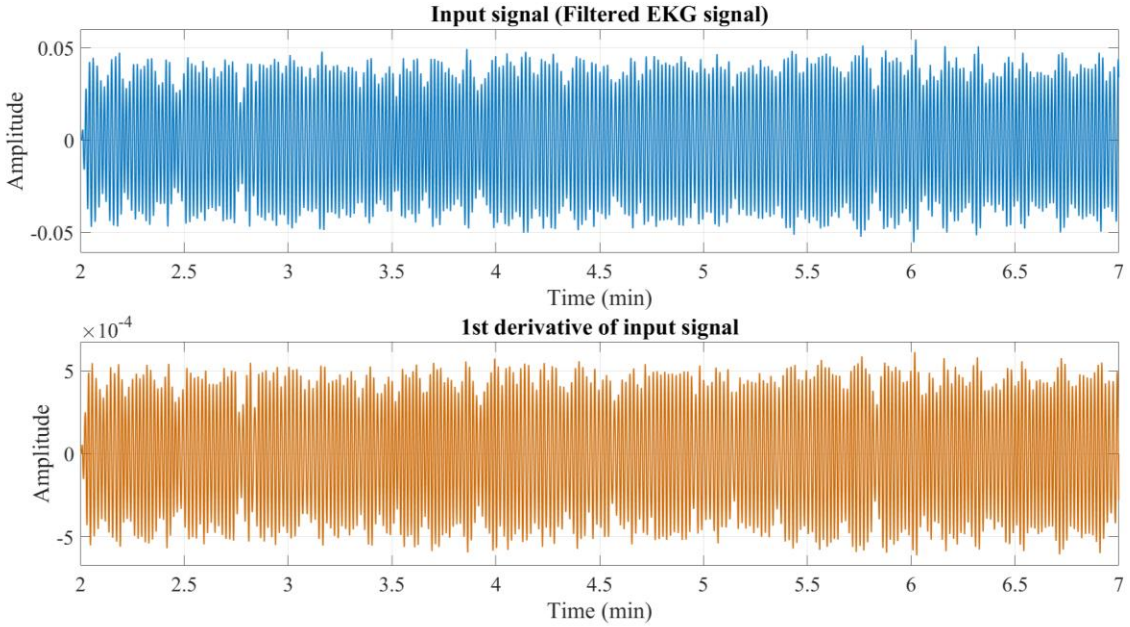

Figure 3.30: The filtered EKG signal (top) and its derivative (bottom).

We will now process this filtered EKG signal as we did the theoretical FM-AM signal mentioned in section 3.5. First, we will calculate the derivative of the input signal. We will consider a 5 min portion of the EKG signal as it is the common measurement length used in HRV analysis, especially in frequency domain analysis. As discussed, the input signal and its derivative are orthogonal. We will then feed both the signals into the instantaneous frequency algorithm and obtain two IF signals. We will use the same terminology as before and call the IF signal calculated using the input signal (filtered EKG signal) as IFIS and the one calculated using its derivative as IFDS.

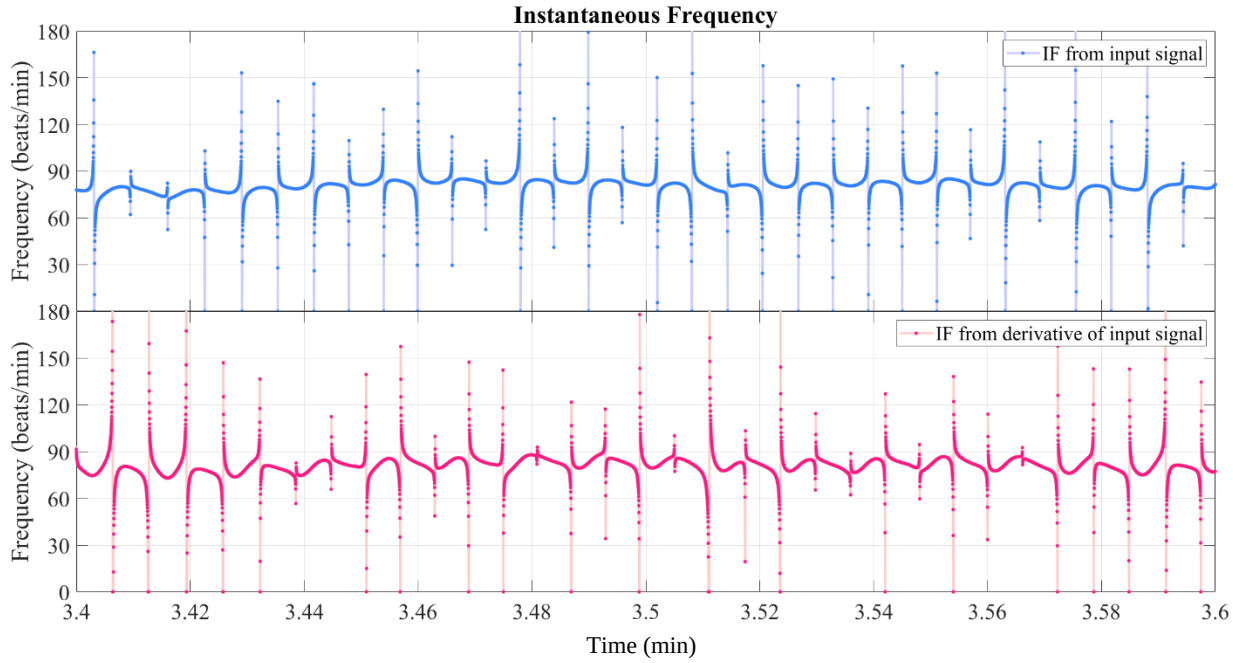

Figure 3.31: Segment of IF signals. IF calculated from filtered EKG signal (top). IF calculated from derivative signal (bottom).

Figure 3.31 show segments of the IF signals calculated from the input signal and its derivative. Observe the asymptotes in the IF signals. We will now assess the effectiveness of the spike removal process on mitigating the effects of the asymptotes in the IF signal. To do so, we will compute the squared derivatives of the IF signals and then send them through the moving window integrator. The window size of the MWI was set to 153 samples. This window size was chosen as it produced the highest SNR value. Calculating the signal to noise ratio for the IF signal is challenging as we have no prior knowledge of the actual IHR signal. For the purpose of calculating the SNR, we assumed that the instantaneous heart rate signal

calculated using RR intervals (RRSIG) as the desired IHR signal. Although this is questionable, we have no other reference signal to work with. The RRSIG is sampled at a varying sampling rate as the time instance of each sample depends on the occurrence of an R peak. Therefore, the RRSIG was first interpolated and resampled at 1KHz. The noise signal can then be calculated by subtracting FINSIG from the resampled RRSIG. FINSIG signals were calculated for MWI window lengths ranging from 11 samples to 301 samples with 2 sample increments. The corresponding noise signals were then calculated. As we now have the desired signal and the noise signals, SNRs can be calculated for each window size. Results of this process are shown in Figure 3.32. As you can see, the maximum SNR value is achieved at a window size of 153 samples.

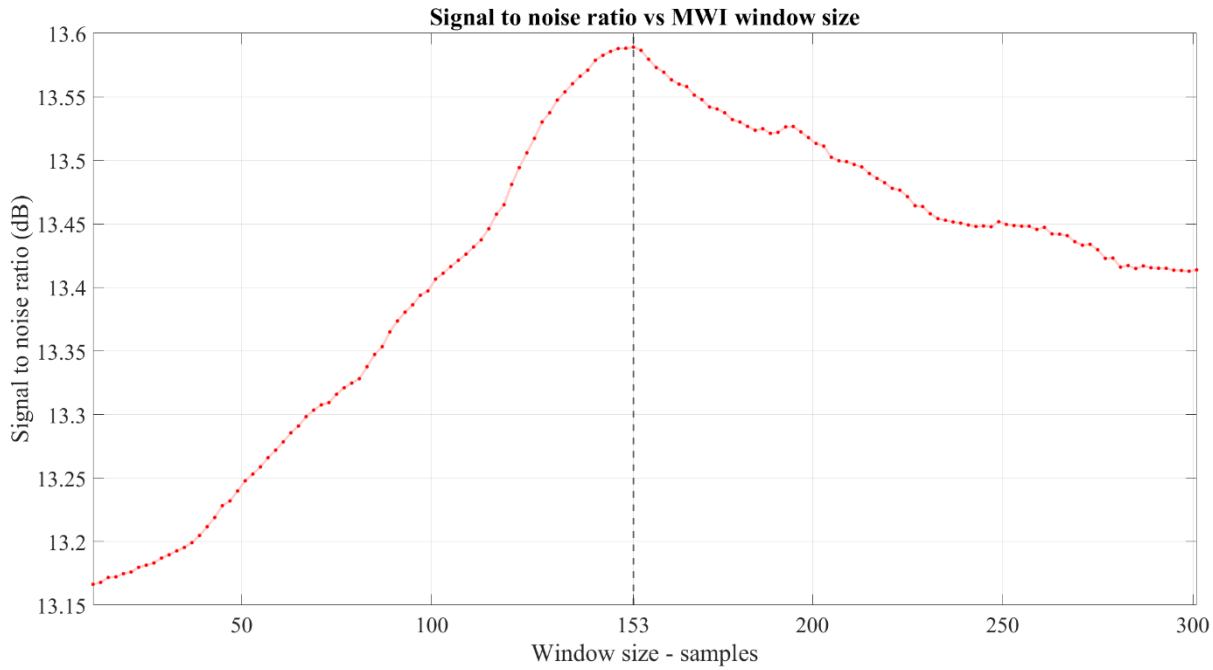

Figure 3.32: SNR for different MWI window sizes. The highest SNR value is achieved at a MWI window size of 153 samples.

Following the same naming convention as before the outputs of the moving window integrator for the IFIS and IFDS are MWIIFIS and MWIIFDS respectively. Figure 3.33 shows the outputs of the MWI for each IF signal. The purple and the orange vertical bands highlight spikes in the IFIS and IFDS signals respectively. Observe how the MWIIFIS is high and MWIIFDS is low in the purple band and vice versa in the orange band. Hence, the location of the spikes in the IF signals have been correctly identified by their

respective MWI outputs. Therefore, we can use the comparison algorithm to remove the spikes from the IF signals.

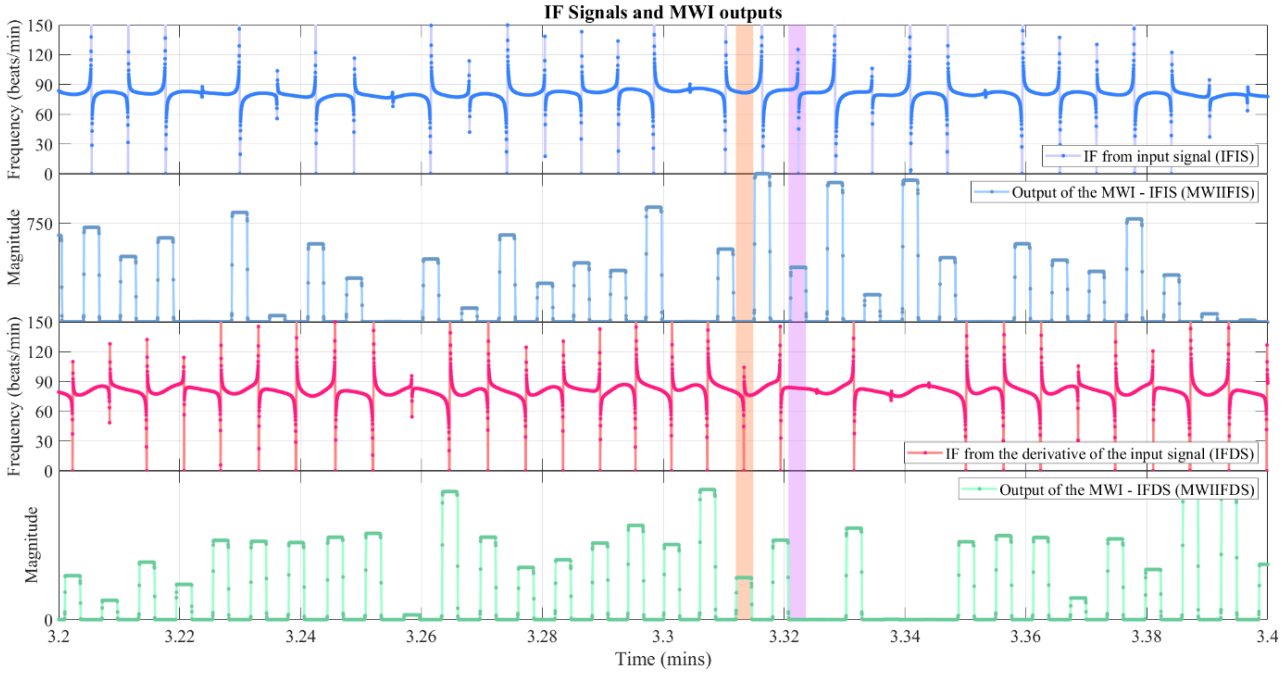

Figure 3.33: IF signals and their corresponding MWI outputs. The purple and the orange vertical bands highlight 2 spikes in the IFIS and IFDS signals respectively.

A segment of the computed final signal (FINSIG) using the comparison algorithm is shown in Figure 3.34.

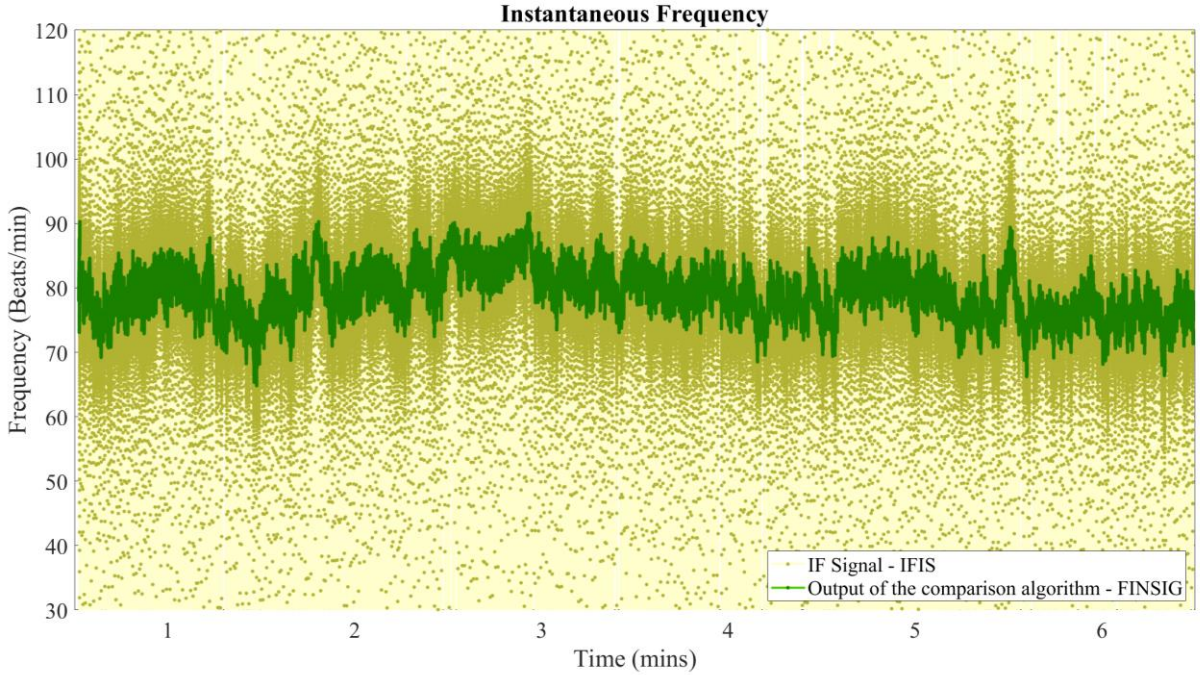

Figure 3.34: Output of the comparison algorithm. The IFIS signal is also plotted (in yellow) for reference.

In Figure 3.34, FINSIG is plotted with the IF signal calculated using the filtered EKG signal (IFIS). For better interpretation, the frequency is presented as beats/min. The effects of the asymptotes have been significantly reduced in the FINSIG. However, the effects have not been eliminated as we can still see small spikes in FINSIG. Some of these spikes result in implausibly rapid fluctuations of the instantaneous heart rate. This can be clearly seen when the FINSIG is compared with the instantaneous heart rate signal calculated using RR intervals (RRSIG). (See Figure 3.35).

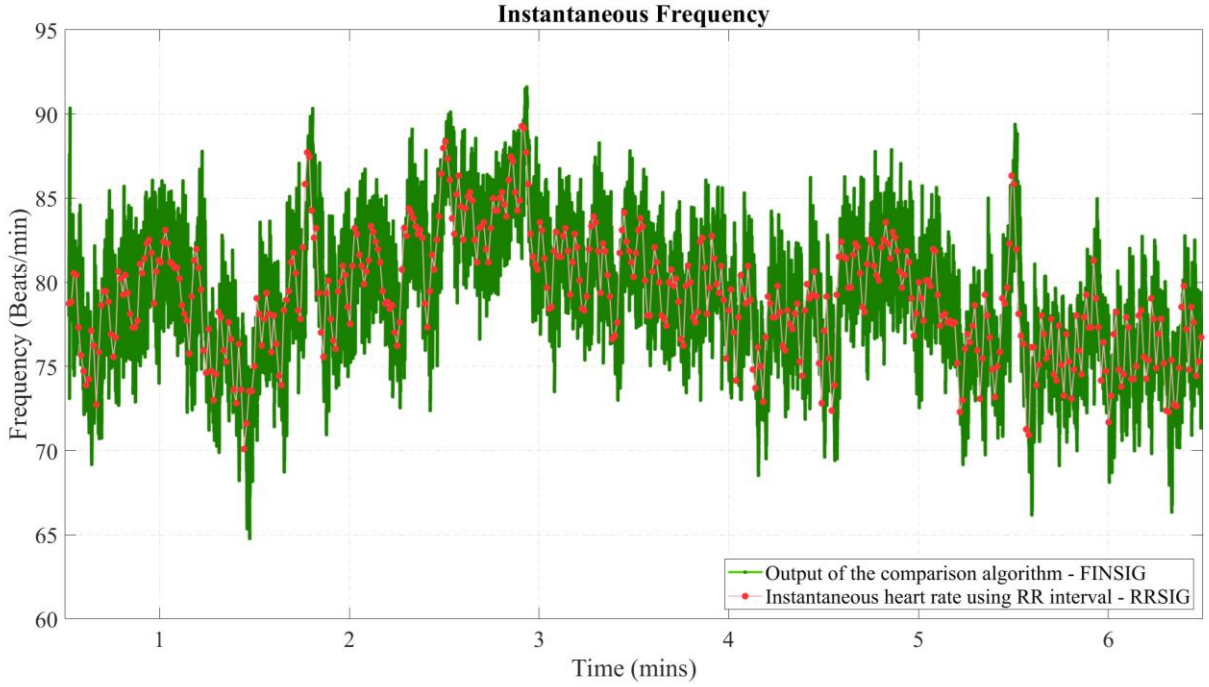

Figure 3.35: Instantaneous Heart rate calculated using different methods.

The overall trend of the FINSIG matches that of the RRSIG. However, FINSIG contains a lot more noise compared to RRSIG because of the effects of the asymptotes. It should be noted however that the RRSIG has considerably lower temporal resolution than FINSIG as it is sampled at an average rate similar to the mean heart rate, which in this case is 1.315 Hz (78.89 beats/min). FINSIG on the other hand is sampled at the same sampling rate as the EKG signal which in this case is 1 kHz. Therefore, one can say that FINSIG contains more information than RRSIG. This notion will be discussed later.

The entire procedure used to calculate FINSIG from the EKG signal can be presented in the flow chart shown in Figure 3.36. In the next chapter, we will assess the suitability of FINSIG and filtered IF signals for HRV calculations and how they compare with the conventional RRSIG.

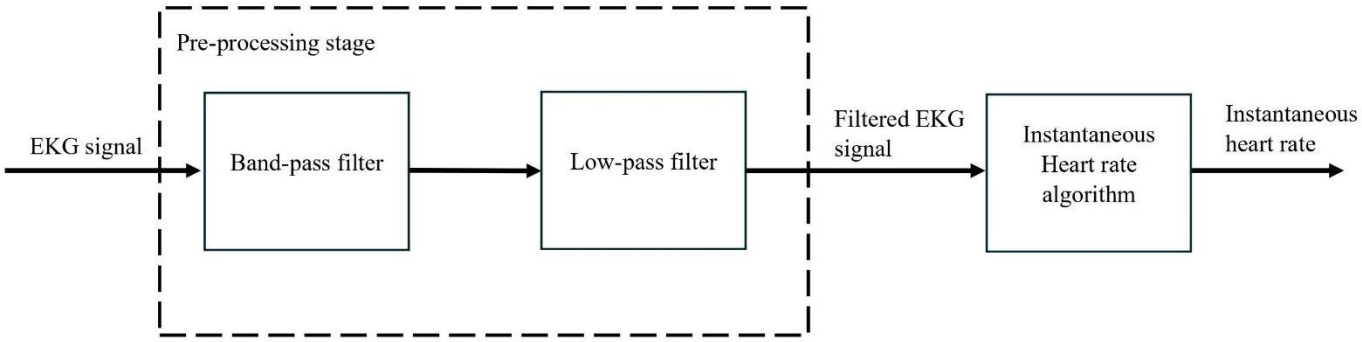

Figure 3.36: Flowchart showing the steps involved in calculating FINSIG from the EKG signal.

3.8 Heart Rate Variability in the Frequency domain.

As discussed before, heart rate variability metrics quantify the variations in the heart rate. In this study, we will mainly focus on the frequency domain analysis of heart rate variability. As discussed in Chapter 2, several digital signal processing techniques can be used to convert instantaneous heart rate signals from the time domain to the frequency domain. These techniques can be applied to the IHR signal calculated using the IF method introduced in this study. However, we will only focus on the most prevalent and popular method which is the Fast Fourier Transform. Before applying the FFT, we will remove the DC offset (bias) from the IHR signal and apply a window to it. The DC offset is present as the mean heart rate is not zero. For frequency domain analysis, we do not care about the actual heart rate values, rather the spectra of the IHR signals. Therefore, removing the DC offset does not affect the spectrum except for the power of the zeroth frequency (DC offset). We apply a simple rectangular window as the signal segment is long enough to render the spectral leakage insignificant. As mentioned before, spectral leakage occurs due to the rapid transitions that could occur at the boundaries of the segmented signal. [61] Many different types of

windowing functions have been used in spectral analysis of HRV signals with functions such as the Hanning window being very popular. The downside to using a window function is that we lose some information near the beginning and end of the signal due to signal attenuation applied by the window. This leads to amplitude reduction and a loss of total energy in the signal. This can be mitigated using correction factors; however, the caveat being that we can never achieve both amplitude and energy correction. [72] We can mitigate the effects of applying the rectangular windowing function with the use of ENBW when computing the PSD. It is important to note that the window function affects the HRV parameters that are calculated. Therefore, the same window should be applied to all signals that are being assessed.

In this section we will compare the spectra of FINSIG and IFIS against the spectrum of RRSIG. As discussed before the RRSIG is sampled at a variable rate. Therefore, the RRSIG is first linearly interpolated at a sampling rate equivalent to the mean heart rate. The MATLAB function interp1 is used for the interpolation. Biases were removed from all signals and the rectangular window function was applied to them before computing the PSD. The PSD calculated from all IHR signals are shown in Figure 3.37.

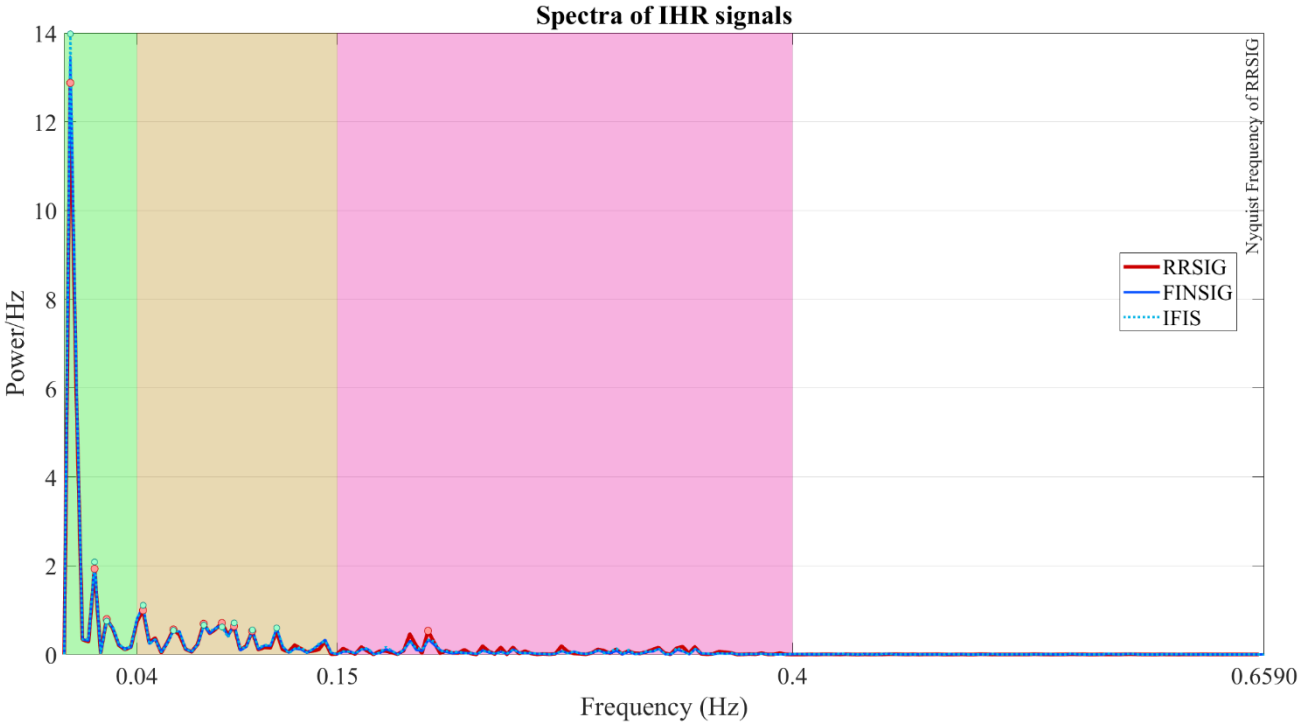

Figure 3.37: PSD of IHR signals. The frequency axis is constructed up to the Nyquist frequency of RRSIG which is equivalent to half the mean heart rate.

The shaded areas of different colors represent different frequency bands in the spectrum. The green region corresponds to the VLF region, the yellow region to LF, and the magenta region to HF. The PSD shows the spectrum up to the Nyquist frequency of the RRSIG, which is equivalent to half the mean heart rate (0.6590 Hz in this example). Note that FINSIG and IFIS have a Nyquist frequency of 500 Hz as the sampling rate is 1 kHz. Therefore, high frequency spectral components, even above the mean heart rate exist in IFIS and FINSIG. However, the relevance of these high frequency components for HRV metric calculations are still not understood. We will elaborate on this in the next chapter.

We can observe that the spectra of FINSIG and IFIS are quite similar to one another. From the PSD we can calculate the total power contained within each frequency band. According to Parseval's theorem, the energy can be calculated by taking the area under the curve of the spectrum. This is applicable to power as well. The area can be calculated by integrating the curve over the specific frequency band. Since the PSD is discrete, this can be approximated by the trapezoidal method.[73]

$$\mathrm{P_f(f)} = \frac{f_b - f_a}{N} \sum_{\mathrm{k=2}}^{N} \frac{\mathrm{PSD[k-1]} + \mathrm{PSD[k]}}{2} \tag{3.55}$$

Where f_a and f_b are the boundary frequencies of the frequency band, PSD[k] is the power density of the k^{th} frequency component and N is the number of discrete data points within the frequency band. Frequency domain HRV metrics are computed by calculating the power contained within certain frequency bands of the spectra of IHR signals. As discussed in Chapter 2, the power can be variable between different recordings and thus it is common to present it as a normalized value by dividing it by the total power (TP) or LF+HF power [74]. TP is the power contained in the spectrum up to the Nyquist rate of the RRSIG. [48] When calculating normalized power, nu1 refers to normalized Powers using TP and nu2 refers to normalized powers using LF+HF. From Figure 3.37 we can observe that IFIS and FINSIG contain more total power compared to RRSIG. Most of this extra power is contained within the high frequency region. On the other hand, RRSIG contains more power in the VLF region. In the next chapter we will further

analyze these metrics and assess the suitability of FINSIG and IFIS for frequency domain HRV parameterization.

Chapter 4 – Results and Discussion

4.1 Overview

In chapter 3 we discussed the theories pertaining to calculating the instantaneous heart rate and analyzing heart rate variability in the frequency domain. In this chapter we will analyze frequency domain HRV metrics calculated using instantaneous heart rate (IFIS), FINSIG and RRSIG of multiple EKG signals. We will then briefly discuss how IFIS can be further processed for time domain analysis and make a comparison between the IF method and RR interval measurement method to estimate the instantaneous heart rate.

4.2 Frequency Domain HRV analysis

In Chapter 3, we walked through the process of calculating the instantaneous heart rate signal using the IF method (IFIS) and generating a relatively cleaned up version of it (FINSIG) from an EKG signal. We then calculated frequency domain HRV metrics from these signals and compared them with the same metrics calculated using the RR interval data (RRSIG). In this section we will do a more thorough analysis of the HRV metrics using multiple EKG signals. These signals are obtained from healthy individuals as well as individuals with heart conditions. We will present the similarities and differences between the HRV metrics but will not analyze them from a medical standpoint as it is out of the scope of this study. However, the results from this study can be used by the medical community to assess if the techniques presented in this study are useful for future HRV related research.

As mentioned before, we are using the publicly available EKG data set published under Kansas State University IRB protocol #9386. This data set includes EKG signals obtained from 40 individuals with and without heart conditions. To assess the robustness of the process to calculate the instantaneous heart rate signal, we will perform the steps presented in Chapter 3 on multiple EKG signals. The following figures are results from some of the EKG signals that were assessed.

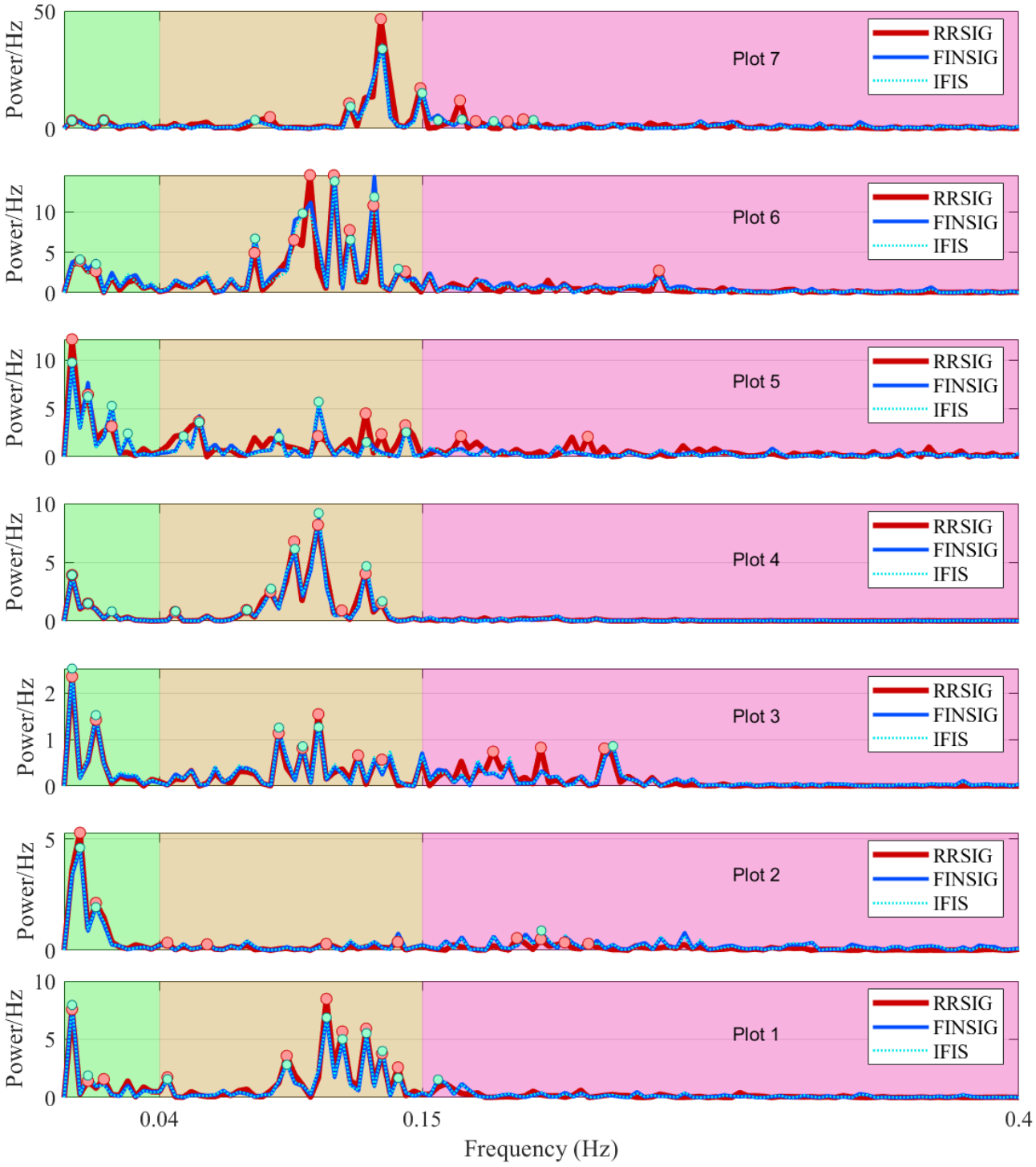

Figure 4.1(a): Power spectral density of IHR signals from different individuals. Each plot contains spectra calculated using RRSIG, IFIS and FINSIG. The markers represent the highest 10 peaks of each IHR signal.

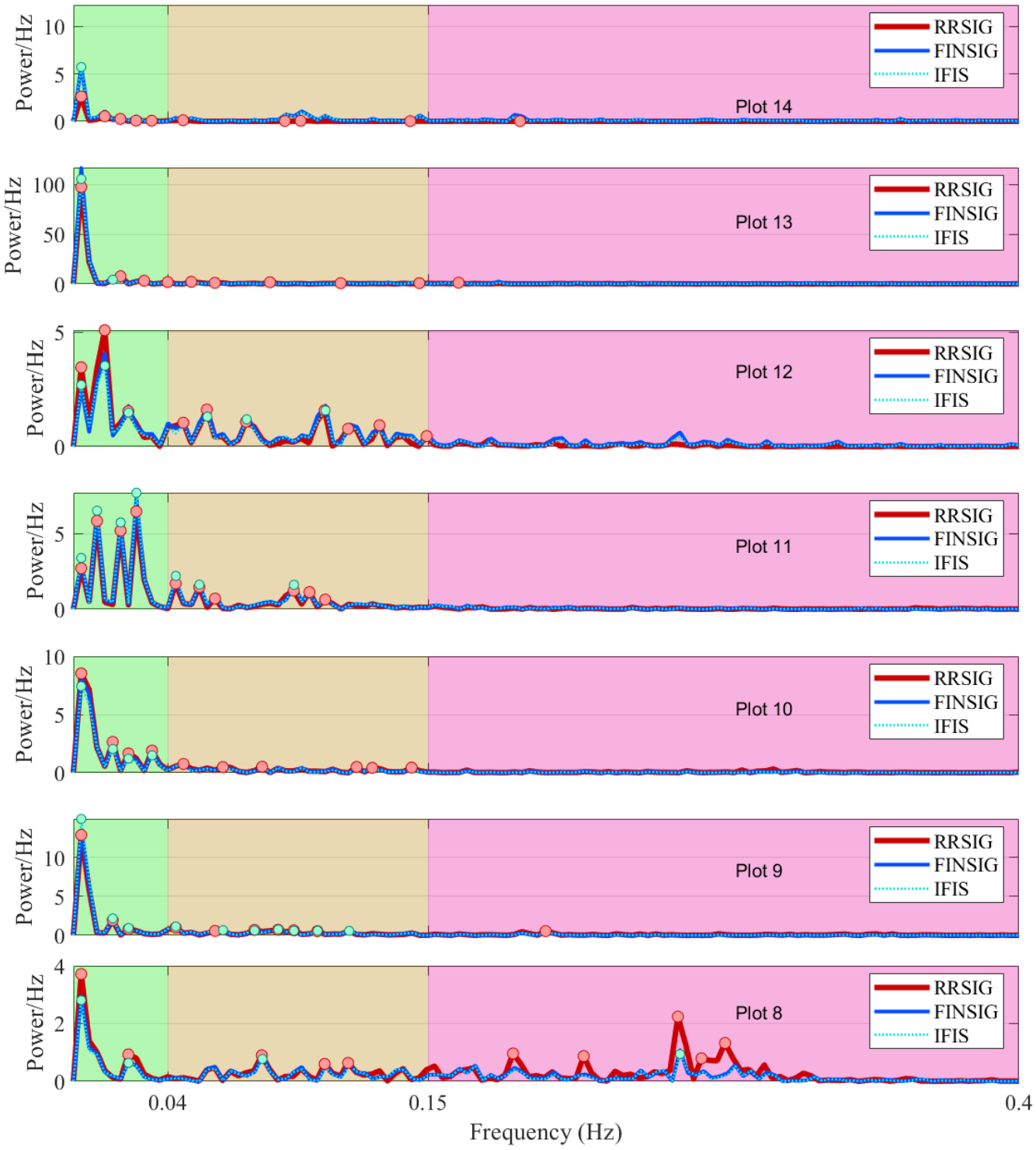

Figure 4.1(b): Power spectral density of IHR signals from different individuals. Each plot contains spectra calculated using RRSIG, IFIS and FINSIG. The markers represent the highest 10 peaks of each IHR signal.

Figure 4.1. shows the power spectral density of IHR signals calculated using 5-minute-long EKG signals from 14 different individuals. Plots 1 to 10 are from individuals without any known heart conditions while plots 11-14 are from individuals with diagnosed heart conditions. The instantaneous heart rate (IHR) signals calculated here are RRSIG, IFIS and FINSIG. The spectrum was then estimated using all 3 IHR signals for each EKG signal. As seen in Figure 4.1, there exists significant variation in the spectra between individuals, but the spectra calculated from different IHR signals (RRSIG, IFIS and FINSIG) of the same person have a somewhat similar distribution. The frequency axis constructed for all signals has the same resolution. This is because the resolution of the frequency axis is dependent on the length of the data vector. For FINSIG and IFIS, the frequencies in the spectrum are multiples of 0.33 Hz. This is because for a 5 min long data vector sampled at 1 kHz the frequency axis resolution is,

$$Res_f = \frac{1000}{5 * 60 * 1000} \tag{4.1}$$

$$Res_f = 0.33 \tag{4.2}$$

The sampling rate of the RRSIG is different for each EKG signal as it is dependent on the mean heart rate. As an example, for a mean heart rate of 75 bpm (1.25 Hz), the RRSIG was first interpolated at a constant sampling rate of 1.25 Hz. The frequency resolution of the RRSIG would then be,

$$Res_{fRR} = \frac{1.25}{5 * 60 * 1.25} \tag{4.3}$$

$$Res_{fRR} = 0.33 \tag{4.4}$$

Therefore, up to the Nyquist frequency of the RRSIG, which is equivalent to ½ of the mean heart rate, all signals contain the same amount of information. In other words, the instantaneous frequency method does not yield any better resolution in the frequency domain than the RR interval method. Signals derived from the IF method has a Nyquist frequency equivalent to ½ the sampling rate of the EKG signal, which in this case is 500 Hz. Therefore, the spectra contain frequencies up to 500 Hz. We know that the spikes in the IFIS signal occur at a rate close to double the instantaneous heart rate. This is because spikes occur at the same rate as the zero-crossing rate of the input signal. Hence frequency components above the zero-crossing

rate are significantly affected by the spikes and do not yield meaningful information related to heart rate variability. However, IFIS provides additional information that is not present in the spectrum of RRSIG between the Nyquist frequency of RRSIG and the zero-crossing frequency of the input signal. As RRSIG is the most prevalent IHR signal used for HRV analysis, we could not find any studies in the literature that analyzed the spectra of IHR signals beyond the Nyquist frequency of RRSIG. Therefore, IFIS is able to provide more information beyond the Nyquist rate of RRSIG for potential future research.

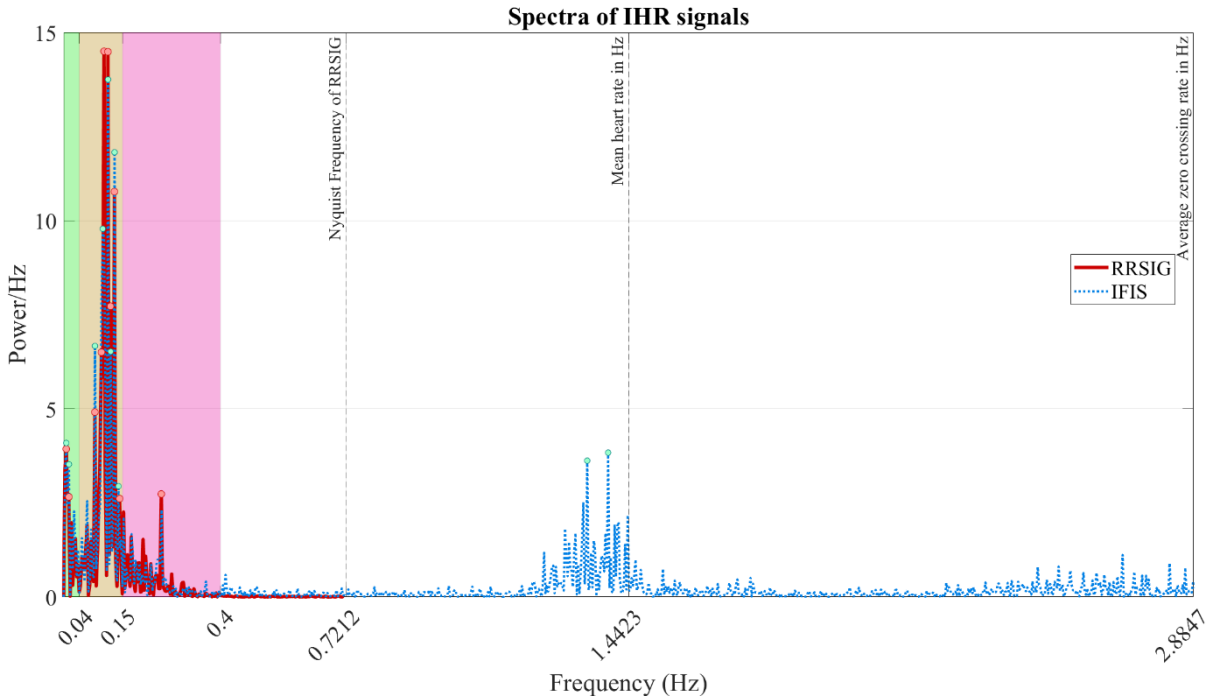

Figure 4.2: Spectra of IHR signals calculated for individual No. 7. The spectrum of RRSIG ends at its Nyquist frequency. The spectrum of IFIS contains frequencies up to 500 Hz (Nyquist frequency of the EKG signal). However, frequency components beyond the average zero crossing rate are heavily affected by the periodic spikes in the IFIS signal. The markers represent the highest 10 peaks of each spectrum.

The importance of frequencies beyond the Nyquist frequency of RRSIG is yet to be determined. Figure 4.2. shows the additional information that IFIS provides in the frequency domain. In addition to the power contained below the Nyquist frequency of RRSIG (typically used for calculating frequency domain HRV metrics), we see some power concentration near the mean heart rate of the EKG signal. We assumed that the filtered EKG signal can be considered as a frequency modulated signal. When looking at the spectrum from that perspective it can be quite difficult to explain why there are frequency components close to the

mean heart rate. If the filtered EKG signal is analogues to an FM signal, the mean heart rate is analogues to the carrier frequency and the IHR signal describes the message signal. If that is the case, we see that the message signal has frequency components very close to the carrier frequency. Usually, the message signal is comprised of frequencies much lower than the carrier frequency. One can argue that these frequencies are remnants of the spikes introduced by the IF algorithm. To see if this is the case we can go back to the example FM-AM signal we introduced in section 3.5. We consider this signal as we have a priori knowledge of the message signal. If the frequency components seen in Figure 4.2 near the mean heart rate are a result of the spikes, we should observe such peaks near the carrier frequency in the FM-AM signal's spectrum as well.

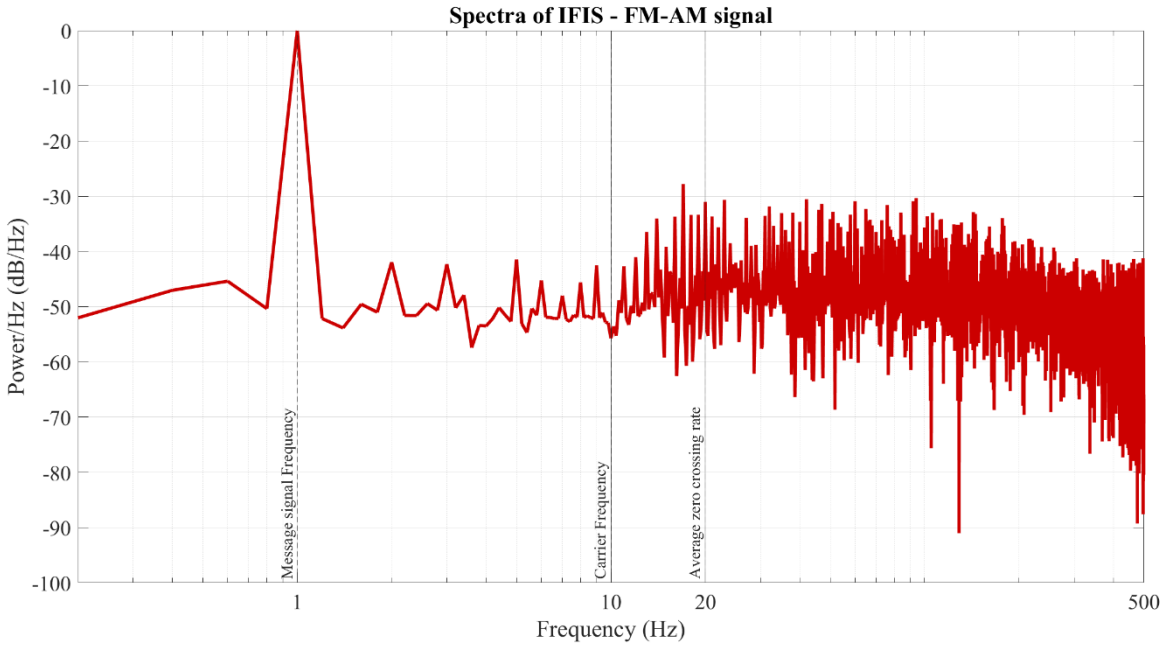

Figure 4.3: Spectrum of the example FM-AM signal presented in section 3.5. The frequency axis (x-axis) is in log scale. There are no significant spectral peaks near the carrier frequency.

Figure 4.3 shows the spectrum of the example FM-AM signal. The magnitude is presented in dB for ease of interpretation. Observe how there are no significant peaks near the carrier frequency (not significant as the magnitude is below -40 dB). We can, therefore, say with some confidence that the spectral peaks present in the IHR signal (see Figure 4.2) near the mean heart rate are not produced by the IF algorithm nor the spikes. Therefore, these spectral peaks may possess information that might be useful for HRV analysis. In

Figure 4.4. the spectra up to 3 Hz of IFIS signals calculated from EKGs obtained from all 14 individuals have been plotted. The black dashed lines represent the mean heart rate in Hz of each EKG signal from which the IFIS signal was computed. Observe how certain spectra do not contain any spectral peaks around the mean heart rate while others do.

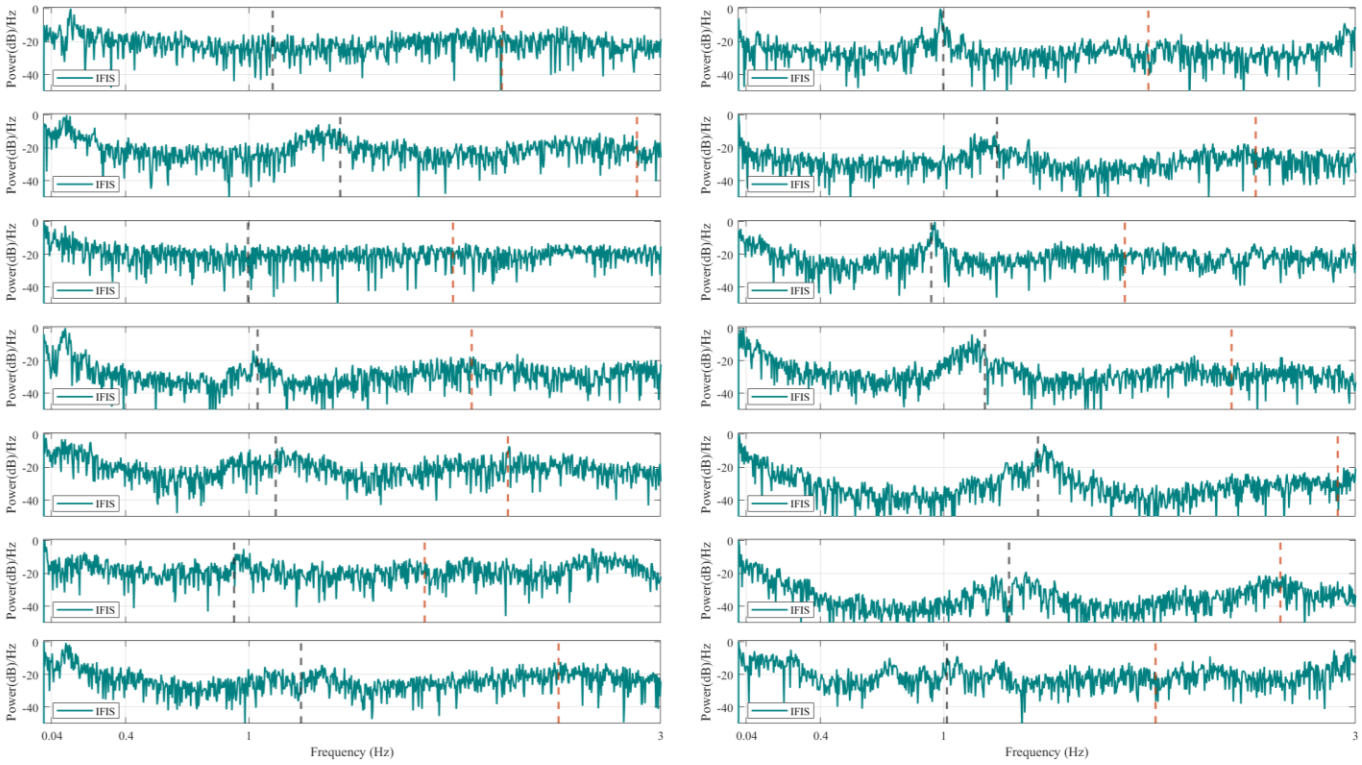

Figure 4.4: Spectra of IFIS signals computed from different EKG signals. The black dashed lines represent the mean heart rate and the orange dashed lines represent the average zero-crossing rate of the filtered EKG signal.

The most challenging aspect of the study is that we have no information of the actual heart rate modulating signal. Without knowing the actual signal, we cannot assess how well RRSIG and the signals calculated using the IF method (IFIS and FINSIG) estimate the modulating signal. This is like demodulating an FM signal and analyzing it without any knowledge of the original message signal. We cannot make a fair comparison between RRSIG and IFIS/FINSIG as well. This is because as discussed, the accuracy of RRSIG is dependent on the robustness of the peak detection method. Further, RRSIG's temporal resolution is significantly less than that of IFIS and FINSIG. Additionally, it is impossible to prevent deformation of the RRSIG during interpolation. Although the IF method addresses some concerns associated with calculating

RRSIG, it introduces a new problem in the form of discontinuities (vertical asymptotes at zero crossings) in IFIS. In section 3.6, we introduced a method to mitigate the effects of such asymptotes that led to the creation of FINSIG. However, this method was not successful at eliminating the effects completely. Due to this reason, in the time domain, FINSIG is relatively noisy and is not recommended for HRV analysis. The actual effect the spikes have on the spectrum of the signal is difficult to predict in the frequency domain. One can assume that these spikes have the same effect as impulses, and therefore the energy within each spike will be distributed uniformly along the spectrum in the frequency domain. This is because for an impulse in the time domain, the spectrum is flat with all frequencies having equal power. [75] However, this assumption is questionable as the spikes present in the IFIS signals are not merely impulses, rather artifacts resulting from vertical asymptotes. Furthermore, as we have no information of the actual heart rate modulating signal (message signal), it is impossible to extract the error signal from IFIS. Therefore, an accurate assessment of how the spikes in the IFIS signal affect the spectrum cannot be done. It is, however, possible to compare the spectra of IFIS and RRSIG within the frequency range of 0 Hz to ½ of the mean heart rate and see how they match up. This is because the spectrum of the RRSIG is the only other available spectrum that estimates the true spectrum of the heart rate modulating signal. From Figure 4.1. we can see that for a given EKG signal the frequency distribution of the RRSIG and IFIS are quite similar. The tallest 10 peaks of the spectra derived from RRSIG (pink markers) and IFIS (turquoise markers) are also marked on Figure 4.1. Peak markers of FINSIG were not plotted for clarity as they land on the same locations as the markers of IFIS. Peaks belonging to the RRSIG and IFIS spectra predominantly occur at the same frequency components for a given EKG signal. The magnitude of peaks of IFIS and FINSIG are almost identical. However, there exists some variation between peak magnitudes of the IF signals and the magnitudes of their counterparts in RRSIG. The effects of these variations will manifest in the frequency domain HRV parameters. This is because these metrics are based on the power contained within certain frequency ranges of the spectrum. To assess this, frequency domain HRV parameters from RRSIG, IFIS and FINSIG for all EKG signals were calculated. Some of the key HRV parameters are summarized in table 4.1. Apart from Total power, all other HRV metrics in table 4.1. are expressed as normalized values.

Normalized HF values are not listed as they can be derived from LF values as LF+HF = 1. We will not discuss the significance of the values of the HRV parameters to assess medical conditions and cardiovascular health as that is out of the scope of this study.

Table 4.1: HRV metrics.

	Plot No.	Mean HR	Total Power			VLF (normalized using TP)			LF (normalized using LF+HF)			LF/HF		
			RRSIG	FINSIG	IFIS	RRSIG	FINSIG	IFIS	RRSIG	FINSIG	IFIS	RRSIG	FINSIG	IFIS
Normal male	1	75	0.2503	0.2412	0.2423	0.1460	0.1452	0.1409	0.8291	0.7723	0.7701	4.8530	3.3921	3.3492
Normal male	2	55.6	0.0859	0.1129	0.1095	0.4902	0.3238	0.3433	0.3822	0.2598	0.2670	0.6185	0.3511	0.3642
Normal male	3	67.7	0.0787	0.0849	0.0873	0.1904	0.1865	0.1935	0.5461	0.5494	0.5527	1.2032	1.2193	1.2355
Normal male	4	62.4	0.2006	0.1983	0.2057	0.1162	0.1181	0.1149	0.9359	0.9217	0.9213	14.5949	11.7792	11.6993
Normal female	5	59.7	0.3684	0.2901	0.2803	0.2352	0.3058	0.3071	0.5931	0.6336	0.6163	1.4574	1.7296	1.6061
Normal female	6	86.5	0.4709	0.5914	0.5269	0.1201	0.1199	0.1206	0.7919	0.7693	0.7824	3.8057	3.3338	3.5961
Normal female	7	66.8	0.8511	0.8584	0.7711	0.0579	0.0623	0.0625	0.6460	0.5457	0.5676	1.8250	1.2009	1.3124
Normal female	8	60.9	0.1264	0.0908	0.0852	0.1825	0.2059	0.2093	0.3021	0.4149	0.4117	0.4329	0.7092	0.6998
Normal female	9	79.1	0.1303	0.1269	0.1391	0.4261	0.4614	0.4662	0.6570	0.7791	0.7778	1.9156	3.5262	3.5004
Normal male	10	87.4	0.1297	0.1186	0.1058	0.5707	0.5946	0.5850	0.7092	0.7813	0.7840	2.4384	3.5715	3.6289
Hypertension - male	11	72	0.1332	0.1503	0.1563	0.5726	0.5547	0.5578	0.8377	0.8245	0.8227	5.1624	4.6979	4.6416
Supraventricular Tachycardia - male	12	56.4	0.1279	0.1491	0.1269	0.4273	0.3153	0.3454	0.8456	0.7159	0.7550	5.4783	2.5203	3.0811
Atrial Filbrillation - female	13	75.5	0.5712	0.7526	0.6336	0.5250	0.4609	0.4879	0.5744	0.4165	0.4818	1.3496	0.7138	0.9297
Coronary Artery Disease - female	14	59.8	0.0164	0.0825	0.0784	0.5706	0.2417	0.2587	0.7491	0.4799	0.5272	2.9860	0.9226	1.1150

To visualize and make a better comparison, the calculated HRV metrics were plotted. From figure 4.5, we can see that the total power calculated for a particular EKG signal has very little variation between the different IHR signals. This is expected as the spectra of the IHR signals calculated from a particular EKG has a somewhat similar distribution. However, Figure 4.5. can be deceiving as it doesn't quite capture the variations between the total power calculated from different IHR signals of the same EKG signal. To get a

better understanding, the absolute differences between the total power values were calculated. These values were computed as follows,

$$TP_{|RRSIG-FINSIG|} = \frac{100|TP_{RRSIG} - TP_{FINSIG}|}{TP_{RRSIG}} \% \quad (4.5)$$

$$TP_{|RRSIG-IFIS|} = \frac{100|TP_{RRSIG} - TP_{IFIS}|}{TP_{RRSIG}} \% \quad (4.6)$$

$$TP_{|IFIS-FINSIG|} = \frac{100|TP_{IFIS} - TP_{FINSIG}|}{TP_{IFIS}} \% \quad (4.7)$$

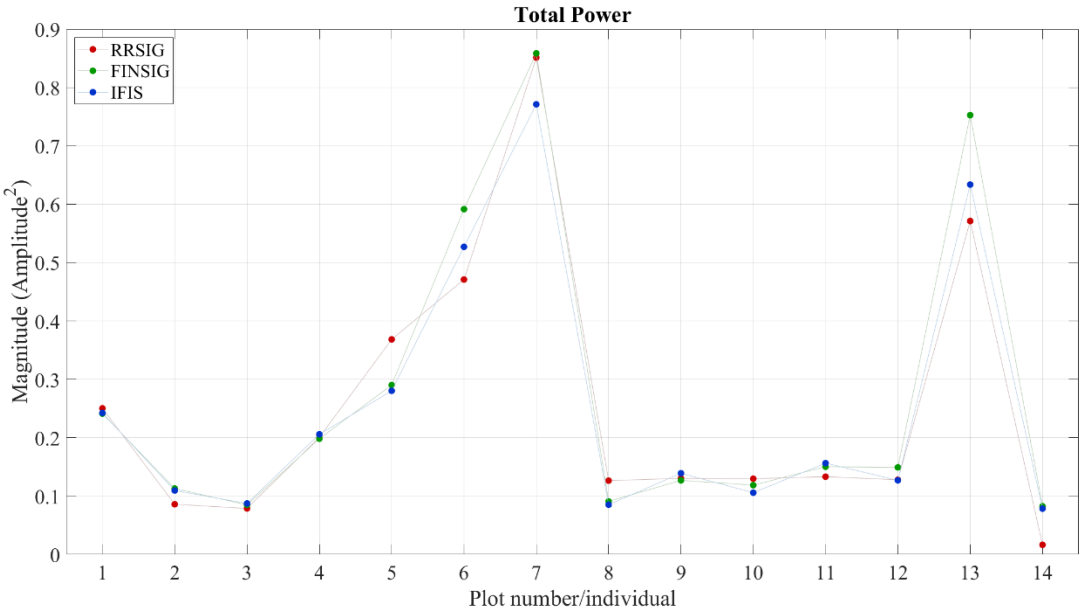

Figure 4.5: Total power in the frequency range of 0 Hz to mean heart rate.

The absolute percentage differences are shown in Figure 4.6. From the plot we can see that the percentage difference between the TP values of IFIS and FINSIG are relatively low for a given EKG signal. The maximum variation occurs in female with atrial fibrillation (plot 13), with a percentage difference of 18.7%. The differences between the TP values calculated using RRSIG and the IF signals show more variability for a given EKG signal. Except for individual No. 14, the absolute difference stays below 33%. The maximum variability occurs for individual No 14. with coronary artery disease. Although the percentage difference is 402% for this subject, the total power contained in the IHR signals is the lowest of all

considered subjects. Although the energy contained within the spectra are significantly different for this individual, the spectral peaks occur at the same frequency components (see plot 14 in Figure 4.1). Through our analysis we can conclude that the TP values follow a similar trajectory regardless of the method used to calculate them. However, there is a significant difference between the actual values calculated from the IF signals and RRSIG of a given EKG signal. The difference between the values calculated from IFIS and FINSIG are comparatively low.

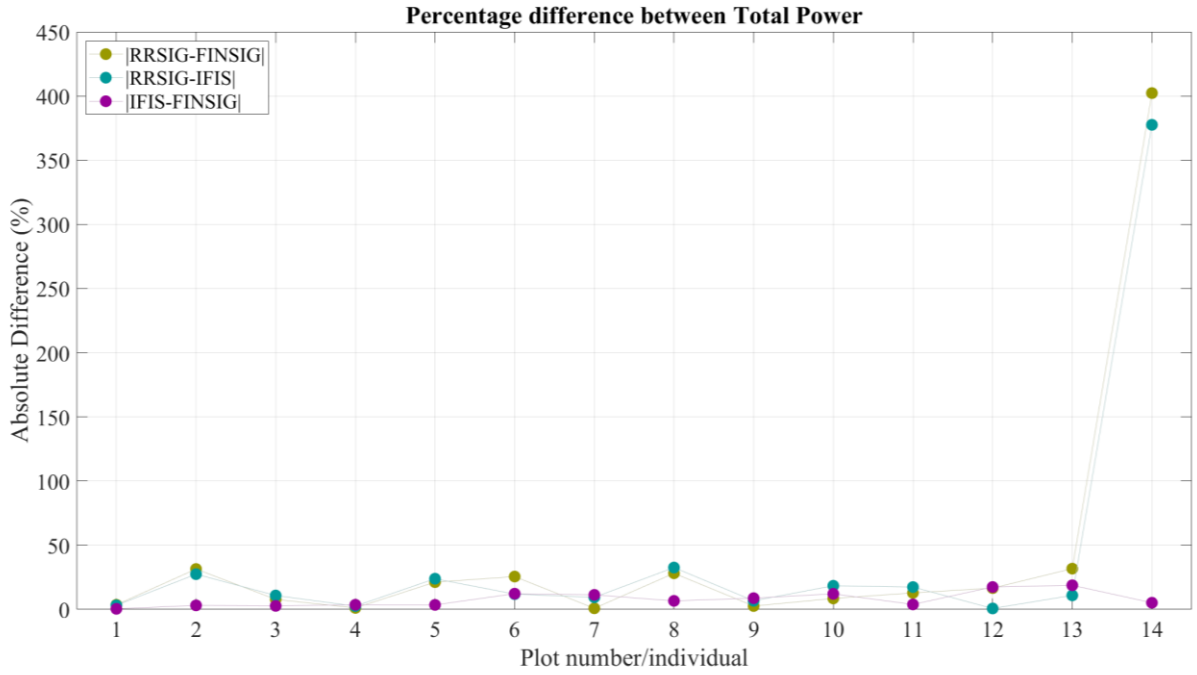

Figure 4.6: Percentage difference in TP values calculated using different IHR signals.

In frequency domain analysis, it is more common to assess normalized power contained withing certain frequency bands of the spectrum. These metrics help researchers assess the body's regulation of autonomic balance among other things. The power within the VLF band normalized using the total power, is presented in Figure 4.7. Again, we can see that excluding the value calculated from EKG measured from subject no.14, all other VLF values calculated from the IF signals and RRSIG show a similar trajectory. Similar to what was done with TP, the absolute difference between signals were calculated and are presented in Figure 4.8. The percentage difference between values derived from RRSIG and IF signals remain below 34% for

all subjects except No.14, for whom it is about 58%. The variation between the values calculated from IFIS and FINSIG remains very low, with a maximum percentage difference of 8%.

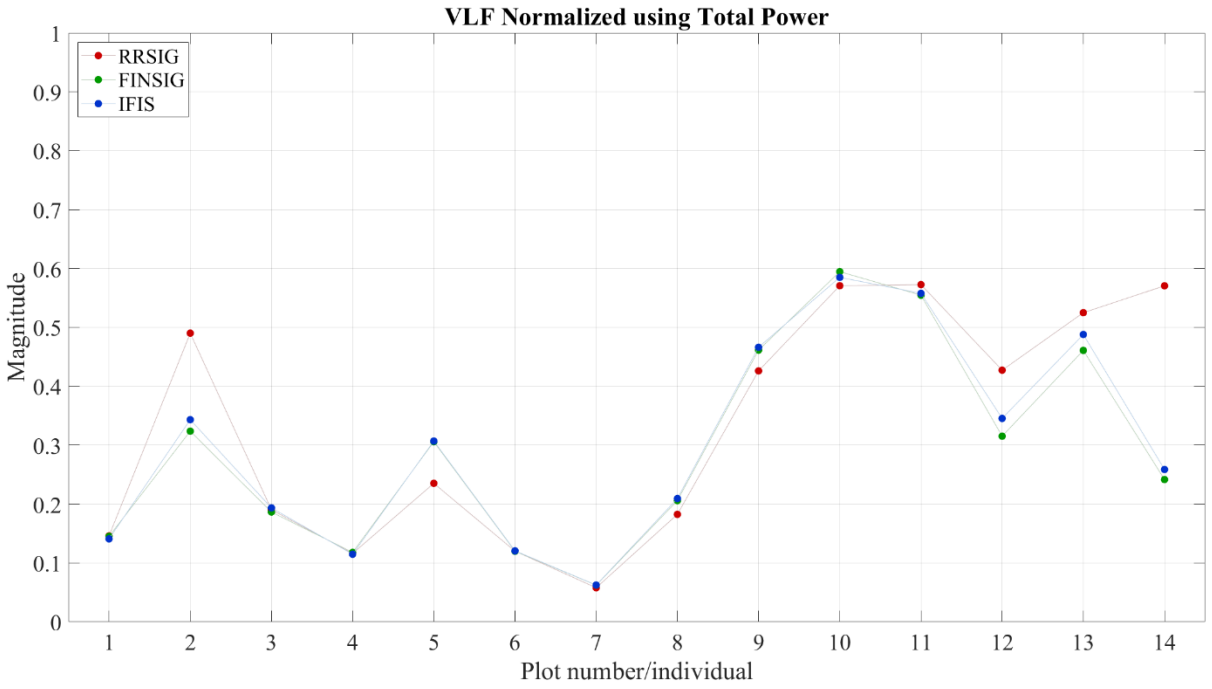

Figure 4.7: VLF Power normalized using Total Power.

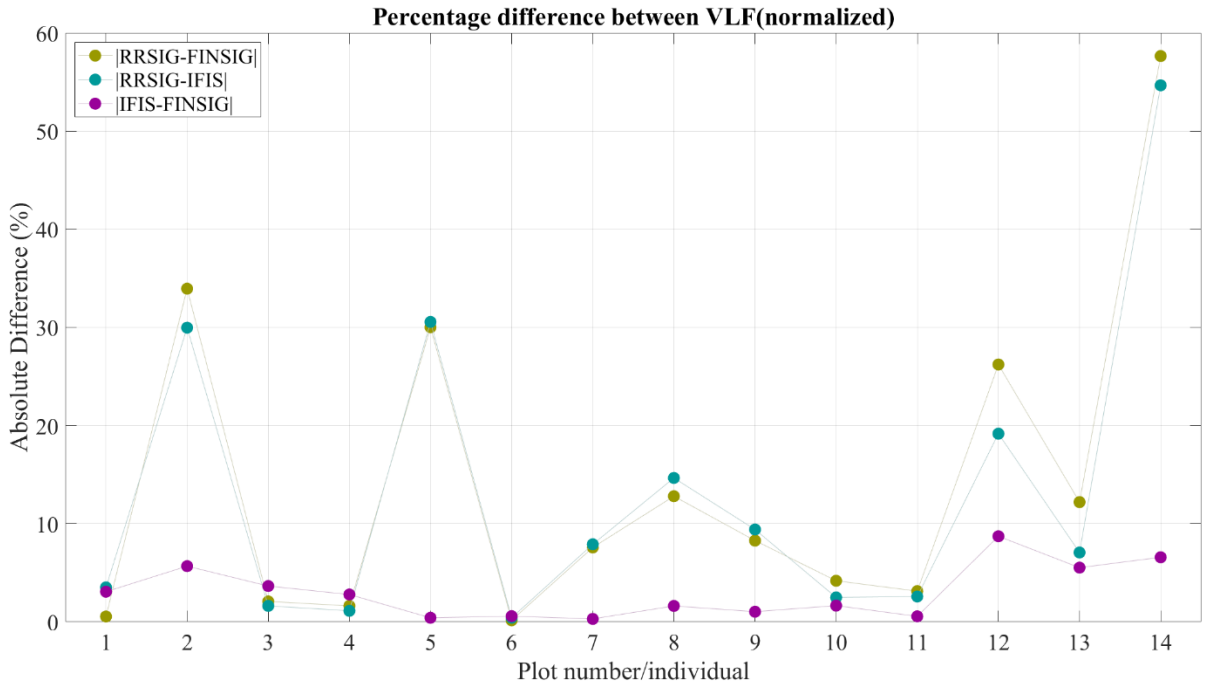

Figure 4.8: Percentage difference between VLF power calculated using different IHR signals.

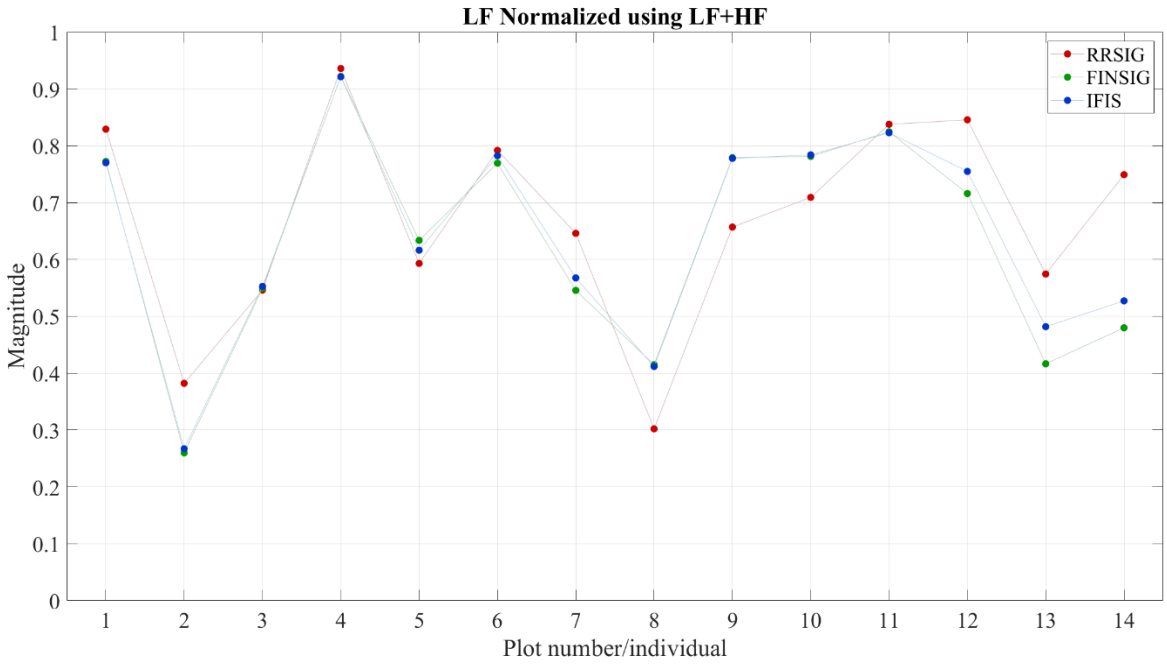

Figure 4.9: LF Power Normalized using Power within LF and HF frequency bands.

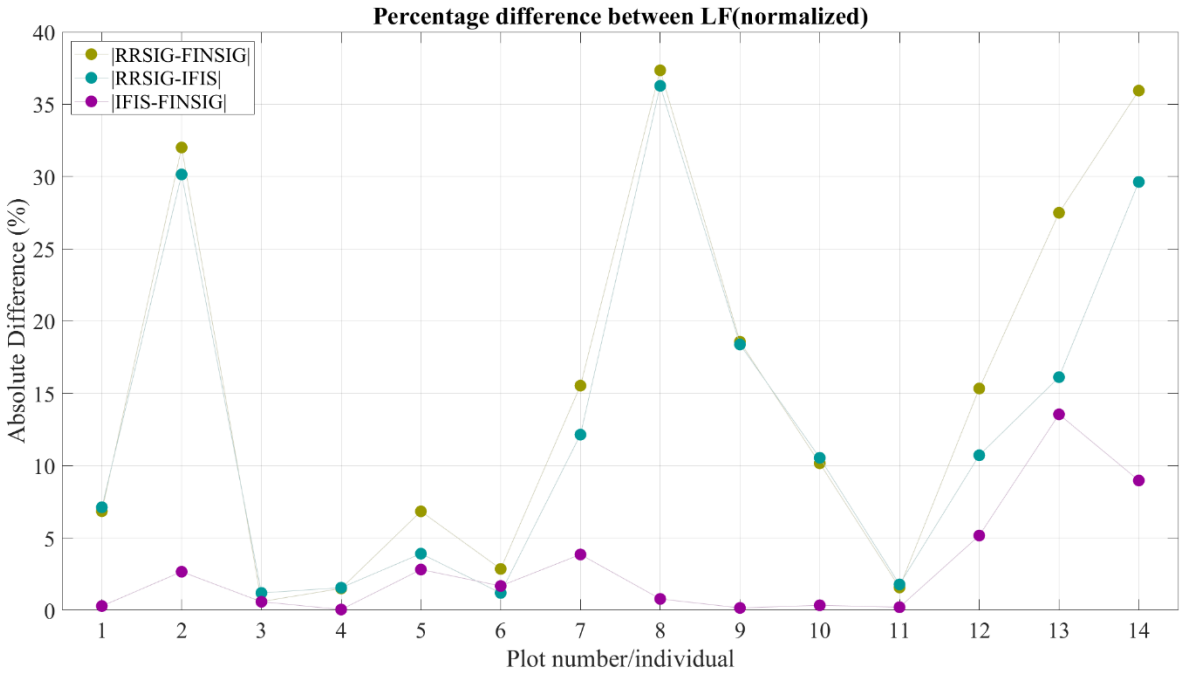

Figure 4.10: Percentage change between LF Power calculated using different IHR signals.

It is common to normalize power within the LF and HF bands by dividing them by the total power contained within the LF and HF bands. Therefore, normalized power in the LF and HF bands follow the relationship,

LF+HF = 1. As such, knowing one normalized metric is enough to derive the other. In Figure 4.9. the normalized power in the LF bands of each EKG signal is presented. The normalized LF powers calculated using different IHR methods somewhat match up, although there is considerable variation between the values calculated using RRSIG and the IF signals. A maximum percentage difference of about 37% is observed between values derived from RRSIG and IFIS for healthy subject no. 8. The percentage difference between the values derived from IFIS and FINSIG remains below 14% for all subjects.

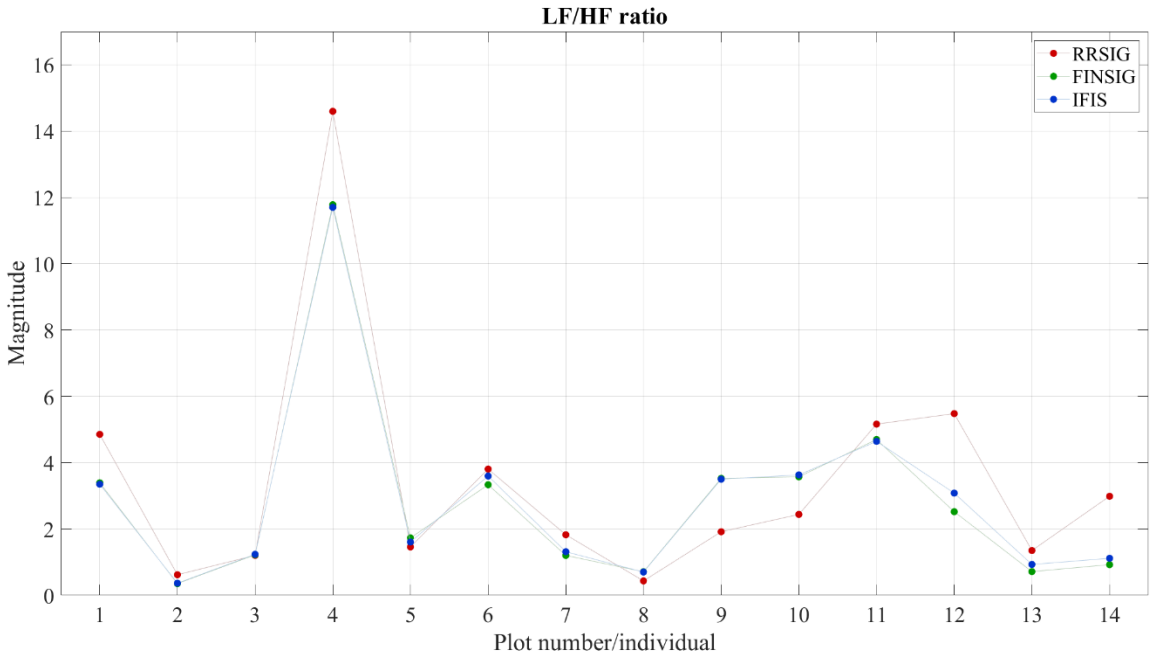

Figure 4.11: LF/HF ratio.

Finally, we observe the ratio between the power within the LF and HF bands (LF/HF). This is a popular HRV metric that may estimate the activity level between the sympathetic and parasympathetic nervous system. [44] Figure 4.11. shows the calculated values and Figure 4.12 shows the absolute differences between the values derived from the different IHR signals. Similar to other calculated HRV metrics, we can observe a higher percentage difference between values calculated using RRSIG and IF signals but a relatively lower percentage difference between values calculated using the two IF signals (IFIS and FINSIG).

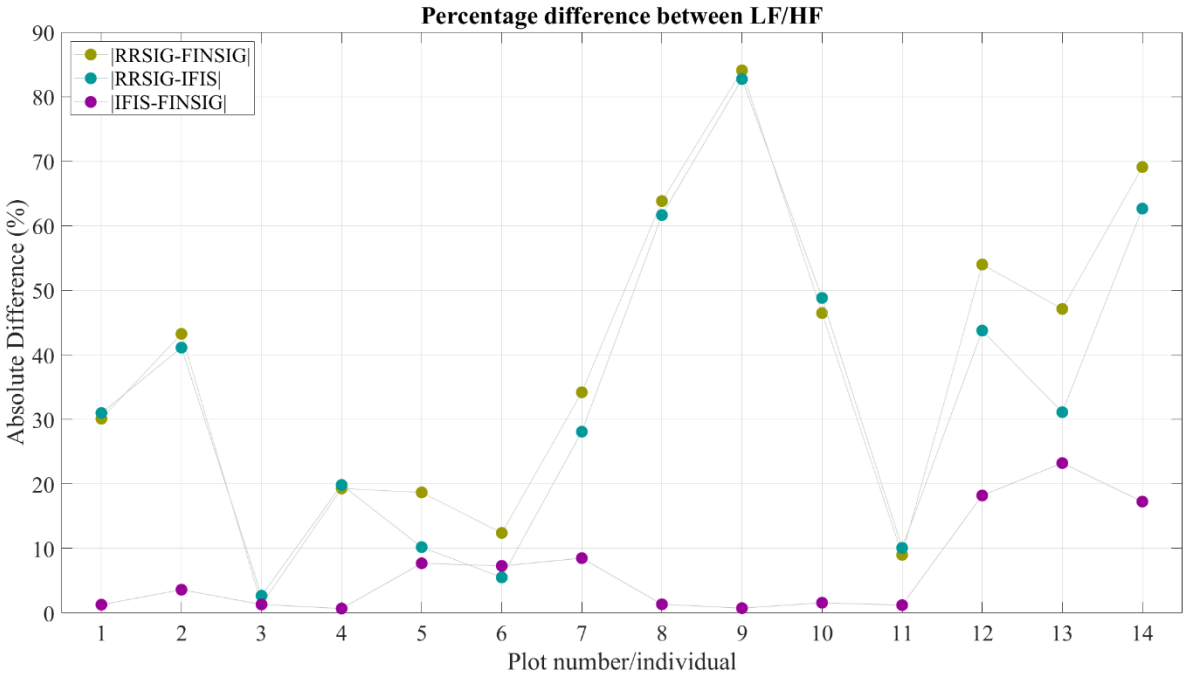

Figure 4.12: Percentage difference between LF/HF ratios calculated using different IHR signals.

As mentioned previously, we cannot perform a true analysis of the HRV metrics calculated using the IF signals introduced in this study. This is because we do not have the true heart rate modulating signal and thus the true HRV metrics to compare our values with. In this chapter, we compared the values of the HRV metrics derived from the IF signals with the corresponding values obtained from RRSIG. This is because RRSIG is the only other IHR signal that estimates the true heart rate modulating signal and is the most prevalent IHR signal used in HRV analysis. We observed that the values of the HRV metrics follow a similar pattern/trajectory regardless of the IHR signal being used. Thus, there is correlation between the values derived from the IF signals and RRSIGs. However, the percentage difference between the values derived from IF signals and RRSIGs are considerably large. Therefore, it is imperative to never compare HRV metrics calculated using different IHR signals. Researchers should always stick to one method of estimating the IHR signal to maintain consistency between calculated values. It was also apparent that for frequency domain analysis at least, the IFIS signal is sufficient for calculating HRV metrics. It is not required to remove spikes in the IFIS signal as the spectrum is not significantly affected by them for the frequency range that is considered for HRV analysis. This is evident by the relatively low percentage

difference between the values calculated using FINSIG and IFIS. Furthermore, low pass filtering the IFIS signal adds additional delay to it which can be undesirable. In the next section of this chapter, we will discuss low-pass filtering the IFIS signal which may enable time domain HRV analysis using the filtered IFIS signal.

4.3 Time domain HRV analysis and Future Work.

In this study we only focused on frequency domain HRV analysis as neither IFIS nor FINSIG are suitable for time domain HRV analysis due to the high level of noise present in them. In this section we will briefly talk about how the IFIS signal can be processed to remove high frequency noise and potentially make it suitable for time domain HRV analysis. It is possible to spend a significant amount of time choosing a filtering method to remove spikes from IFIS. In chapter 3 of this thesis, we introduced a spike removal method that was able to somewhat attenuate the high frequency noise in the signal. However, the resultant signal was still not suitable for time domain HRV analysis. In this section we will filter the IFIS signal in the frequency domain using an ideal low pass filter and compare it with RRSIG visually. Further research should be done to assess the suitability of the filtered IFIS signal for time domain HRV analysis.

In chapter 3, we discussed how a time domain signal can be transformed into the frequency domain using the Fourier Transform. We also saw that a time domain signal can be reconstructed from the spectrum using the inverse Fourier Transform. We will use this reversibility of the Fourier Transform to filter the IFIS signal in the frequency domain and reconstruct a clean signal in the time domain. For HRV analysis, researchers use the instantaneous heart rate signal calculated using RR intervals (RRSIG) which, once interpolated, has a Nyquist frequency equivalent to ½ the mean heart rate of the signal. For consistency, we can design an ideal low pass filter with a cut off frequency equivalent to ½ the mean heart rate of the signal. We can obviously use a cut-off frequency much higher than this but with a higher cut-off frequency, the less effective the filtering process will be at removing spikes. Again, we will not focus on the effects of the cut-off frequency on the IFIS signal and how much information is lost by choosing the cut-off frequency

equivalent to the Nyquist Frequency of RRSIG. This will requires further analysis. An ideal filter has a step shape in the frequency domain as seen in Figure 4.13.

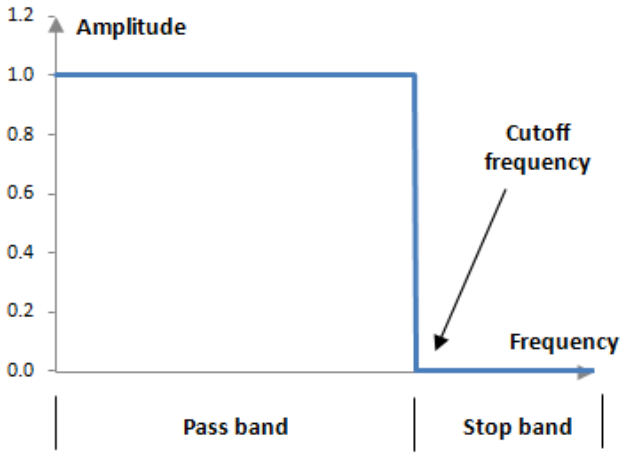

Figure 4.13: Frequency Domain representation of an Ideal Low Pass Filter.

Filtering a signal in the time domain involves convolving the signal with the impulse response of the filter. It is known that convolution in the time domain is equivalent to multiplication in the frequency domain. [76] As such, we can simply multiply the Fourier Transform of the IFIS signal with the frequency response of the ideal low pass filter shown in Figure 4.13 to filter the IFIS signal. We can then compute the inverse Fourier Transform of the filtered IFIS spectrum to generate a clean IFIS signal. The green curves in Figure 4.14. corresponds to the filtered IFIS signals and the red curves are the RRSIGs. Visually, the filtered IFIS signals closely resemble their corresponding RRSIGs except for No. 14. This variation was also observed in the frequency domain HRV metrics of subject No. 14, where the HF power was significantly higher in the IF signals compared to RRSIG. In plot 7 of Figure 4.14. we see a sharp spike in the RRSIG. This is a result of the selected threshold capturing a peak in the EKG signal which is not an R peak. The extra peak detected is shown in Figure 4.14. This is an excellent demonstration of one of the biggest pitfalls of measuring heart rate based on R peaks.

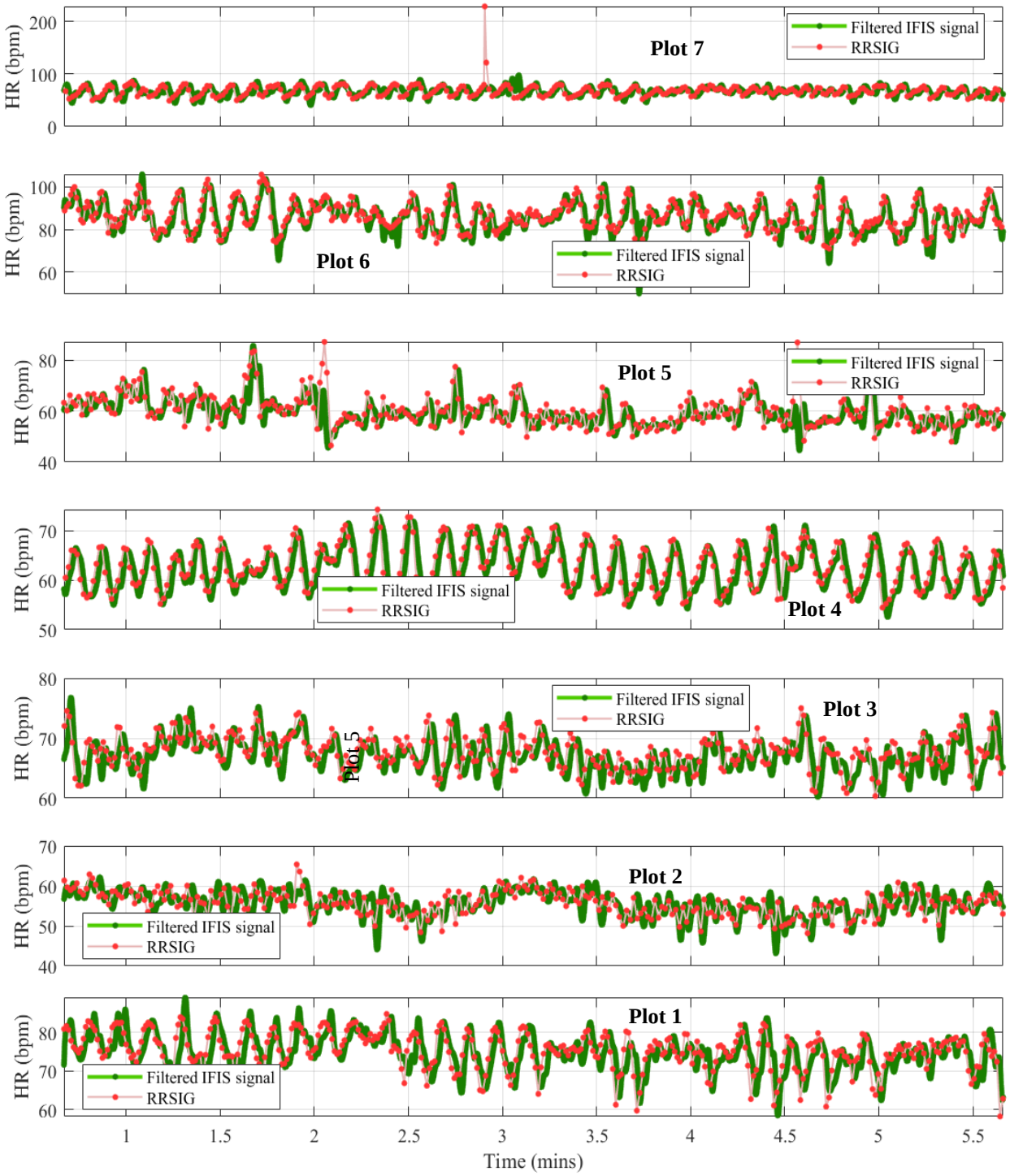

Figure 4.14(a): Filtered IFIS signal (using ideal low-pass filter) shown in green. The red curve is the RRSIG plotted for reference.

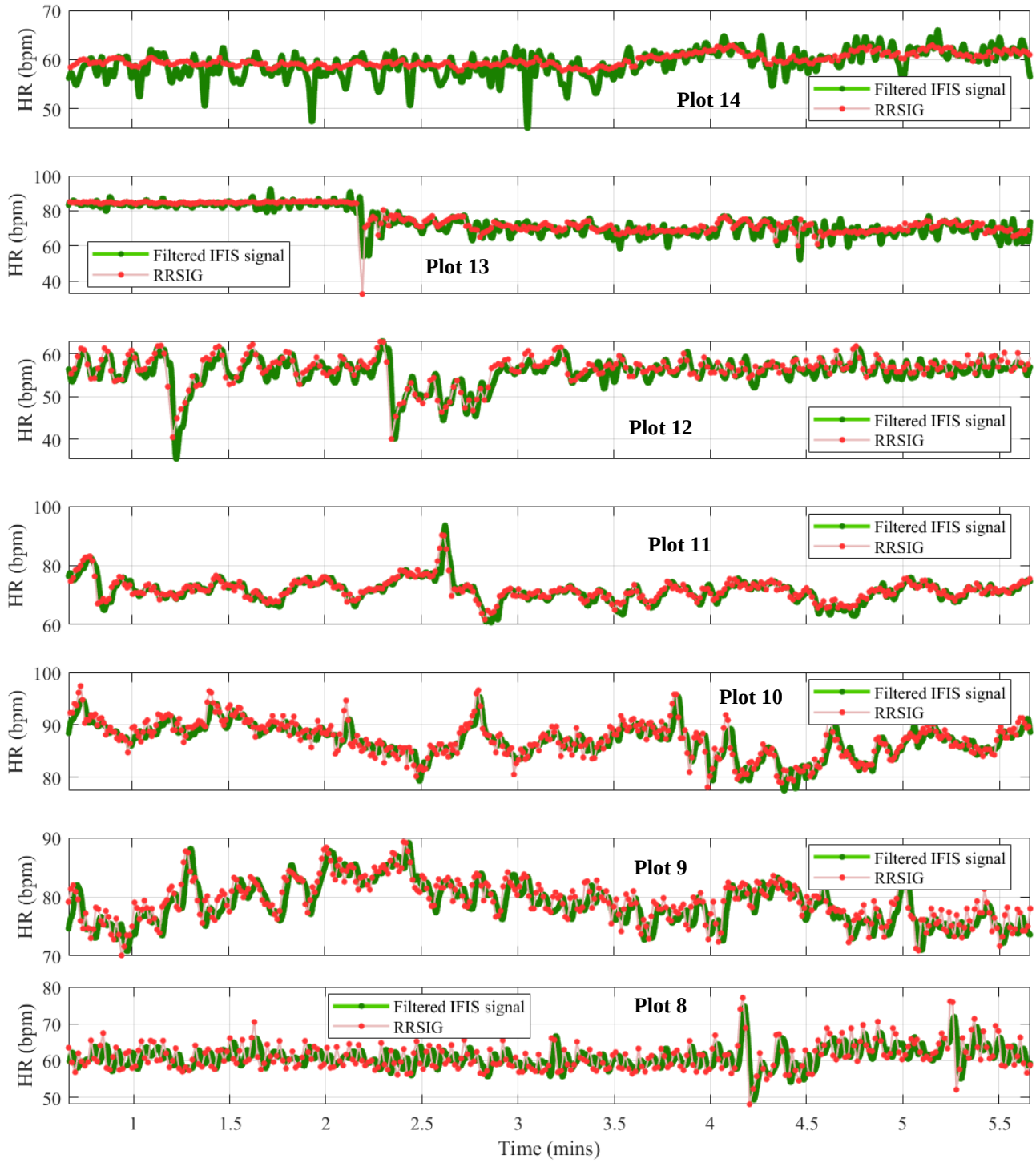

Figure 4.14(b): Filtered IFIS signal (using ideal low-pass filter) shown in green. The red curve is the RRSIG plotted for reference.

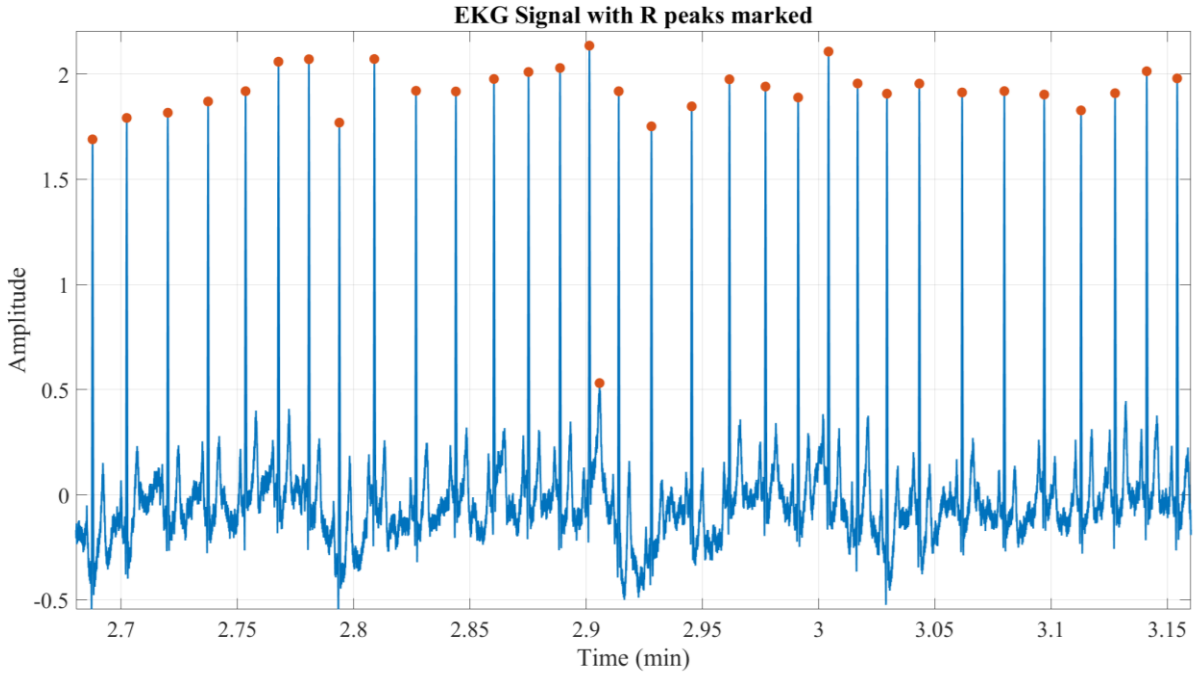

Figure 4.15: Incorrectly set threshold capturing a non-R peak as an R peak that led to the incorrect IHR estimate that is observed as a spike in Figure 4.14 plot 7.

If the threshold to detect peaks is not set correctly, there is a possibility of some R peaks being missed and/or non-R peaks being detected, both of which will significantly affect the instantaneous heart rate measurements. R peak detection algorithms rely on the fact that the most prominent peaks in the EKG signal are R peaks. However, some EKG signals, especially measured from ambulatory EKG devices can contain spikes due to noise. A low pass filter might not be effective at removing these spikes without affecting the R peaks. To further demonstrate this, one of the EKG signals was corrupted by adding white Gaussian noise. The noise level was set so that the signal to noise ratio was 20. Figure 4.16 shows how the thresholding algorithm fails to correctly identify R peaks of the noisy signal. Therefore, it is clear that even if the noise level is 100x less than the EKG signal, simple thresholding methods can fail to detect R waves correctly. However, since the instantaneous heart rate calculated using the IF method does not rely on R peak detection, it is more robust at estimating instantaneous heart rate from EKG signals with low SNR values.

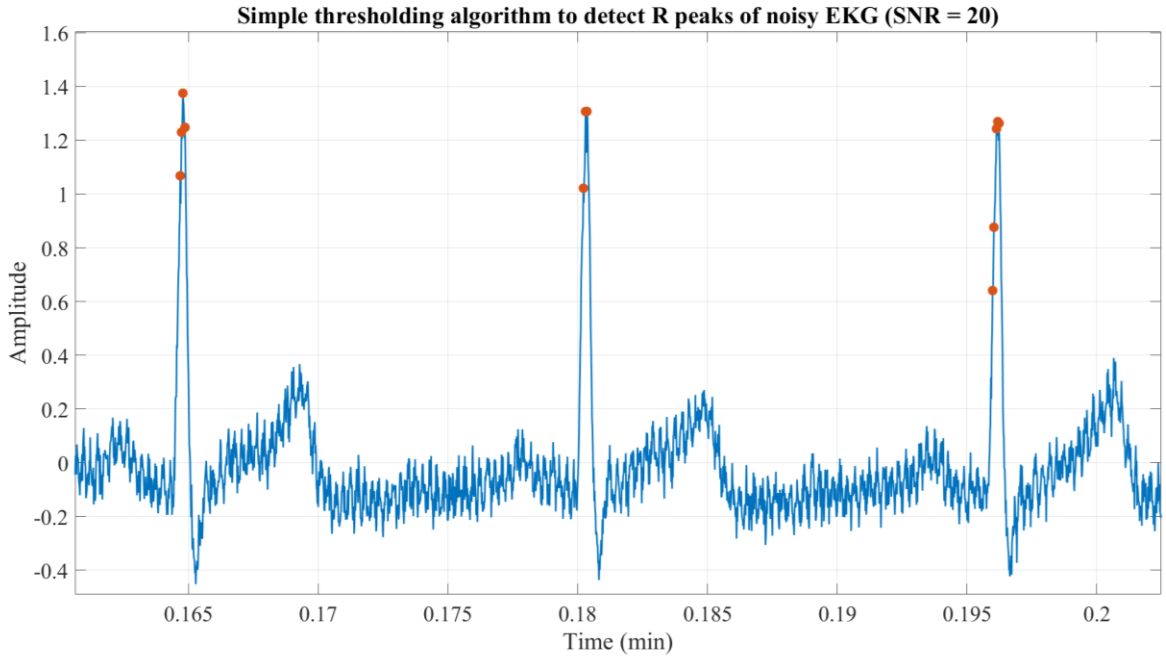

Figure 4.16: An EKG signal corrupted by adding white Gaussian noise. Observe how the thresholding method is unable to correctly detect the inflection point of the R wave (R peak). Since multiple peaks are detected as R peaks, the resulting heart rate is erroneous.

In this study we set the center frequency of the bandpass filter used in the preprocessing stage to the mean heart rate. One can argue that to estimate the mean heart rate we had to use RR interval measurements and thus, this procedure is not completely independent of R peak detection. Although this is true, the focus of this study was to introduce an IF based method to estimate IHR and not to introduce a method to set the center frequency of the bandpass filter. Therefore, we resorted to the simple method of estimating the mean heart rate through RR interval measurements. However, we do not have to rely on R peak detection or RR interval measurements to estimate the center frequency of the bandpass filter. We can instead use methods such as the one introduced in [32] to set the center frequency of the bandpass filter. Other possible approaches are to use adaptive filters or parallel filters.

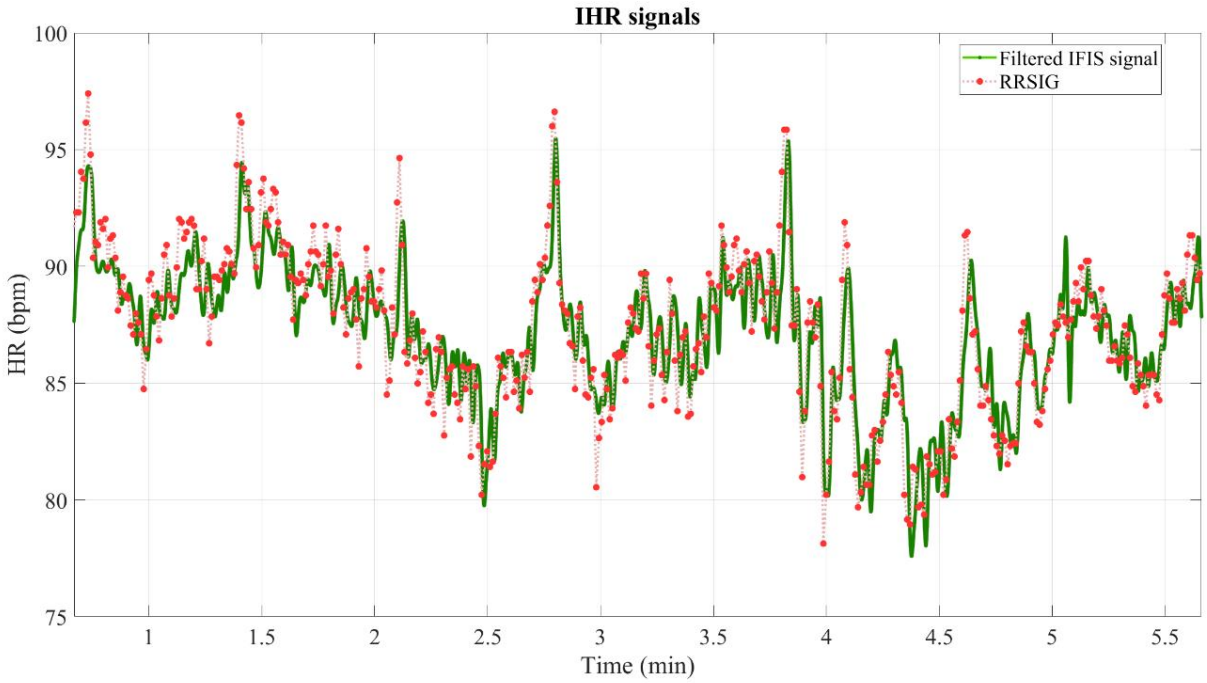

Figure 4.17: IHR signals of individual No 11. Data points are plotted as dots.

The IHR signal computed using the filtered IFIS signal also provides better temporal resolution than RRSIG. Observe Figure 4.17 where the IHR signals of individual 11 are plotted. The red dots represent the instantaneous heart rates calculated using RR intervals and the dotted lines represent linearly interpolated IHR values between them. The green dots represent the IHR values calculated using the IF method. Since the filtered IFIS signal produces data points at a rate equivalent to the sampling rate of the EKG signal it has significantly higher temporal resolution than RRSIG. Therefore, the error of an interpolated IHR value is less in the filtered IFIS signal than that of RRSIG. Further, the effect that the interpolation technique (e.g. linear, spline etc.) has on the RRSIG value is much higher.

Chapter 5 - Conclusion

In this study we used an algorithm based on instantaneous frequency to estimate the instantaneous heart rate (IHR) from an electrocardiogram (EKG) signal to perform heart rate variability (HRV) analysis. We were motivated to find an alternative method to calculate the instantaneous heart rate as the prevalent method of using RR interval measurements has inherent shortcomings. These drawbacks stem from the reliance on R peak detection for measuring heart rate. Correctly detecting R peaks can get extremely challenging for EKG signals contaminated by high levels of noise as well as EKG signals containing anomalies. Further, placement of the EKG electrodes affects the amplitude and prominence of the R waves, lending some EKG leads unsuitable for heart rate estimation using R peaks. Additionally, the IHR signal constructed using RR intervals (RRSIG) is not a uniformly sampled signal and has low temporal resolution in the time domain. To address these concerns a methodology based on instantaneous frequency (IF) was introduced to calculate the IHR signal. This signal was termed IFIS. Although IFIS was able to address these shortcomings, the new method introduced new implications in the form of spikes in the calculated IFIS. Two different methods were introduced in the study to potentially address this issue: using a low-pass filter to remove spikes from IFIS and a spike removing algorithm. We observed that for frequency domain HRV analysis, spikes in IFIS did not significantly affect the final calculated HRV metrics. For time domain analysis, the low-pass filtering method is more suitable for removing spikes.

We were able to demonstrate the weaknesses of algorithms that rely on R peak detection to calculate IHR from noisy EKGs. We also observed how the IF method is robust enough to handle noise and anomalies in the EKG signal. This is because it does not rely on R peaks to calculate IHR. Further, since IFIS produces samples at a constant rate equivalent to the sampling rate of the EKG signal, there is no need for interpolation. The RRSIG on the other hand is sampled at a varying rate and interpolation is necessary before frequency domain analysis which can distort the shape of the signal.

The amount of useful information contained within the IHR signal calculated using the IF method compared to RRSIG is up for contention. For HRV analysis in the frequency domain, the resolution of the spectra is dependent on the length of the signal and not the sampling rate. Although the spectrum is broader for the IHR signal calculated using IF method, HRV metrics are calculated using the spectral components up to ½ times the mean heart rate. It is not clear if this limit is set due to the lack of information beyond the Nyquist frequency of the RRSIG or due to lack of correlation between high frequency components and physiological functions. However, the spectrum of IFIS provides more potentially useful information up to the average zero crossing rate of the filtered EKG signal. This information can potentially be used by researchers to introduce new HRV metrics and find links to physiological functions and conditions.

In the time domain, RRSIG produces data points at intervals equivalent to the RR interval. Therefore, the maximum sampling rate that can be achieved is equivalent to the maximum heart rate and is independent of the sampling rate of the actual EKG signal. The IHR signal produced by the IF method on the other hand produces samples at a constant sampling rate equivalent to the sampling rate of the EKG signal. Therefore, a filtered IFIS signal is more detailed: gives a better estimate of the IHR at a data point between R peaks compared to RRSIG.

Therefore, through this study we were able to utilize concepts of IF to calculate the IHR from EKG signals and calculate HRV metrics. We were also able to address the shortcomings associated with the conventional method of estimating the IHR signal which relies on R peak detection through the method introduced in this study.

Bibliography

[1] H. H. P. Staff, “Heart rate variability: How it might indicate well-being,” Harvard Health. Accessed: Feb. 10, 2024. [Online]. Available: https://www.health.harvard.edu/blog/heart-rate-variability-new-way-track-well-2017112212789

[2] H. M. Stauss, “Heart rate variability,” *Am. J. Physiol.-Regul. Integr. Comp. Physiol.*, vol. 285, no. 5, pp. R927–R931, Nov. 2003, doi: 10.1152/ajpregu.00452.2003.

[3] G. E. Billman, H. V. Huikuri, J. Sacha, and K. Trimmel, “An introduction to heart rate variability: methodological considerations and clinical applications,” *Front. Physiol.*, vol. 6, Feb. 2015, doi: 10.3389/fphys.2015.00055.

[4] J. S. PerkiÃ¶mÃ¤ki, “Heart Rate Variability and Non-Linear Dynamics in Risk Stratification,” *Front. Physiol.*, vol. 2, Nov. 2011, doi: 10.3389/fphys.2011.00081.

[5] E. Tobaldini, L. Nobili, S. Strada, K. R. Casali, A. Braghiroli, and N. Montano, “Heart rate variability in normal and pathological sleep,” *Front. Physiol.*, vol. 4, 2013, doi: 10.3389/fphys.2013.00294.

[6] Z. Zhang, “An online algorithm for least-square spectral analysis: Applied to time-frequency analysis of heart rate”.

[7] “Heart | SEER Training.” Accessed: Jan. 31, 2024. [Online]. Available: https://training.seer.cancer.gov/anatomy/cardiovascular/heart/

[8] “Right Ventricle Function, Definition & Anatomy | Body Maps,” Healthline. Accessed: Feb. 11, 2024. [Online]. Available: https://www.healthline.com/human-body-maps/right-ventricle

[9] M. N. Berman, C. Tupper, and A. Bhardwaj, “Physiology, Left Ventricular Function,” in *StatPearls*, Treasure Island (FL): StatPearls Publishing, 2024. Accessed: Feb. 11, 2024. [Online]. Available: http://www.ncbi.nlm.nih.gov/books/NBK541098/

[10] L. M. Biga *et al.*, “19.3 Cardiac Cycle,” Sep. 2019, Accessed: Feb. 10, 2024. [Online]. Available: https://open.oregonstate.education/aandp/chapter/19-3-cardiac-cycle/

[11] “The P Wave - Sinus Rhythm - Normal Function of the Heart - Cardiology Teaching Package - Practice Learning - Division of Nursing - The University of Nottingham.” Accessed: Feb. 11, 2024. [Online]. Available: https://www.nottingham.ac.uk/nursing/practice/resources/cardiology/function/p_wave.php

[12] “Cardiac conduction system - Health Video: MedlinePlus Medical Encyclopedia.” Accessed: Feb. 11, 2024. [Online]. Available: https://medlineplus.gov/ency/anatomyvideos/000021.htm

[13] “The T Wave - Sinus Rhythm - Normal Function of the Heart - Cardiology Teaching Package - Practice Learning - Division of Nursing - The University of Nottingham.” Accessed: Feb. 11, 2024. [Online]. Available: https://www.nottingham.ac.uk/nursing/practice/resources/cardiology/function/t_wave.php

[14] “What is an electrocardiogram (ECG)?,” in *InformedHealth.org [Internet]*, Institute for Quality and Efficiency in Health Care (IQWiG), 2019. Accessed: Mar. 30, 2024. [Online]. Available: https://www.ncbi.nlm.nih.gov/books/NBK536878/

[15] “Holter Monitor.” Accessed: Apr. 01, 2024. [Online]. Available: https://www.hopkinsmedicine.org/health/treatment-tests-and-therapies/holter-monitor

[16] “1-lead to 12-lead and exercise ECG.” Accessed: Apr. 10, 2024. [Online]. Available: https://www.ndsu.edu/pubweb/~grier/1to12-lead-ECG-EKG.html

[17] “EKG Interpretation.” Accessed: Mar. 30, 2024. [Online]. Available: https://www.nurseslearning.com/courses/nrp/nrp1619/Section%205/index.htm

[18] “Introduction to ECG.” Accessed: Apr. 01, 2024. [Online]. Available: https://www.healio.com/cardiology/learn-the-heart/ecg-review/ecg-interpretation-tutorial/introduction-to-the-ecg

[19] Y. Sattar and L. Chhabra, “Electrocardiogram,” in *StatPearls*, Treasure Island (FL): StatPearls Publishing, 2024. Accessed: Apr. 01, 2024. [Online]. Available: http://www.ncbi.nlm.nih.gov/books/NBK549803/

[20] “Target Heart Rate and Estimated Maximum Heart Rate | Physical Activity | CDC.” Accessed: Dec. 09, 2023. [Online]. Available: https://www.cdc.gov/physicalactivity/basics/measuring/heartrate.htm

[21] J. Allen, “Photoplethysmography and its application in clinical physiological measurement,” *Physiol. Meas.*, vol. 28, no. 3, pp. R1–R39, Mar. 2007, doi: 10.1088/0967-3334/28/3/R01.

[22] E. A. Pelaez and E. R. Villegas, “LED power reduction trade-offs for ambulatory pulse oximetry,” in *2007 29th Annual International Conference of the IEEE Engineering in Medicine and Biology Society*, Lyon, France: IEEE, Aug. 2007, pp. 2296–2299. doi: 10.1109/IEMBS.2007.4352784.

[23] S. Lu *et al.*, “Can Photoplethysmography Variability Serve as an Alternative Approach to Obtain Heart Rate Variability Information?,” *J. Clin. Monit. Comput.*, vol. 22, no. 1, pp. 23–29, Jan. 2008, doi: 10.1007/s10877-007-9103-y.

[24] K. Georgiou, A. V. Larentzakis, N. N. Khamis, G. I. Alsuhaibani, Y. A. Alaska, and E. J. Giallafos, “Can Wearable Devices Accurately Measure Heart Rate Variability? A Systematic Review,” *Folia Med. (Plovdiv)*, vol. 60, no. 1, Jan. 2018, doi: 10.2478/folmed-2018-0012.

[25] J. R. Jago and A. Murray, “Repeatability of peripheral pulse measurements on ears, fingers and toes using photoelectric plethysmography,” *Clin. Phys. Physiol. Meas.*, vol. 9, no. 4, pp. 319–329, Nov. 1988, doi: 10.1088/0143-0815/9/4/003.

[26] M. Cadogan, R. Buttner, and M. C. and R. Buttner, “ECG Rate Interpretation,” Life in the Fast Lane • LITFL. Accessed: Dec. 16, 2023. [Online]. Available: https://litfl.com/ecg-rate-interpretation/

[27] J. Pan and W. J. Tompkins, “A Real-Time QRS Detection Algorithm,” *IEEE Trans. Biomed. Eng.*, vol. BME-32, no. 3, pp. 230–236, Mar. 1985, doi: 10.1109/TBME.1985.325532.

[28] L. Sörnmo and P. Laguna, “Electrocardiogram (ECG) Signal Processing,” in *Wiley Encyclopedia of Biomedical Engineering*, 1st ed., M. Akay, Ed., Wiley, 2006. doi: 10.1002/9780471740360.ebs1482.

[29] L. Sörnmo and P. Laguna, “The Electrocardiogram—A Brief Background,” in *Bioelectrical Signal Processing in Cardiac and Neurological Applications*, pp. 411–452. Accessed: Jan. 23, 2024. [Online]. Available: https://www.researchgate.net/publication/279429143_The_Electrocardiogram-A_Brief_Background

[30] S. Pal and M. Mitra, “Detection of ECG characteristic points using Multiresolution Wavelet Analysis based Selective Coefficient Method,” *Measurement*, vol. 43, no. 2, pp. 255–261, Feb. 2010, doi: 10.1016/j.measurement.2009.10.004.

[31] T. Berset, I. Romero, A. Young, and J. Penders, “Robust heart rhythm calculation and respiration rate estimation in ambulatory ECG monitoring,” in *Proceedings of 2012 IEEE-EMBS International Conference on Biomedical and Health Informatics*, Hong Kong: IEEE, Jan. 2012, pp. 400–403. doi: 10.1109/BHI.2012.6211599.

[32] A. K. Barros and N. Ohnishi, “Heart instantaneous frequency (HIF): an alternative approach to extract heart rate variability,” *IEEE Trans. Biomed. Eng.*, vol. 48, no. 8, pp. 850–855, Aug. 2001, doi: 10.1109/10.936361.

[33] S. Saliu, “Definition of instantaneous frequency on real signals”.

[34] B. Boashash, “Estimating and interpreting the instantaneous frequency of a signal. I. Fundamentals,” *Proc. IEEE*, vol. 80, no. 4, pp. 520–538, Apr. 1992, doi: 10.1109/5.135376.

[35] B. Van Der Pol, “The fundamental principles of frequency modulation,” *J. Inst. Electr. Eng. - Part III Radio Commun. Eng.*, vol. 93, no. 23, pp. 153–158, May 1946, doi: 10.1049/ji-3-2.1946.0024.

[36] C. Berthomier and N. Cornilleau-Wehrlin, “APPLICATION DE LA NOTION DE SIGNAL ANALYTIQUE A LA D]~TERMINATION DE L’AMPLITUDE ET DE LA FRI~QUENCE INSTANTANI~E D’UN SIGNAL,” 1975.

[37] J. C. Goswami and A. E. Hoefel, “Algorithms for estimating instantaneous frequency,” *Signal Process.*, vol. 84, no. 8, pp. 1423–1427, Aug. 2004, doi: 10.1016/j.sigpro.2004.05.016.

[38] R. M. Adelson, “Frequency Estimation from Few Measurements,” *Digit. Signal Process.*, vol. 7, no. 1, pp. 47–54, Jan. 1997, doi: 10.1006/dspr.1997.0280.

[39] D. N. Vizireanu, “A simple and precise real-time four point single sinusoid signals instantaneous frequency estimation method for portable DSP based instrumentation,” *Measurement*, vol. 44, no. 2, pp. 500–502, Feb. 2011, doi: 10.1016/j.measurement.2010.11.001.

[40] R. Romulus, “A comparison between instantaneous frequency estimation methods of frequency modulated signals covered with Gaussian noise,” in *2012 10th International Symposium on Electronics and Telecommunications*, Timisoara, Timis, Romania: IEEE, Nov. 2012, pp. 331–334. doi: 10.1109/ISETC.2012.6408120.

[41] N. A. Khan, M. Mohammadi, and S. Ali, “Instantaneous frequency estimation of intersecting and close multi-component signals with varying amplitudes,” *Signal Image Video Process.*, vol. 13, no. 3, pp. 517–524, Apr. 2019, doi: 10.1007/s11760-018-1377-7.

[42] D. Wei and A. C. Bovik, “On the instantaneous frequencies of multicomponent AM-FM signals,” *IEEE Signal Process. Lett.*, vol. 5, no. 4, pp. 84–86, Apr. 1998, doi: 10.1109/97.664173.

[43] N. Karim, J. A. Hasan, and S. S. Ali, “HEART RATE VARIABILITY – A REVIEW”.

[44] F. Shaffer and J. P. Ginsberg, “An Overview of Heart Rate Variability Metrics and Norms,” *Front. Public Health*, vol. 5, p. 258, Sep. 2017, doi: 10.3389/fpubh.2017.00258.

[45] R. E. Kleiger, P. K. Stein, and J. T. Bigger, “Heart Rate Variability: Measurement and Clinical Utility,” *Ann. Noninvasive Electrocardiol.*, vol. 10, no. 1, pp. 88–101, Jan. 2005, doi: 10.1111/j.1542-474X.2005.10101.x.

[46] R. E. Kleiger, J. P. Miller, J. T. Bigger, and A. J. Moss, “Decreased heart rate variability and its association with increased mortality after acute myocardial infarction,” *Am. J. Cardiol.*, vol. 59, no. 4, pp. 256–262, Feb. 1987, doi: 10.1016/0002-9149(87)90795-8.

[47] F. Shaffer, R. McCraty, and C. L. Zerr, “A healthy heart is not a metronome: an integrative review of the heart’s anatomy and heart rate variability,” *Front. Psychol.*, vol. 5, Sep. 2014, doi: 10.3389/fpsyg.2014.01040.

[48] T. Kuusela, “Methodological Aspects of Heart Rate Variability Analysis,” in *Heart Rate Variability (HRV) Signal Analysis*, CRC Press, 2012, pp. 9–42. doi: 10.1201/b12756-4.

[49] E. Miranda Dantas *et al.*, “Spectral analysis of heart rate variability with the autoregressive method: What model order to choose?,” *Comput. Biol. Med.*, vol. 42, no. 2, pp. 164–170, Feb. 2012, doi: 10.1016/j.compbiomed.2011.11.004.

[50] M. Armstrong, C. C. Kerndt, and R. A. Moore, “Physiology, Baroreceptors,” in *StatPearls*, Treasure Island (FL): StatPearls Publishing, 2024. Accessed: Apr. 11, 2024. [Online]. Available: http://www.ncbi.nlm.nih.gov/books/NBK538172/

[51] H. Usui and Y. Nishida, “The very low-frequency band of heart rate variability represents the slow recovery component after a mental stress task,” *PLOS ONE*, vol. 12, no. 8, p. e0182611, Aug. 2017, doi: 10.1371/journal.pone.0182611.

[52] C. Carlson, V.-R. Turpin, A. Suliman, C. Ade, S. Warren, and D. E. Thompson, “Bed-Based Ballistocardiography: Dataset and Ability to Track Cardiovascular Parameters,” *Sensors*, vol. 21, no. 1, p. 156, Dec. 2020, doi: 10.3390/s21010156.

[53] Zhidong Zhao, Min Pan, and Yuquan Chen, “Instantaneous frequency estimate for non-stationary signal,” in *Fifth World Congress on Intelligent Control and Automation (IEEE Cat. No.04EX788)*, Hangzhou, China: IEEE, 2004, pp. 3641–3643. doi: 10.1109/WCICA.2004.1343274.

[54] C. Sekar, *Analog Communication*, 1st ed. Oxford University Press, 2010.

[55] S. Palani, *Discrete Time Systems and Signal Processing*. Cham: Springer International Publishing, 2023. doi: 10.1007/978-3-031-32421-5.

[56] “DFT Frequency Resolution Explained - Wave Walker DSP.” Accessed: Apr. 18, 2024. [Online]. Available: https://www.wavewalkerdsp.com/2022/03/16/dft-frequency-resolution-explained/

[57] “Scalloping loss | RecordingBlogs.” Accessed: Apr. 18, 2024. [Online]. Available: https://www.recordingblogs.com/wiki/scalloping-loss

[58] “Understanding Power Spectral Density and the Power Spectrum.” Accessed: Apr. 21, 2024. [Online]. Available: https://www.mathworks.com/videos/understanding-power-spectral-density-and-the-power-spectrum-1707740400025.html

[59] G. Heinzel, A. Rudiger, and R. Schilling, “Spectrum and spectral density estimation by the Discrete Fourier transform (DFT), including a comprehensive list of window functions and some new flat-top windows.”.

[60] F. J. Harris, “On the use of windows for harmonic analysis with the discrete Fourier transform,” *Proc. IEEE*, vol. 66, no. 1, pp. 51–83, 1978, doi: 10.1109/PROC.1978.10837.

[61] “Window Types: Hanning, Flattop, Uniform, Tukey, and Exponential.” Accessed: Mar. 18, 2024. [Online]. Available: https://community.sw.siemens.com/s/article/window-types-hanning-flattop-uniform-tukey-and-exponential

[62] “Spectrogram using short-time Fourier transform - MATLAB spectrogram.” Accessed: Apr. 01, 2024. [Online]. Available: https://www.mathworks.com/help/signal/ref/spectrogram.html#mw_c6dfa97d-9a98-4238-a6bd-d58825fb47e0

[63] “Overlap Percentage.” Accessed: Apr. 18, 2024. [Online]. Available: https://www.spectraplus.com/DT_help/overlap_percentage.htm

[64] R. Bristow-Johnson, “Audio EQ Cookbook,” Audio EQ Cookbook. Accessed: Jan. 30, 2024. [Online]. Available: https://www.w3.org/TR/audio-eq-cookbook/

[65] K. Umetani, D. H. Singer, R. McCraty, and M. Atkinson, “Twenty-Four Hour Time Domain Heart Rate Variability and Heart Rate: Relations to Age and Gender Over Nine Decades,” *J. Am. Coll. Cardiol.*, vol. 31, no. 3, pp. 593–601, Mar. 1998, doi: 10.1016/S0735-1097(97)00554-8.

[66] H. Zumbahlen, *Chapter 8: Analog Filters*. Accessed: Feb. 19, 2024. [Online]. Available: https://learning.oreilly.com/library/view/linear-circuit-design/9780750687034/OEBPS/B9780750687034000080.htm

[67] “All About Heart Rate (Pulse),” www.heart.org. Accessed: Feb. 19, 2024. [Online]. Available: https://www.heart.org/en/health-topics/high-blood-pressure/the-facts-about-high-blood-pressure/all-about-heart-rate-pulse

[68] “Monocomponent Signal - an overview | ScienceDirect Topics.” Accessed: Jan. 01, 2024. [Online]. Available: https://www.sciencedirect.com/topics/computer-science/monocomponent-signal

[69] “Inverse cosine in radians - MATLAB acos.” Accessed: Apr. 21, 2024. [Online]. Available: https://www.mathworks.com/help/matlab/ref/acos.html

[70] “2.3 The Dot, oops, INNER Product.” Accessed: Feb. 21, 2024. [Online]. Available: https://web1.eng.famu.fsu.edu/~dommelen/quantum/style_a/dot.html

[71] A. Aishwarya, N. S. Bharath, M. Swathi, and R. Prabha, “Detection of Obstructive Sleep Apnoea Using ECG Signal,” in *Recent Advancements in System Modelling Applications*, vol. 188, R. Malathi and J. Krishnan, Eds., in Lecture Notes in Electrical Engineering, vol. 188. , India: Springer India, 2013, pp. 381–392. doi: 10.1007/978-81-322-1035-1_33.

[72] “Window Correction Factors.” Accessed: Apr. 20, 2024. [Online]. Available: https://community.sw.siemens.com/s/article/window-correction-factors

[73] “Trapezoidal numerical integration - MATLAB trapz.” Accessed: Apr. 12, 2024. [Online]. Available: https://www.mathworks.com/help/matlab/ref/trapz.html#d126e1747307

[74] J. A. J. Heathers, “Everything Hertz: methodological issues in short-term frequency-domain HRV,” *Front. Physiol.*, vol. 5, May 2014, doi: 10.3389/fphys.2014.00177.

[75] “AppendixA.” Accessed: Mar. 17, 2024. [Online]. Available: https://terpconnect.umd.edu/~toh/spectrum/AppendixG.html

[76] S. Brunton and N. Kutz, *Data-Driven Science and Engineering - Machine Learning, Dynamical Systems, and Control*, 2nd ed. Cambridge University Press, 2021.